Seasonal variation of the sea off Sanriku and data analysis method

by

Sachiko Oguma

Marine Information Research Center, Japan Hydrographic Association
Mishima Bldg. 5F, 7-15-4 Ginza, Chuo-ku, Tokyo, 104-0061 Japan

July 2003

Abstract

In this study, monthly observation data and their standard depth data are analyzed to understand seasonal variations of mean temperature and salinity of the sea off Sanriku. Oceanic dataset obtained by the Iwate Fisheries Technology Center during 1971-1995 is mainly used and a new data interpolation scheme and a skewed occurrence frequency of temperatures are also described.

In chapter 1, a new interpolation scheme is discussed to avoid generation of pseudo density inversions. Oceanic datasets, which are arranged for standard depths have various applications for numerous users. Since observations are not always conducted exactly at the standard depths, especially in the case of historical bottle observations, data interpolation at standard depths is needed. Usually, data interpolation is conducted for temperature and salinity values, and then density values are calculated from those interpolated values of temperature and salinity. However, pseudo density inversions are often generated among interpolated data in the areas such as the sea off Sanriku, east of Japan, since vertical structures of water mass distributions at those areas are extremely complex. In order to solve this problem, a new interpolation scheme is designed, in which temperature and density are used as independent variables. In this scheme, temperature and density values are firstly interpolated using observed values, and salinity is back-calculated from interpolated temperature and density values at standard depths. This scheme is applied to obtain standard depth dataset. The standard depth data interpolated by this new scheme are used in this study.

In chapter 2, "skewness" of occurrence frequency of temperature data is discussed comparing with oceanic condition when extreme values were observed. It is suggested that occurrence frequency distributions of temperature and salinity are very skewed at depths deeper than 150 m, and that temperatures sometimes exceed $m+5\sigma$ (m: mean and σ: standard deviation). It was found that this abnormally high temperature (and high salinity) water could be regarded as the pure Kuroshio water intruding into the region due to some special conditions, such as abnormal approach of large warm-core ring to the Sanriku Coast in 1972, or abnormal northward extension of the Kuroshio along the coast in 1979. These events are very rare, occurring only twice in the analysis period of 25 years, but the abnormally high temperatures observed are real.

In chapter 3, seasonal variations in the sea off Sanriku are discussed using horizontal distributions of temperature and salinity. The variations of three typical waters found in this region, the Tsugaru Current water, the Oyashio water, and the Kuroshio water, are discussed in terms of a T(temperature) - S(salinity) scatter diagram referring to the water

mass classification proposed by Hanawa and Mitsudera (1986). The mean temperature and salinity fields averaged for each month show clear seasonal variation. At 100 m depth, the mean fields of temperature and salinity indicate remarkable seasonal variation, especially in the frontal area between the Tsugaru Current and the first branch of the Oyashio. The temperature and salinity fronts between the Tsugaru Current water and the Oyashio water gradually disappear in January through April, appear again in May, and then become clearest in September. However, at 200 m depth, distributions of the Tsugaru Current water and the Oyashio water can barely be distinguished, since those water masses occupy in shallow layers.

In chapter 4, the forerunner of Tsugaru Current is discussed using vertical sections of monthly mean temperature and salinity. The forerunner of Tsugaru Current appears as temperature or salinity maximum on the shelf bottom in spring, mainly in March or April. It seems to be similar to the forerunner of Soya Current. Although it is hard to show typical seasonal variations from time series of temperature and salinity fields in individual months, the forerunner of Tsugaru Current could be suggested as a special water mass in spring season.

Contents

General Introduction

In the management of oceanographic data, it is very important to understand oceanic condition of the area where the data were obtained. In order to check whether the data reported are appropriate for the observation area, range values of each variable for data checking must be changed owing to location or seasonal variation of the region. If a dataset for a basin-scale area is targeted, range values should be set up widely, since the range should cover all possible values of variables in the target area. On the other hand, if a dataset for a narrow region such as marginal sea is treated, more strict range would be set up, because possible values of variables are limited to some degree. Therefore, understanding of oceanic condition of targeted area becomes more important when the area becomes more limited.

In order to discuss appropriate range for data checking in the targeted region, the maximum and the minimum values, occurrence frequency distributions, and values of mean and standard deviations are generally used so far. These statistical specifics are usually calculated at each standard depth. Mostly, standard depth data are interpolated to the depths defined by the International Association for the Physical Sciences of the Ocean (IAPSO). Standard depth dataset of World Ocean Database 1998 (WOD98) produced by National Oceanographic Data Center (NODC) is a typical example. Japan Oceanographic Data Center (JODC) had provided standard depth dataset via online until 2000. However, they decided to provide only observation data since then. Therefore, Marine Information Research Center (MIRC) of Japan Hydrographic Association has developed data interpolation scheme to produce standard depth dataset using observation data archived in JODC. Initially, MIRC followed the interpolation scheme used by NODC for compilation of WOD98. However, pseudo density inversions were frequently occurred among interpolated values, especially in the area where different water masses occupy complicatedly, such as the sea off Sanriku. This means that interpolation scheme itself should also be developed under taking oceanic condition of the targeted region into account.

The sea off Sanriku is extraordinary complicated area; the Tsugaru Current in coastal area, the Oyashio and the Kuroshio Extension in offshore and warm/cold water rings intrude each other, and they also exhibit considerable seasonal variations. Because of the complexity of oceanic condition, the sea off Sanriku has been named in several ways, for example, "Perturbed Area" (e.g., Uda, 1935), "Transition Area" (e.g., Kawai, 1972), and "Mixed Water Region" (e.g., Talley et al., 1995). The sea off Sanriku has been studied as not only a nutritious area for fisheries, but also a source area of the North Pacific Intermediate Water (e.g., Hasunuma, 1978; Hirai et al., 1988; Talley et al., 1995). Although there are many previous

studies about seasonal variations of each water mass distributed in the sea off Sanriku (e.g., Muto et al., 1969; Mizuno, 1984; Okuda, 1986; Sekine, 1988; Takasugi, 1992), descriptions based on individual observation were too diverse to discuss typical seasonal variations of mean fields in temperature and salinity.

The purposes of the present study are, firstly to suggest an importance of discussion for data interpolation and oceanic condition, and secondary to indicate the seasonal variations of mean fields of temperature and salinity in the sea off Sanriku. Since it is necessary to use, at least, monthly observed data for describing seasonal variation, oceanic dataset obtained regularly by the Iwate Fisheries Technology Center is mainly analyzed in the present study. Before data analysis, the dataset is checked following the data quality control procedure developed at MIRC (MIRC, 2001).

The present thesis is organized as follows. In chapter 1, a new interpolation scheme is described, which can be applied to produce standard depth dataset, preventing from generation of pseudo density inversions. In chapter 2, "skewness" of occurrence frequency of temperature data is discussed comparing with oceanic condition, when extreme values are observed. In chapter 3, seasonal variations in the sea off Sanriku are discussed. Horizontal distributions of monthly mean temperature and salinity at 100 m and 200 m depths are shown as typical patterns of seasonal variations. In chapter 4, seasonal variations of vertical distributions of temperature and salinity in the sea off Sanriku is discussed, focusing on the forerunner of Tsugaru Current in coastal area, which appears mainly in March or April. Finally, general conclusion is given.

1 Interpolation scheme for standard depth data applicable for areas with a complex hydrographical structure

1.1 Introduction

Datasets based on standard depths are requested by many data users, because they are very useful for numerical model studies which require gridded data. For example, the World Ocean Atlas 1998 (WOA98) which was published by the Ocean Climate Laboratory, National Oceanographic Data Center (thereafter NODC) gives various statistical results for standard depths, and provides the initial conditions or boundary conditions of the numerical models.

On the other hand, the Japan Oceanographic Data Center (JODC) until 2000 provided both observed data and standard depth data via an online service, however, currently only the observed data is available, since the standard depth data can be obtained from the observed data. A further reason is that recent instruments such as CTD, XBT, and so on can record data continuously and an observer can then select the data at the required standard depths. The Marine Information Research Center (MIRC) provides oceanographic datasets at standard depths calculated from the JODC observation datasets. Pre-2000, the standard depth data provided by JODC were constructed basically from the reported values from each organization where the data originated, with methods of interpolation differing among the organizations. It is desirable to use a unified and reliable interpolation scheme to prepare the standard depth data. The NODC applied an elaborative interpolation scheme for the compilation of World Ocean Database 1998 (WOD98) (e.g., Antonov et al., 1998) following the procedures set by UNESCO (1991). MIRC also followed their interpolation procedures, and after this scheme was initiated almost no pseudo density inversions were observed in the datasets for the subtropical region and for the Kuroshio region.

However, we found that use of the interpolation scheme produces occasionally pseudo density inversion layers, when it is applied to very complex areas such as the Kuroshio/Oyashio mixed water region east of Japan (e.g., Talley et al., 1995) shown in Fig. 1.1. Among the Kuroshio/Oyashio mixed water region, the sea area off Sanriku in the westernmost of the region is especially complicated. In this sea area, the warm and saline Tsugaru Current Water encounters the cold and fresher Oyashio Water in this region, and the much warmer and more saline water originating from the Kuroshio Water frequently intrudes (Oguma and Nagata, 2002; Oguma et al., 2002). As a result, they create a very complex layered-structure, and their vertical temperature and salinity profiles may form in a zigzag shaped

pattern. The CTD profile in Fig. 1.2 obtained by the Iwate Fisheries Technology Center suggests that the typical thickness scale of the interleaving layers is generally much less than the vertical intervals of measurements in serial observations. Because of the coarseness of the large depth intervals, vertical profiles of temperature and salinity observed at standard depths show a somewhat smooth curve. The smooth profiles obtained in areas of complex hydrographic structure suggest that the gross features of the profiles might be reproduced by the conventional interpolation scheme.

We plan to apply the NODC interpolation scheme in order to compile MIRC standard depth database, and attempt to obtain an interpolation scheme which does not produce pseudo density inversions, even in the Kuroshio/Oyashio mixed water region of east of Japan. In this study, we discuss a modification to the interpolation scheme to make it applicable for such areas of complex hydrographic structure.

1.2 Interpolation scheme used by NODC

Before interpolation, we conducted data quality checks. We did not use any of erroneous data, which conflict with the range check or the density inversion check. In this study, a gradient check was not conducted to test the interpolation scheme for the area where temperature and salinity change markedly in the vertical direction, such as the sea area off Sanriku.

Ranges used are in the function of depth, and are the same as those used by NODC at the compiling stage of WOD98 (Antonov et al., 1998). For density inversion, *in-situ* density

$$\rho = \rho(T, S, p)$$

was applied, which were calculated from the *in-situ* temperature T, salinity S and depth p. NODC applied acceptable values in function of depth for density inversion: the density of the upper level is heavier over 0.03 kg m^{-3} than that of the lower level for the depth range from 0 to 30 m, or heavier over 0.02 kg m^{-3} for the depth range from 30 to 400 m, or heavier over 0.001 kg m^{-3} for the depth range deeper than 400 m. Note that these values are not for the density gradient, but for the density difference between two adjacent observed depths no matter how far the two depths are separated. It should be noted that the *in-situ* density is used only for data quality check. To discuss the generation of pseudo density inversions, potential density (σ_θ)

$$\sigma_\theta = \rho(\theta(T, S, p), S, 0) - 1000,$$

where θ is potential temperature, will be used.

After the data quality check, we interpolated the data to the objective standard depths (see Table 1.1), using data obtained at the observation point. In the NODC interpolation scheme, observed data at depths as near as possible are selected to interpolate data to the standard depths. Table 1.1 lists the acceptable distances (m), which are used for defining the interior value (I) and the exterior value (E) of distance between the objective standard depth and the observed data depth. The observed data (depth z) which are located outside the exterior domain ($z <$ S$-$E or $z >$ S$+$E, where S is the depth of the objective standard depth) for the objective standard depth, are not used.

Although I and E for the sea surface (0 m) and 10 m depth are defined by NODC, we did not make interpolations or extrapolations for these depths. If observed data at a depth shallower than 5 m is available, we use this value as the data at the sea surface, because the definition of the surface is not clear both for bucket water sampling and for CTD observations. Also, the water temperature of the intake water to the ship engine can be reported as the sea surface temperature. The accuracy of the sea surface temperature is in general limited as discussed by Nagata et al. (1999). Since the interpolated value for the 10 m standard depth can be strongly affected by the surface temperature, we used the observed value taken within the depth range between 9 and 11 m depth as the value at 10 m depth.

Cases whether the interpolation is applied or not are illustrated in Figs. 1.3 to 1.6. Fig. 1.3 indicates the cases that no interpolation is made even if some data are available within the exterior domain (S$-$E $\leq z <$ S$-$I or S$+$I $< z \leq$ S$+$E). As shown in Fig. 1.3(a), if no data is available inside the interior domain (S$-$I $\leq z \leq$ S$+$I), the interpolation is not applied. Also in the cases indicated in Fig. 1.3(b) that one data is available inside the interior domain but no data in the exterior domain, or as indicated in Fig. 1.3(c) that the data are available only on one side, the interpolation is not applied.

Fig. 1.4 shows the cases when linear interpolation can be applied. If one data is available on one side of the interior domain and if another one data is available on the other side of the region inside of the exterior range (S$-$E $\leq z \leq$ S$+$E), linear interpolation to the standard depth is made using these two data.

As seen in Figs. 1.5 and 1.6, the interpolation is made using three or four observed data under the conditions (1) at least one observation data occurs in the interior domain, and (2) the two data nearest to the objective standard depth are on either side of the standard depth. When three data are available under the suggested conditions, the parabolic Lagrangian interpolation is applied, and, when four data are available, the cubic interpolation scheme given by Reiniger and Ross (1968) is applied. In all the cases in Figs. 1.5 and 1.6, the observed data in the interior domain are preferred to those in the exterior domain. On one side of the

exterior domain, only the one data nearest to the standard depth is used even if more than two data occur.

In the NODC interpolation schemes or other compatible schemes, interpolation is usually applied to temperature and salinity values, and the density value at the objective standard depth is calculated from the interpolated temperature and salinity values. However, if we apply the interpolation scheme to data taken in areas of complex hydrographic structure such as the Kuroshio/Oyashio mixed water region, pseudo density inversions may generated; namely the interpolated density may be denser than the observed density at a deeper depth, or be lighter than that observed at a shallower layer. We discuss this problem in the next section.

1.3 Generation of pseudo density inversions

In order to check how frequently pseudo density inversions are generated by the NODC interpolation scheme, we use the data for the sea area off Sanriku, the westernmost part of the Kuroshio/Oyashio mixed water region (see Fig. 1.1). The dataset we used was obtained by the Iwate Fisheries Technology Center between 1971-1995. Data obtained before 1970 are also available, however, the low quality of salinity data in this period may cause excessive pseudo density inversions. During the 1970s, the quality of the oceanographic observations conducted by the prefectural fisheries agencies in Japan was much improved, because accurate salinometers (manufactured by Auto-Lab Industries PTY. LTD., Australia) were installed by many of the agencies (Nagata et al., 1999; Oguma et al., 1999). After the 1990s, STD or CTD allowed measurement of data exactly at the standard depths, and few interpolations were needed thereafter. To assess the interpolation scheme for density, only observation points including both temperature and salinity data were used.

As mentioned in the former section, firstly we conducted a range check and inversion check of density (for *in-situ* density) for the observed data in the sea area off Sanriku. Acceptable ranges for range checks are the same as in the NODC quality check scheme. The acceptable values for a density inversion used here are the same as the values used by NODC. The criterion 0.001 which is applied for the depths deeper than 400 m is used to assess the manner of how pseudo density inversions appear. The data of profiles including the density inversion depths are excluded from the interpolation procedure.

For concerning the range checked 25-year (1971-1995) dataset in the sea area off Sanriku obtained by the Iwate Fisheries Technology Center, the total number of observation stations was 9382, however 3555 stations were eliminated from the interpolation procedure after

the density inversion check described above. Additionally, the potential density (σ_θ) was estimated before the assessment of the interpolation scheme. There were 1590 stations which include potential inversions, namely their density profile was statically instable. This may indicate the complexity of the sea area off Sanriku, where water masses of Kuroshio, Oyashio and Tsugaru current intrude into each other. These stations were also eliminated from the interpolation procedure. Finally the 4237 observation stations remaining were used for the assessment of interpolation scheme.

In this section, temperature and salinity were selected as independent values, and were interpolated to assess the objective standard depths following the NODC interpolation scheme noted in the previous section. At the 4237 stations, 30063 temperature data, 30033 salinity data, and 30029 potential density data were obtained as observed data at the standard depths. Temperature and salinity interpolation were conducted respectively at the objective standard depths, at which no observed data occurred. As a result, 12571 temperature data and 12569 salinity data were interpolated, and then 12583 potential density data were calculated using those interpolated data. For all 4237 interpolated stations, a pseudo density inversion check was performed. There are some cases that interpolated temperature or salinity values may lie outside the range between the values directly above and below the observation depths because of the parabolic or cubic interpolation. Following the NODC procedure, the interpolation scheme is replaced by linear interpolation, if the interpolated value lies outside of the range between the values directly above and below the observation depths. Finally, the number of pseudo density inversions were 160, 1.3 % of interpolated density data. It should be noticed that a pseudo density inversion can be created even by the linear interpolation of temperature and salinity, when density differences between upper and lower observed layers are significantly small and the vertical temperature (salinity) gradient is large (Cabbeling effect).

On the basis of these results, we have tried to use temperature and potential density as independent variables, and the interpolation is applied for these two values. The reason is that the accuracy of the temperature measurements is generally better than that of salinity, and that pseudo density inversion may not be generated at least in the linear interpolation of potential density values.

1.4 Interpolation using temperature and potential density values

We interpolated the temperature and potential density for the 25-year dataset as in the interpolation for temperature and salinity detailed in the previous section. The number of

standard depths to be interpolated were 12571 for temperature, 12569 for density, and 12566 for salinity. By parabolic and cubic interpolation, the number of pseudo density inversions was 133, 1.06 % of the objective standard depths. As discussed in the previous section, when the interpolated temperature or density lies outside of the range of the observed values directly above and below depths, the parabolic or cubic interpolation was replaced by a linear interpolation. Consequently, 24 (0.19 %) pseudo inversions were generated. These inversions were generated among the interpolated values, while they were not outside of the range of directly above and below observed values. These cases can occur if the observed data directly above and below are at a long distance and several standard depths occur between them.

Examples of generation of pseudo density inversions are shown in Fig. 1.7. In Fig. 1.7, there is no observation for the 125 m depth, therefore we interpolated from the observed values at 75 m, 100 m and 150 m according to the criterion shown in Table 1.1 and Fig. 1.3. The results of the parabolic interpolation applied for temperature and salinity are shown with white squares. The calculated density value at 125 m depth is denser than the observed density at 150 m depth. When we applied the interpolation for temperature and density, the interpolated density at 125 m also exceeded the observed density at 150 m as shown with white triangles. In this case, the generated density inversion in our scheme is a little larger than that produced by the conventional scheme. This example indicates that the generation of pseudo density inversion is not always suppressed by simply replacing salinity by density, and explains why some pseudo density inversions are newly generated in interpolation applied for temperature and density. After the linear interpolation, potential density profile becomes reasonable as shown in Fig. 1.7 with white circles.

However, Fig. 1.7 indicates another problem. The salinity value calculated from the interpolated temperature and potential density is outside of the values for the directly above and below observed data (termed as outside values). As a result, 457 outside interpolated salinity values, 3.6 % of the interpolated salinity data (12556), remained like the outside salinity value in Fig. 1.7.

For this problem, we discuss the salinity readjustment method in next section.

1.5 Readjustment of salinity values

In the sea area off Sanriku, salinity profile with a zigzag pattern such as in Fig. 1.2 are not unusual. Among 30033 observed standard depth salinity data at 4237 observation stations, 10754 observed salinities (35.8 %) were outside of the range of salinity values of the directly above and below observation depths. Calculated salinity values at the objective

standard depths should not be outside artificially, however, 457 outside salinity values, 3.6 % of interpolated salinity data, were appeared as mentioned in previous section.

For the remaining 457 outside salinity values, two typical examples of outside salinity generations are shown in Tables 1.2 and 1.3 for the parabolic and cubic interpolations, respectively. In the case of Table 1.2, observation was lacking at 30 m depth, and the cubic interpolation was applied for temperature and density, then salinity was calculated from the interpolated temperature and density values. The obtained salinity value lies outside of the range between the salinities at the 25 m and 50 m observation levels. Cubic interpolation was replaced by linear interpolation, however, also in this case the value remained outside of the range. Therefore, we readjusted the salinity value replacing it with the averaged value of those at just above and below observation depths, and then the temperature is re-calculated from the density and salinity values. In the case of Table 1.3, almost the same process was performed for the outside salinity value at 125 m depth calculated by parabolic interpolation.

In these cases, no pseudo density inversion is generated, but the calculated salinity values lie clearly outside of the salinity range between at just upper and lower observed depths. The situation is not improved in these typical cases, even if we use a linear interpolation for temperature and density; the salinity values shift to lower salinity values and become less acceptable. These cases explain why unacceptable interpolated salinity values occur even in the case of linear interpolation of temperature and density. As can be seen in these cases, they can occur when the temperature gradient between the observed depths directly above and below the objective standard depth is large. Actually, these cases would be flagged as "profile holding large gradient (of temperature, etc.)" if we apply the gradient check used by NODC. However, such large temperature gradients are often observed in the Kuroshio/Oyashio mixed water region, and occur as real phenomena, not erroneous one.

The mechanism of the generation of outside salinity values is schematically shown in Fig. 1.8. The isohalines curvature is shown in the T–σ_θ diagrams in the figure. If the temperature difference is large between the directly above and below observed depths, and if the density difference is small, the salinity difference becomes large. The water types at directly above and below depths are shown schematically with black circles A and B, respectively. The linearly interpolated value is given at point C shown with a white circle. The resultant salinity value is lower than the salinity values of both the directly above and below observed depths. The situation is just the same as the Cabbeling effect in the T–S diagram.

Although a zigzag salinity profile such as Fig. 1.2 is not unusual, readjustment of interpolated salinity is needed to be inside of the range of values of both the directly above

and below observed depths as possible.

To readjust the salinity value, firstly linear interpolation for salinity at the objective standard depth, using salinities s_a at the directly above depth and s_b at the below observed depths, while the density value d is kept equal to the result of the linear interpolation. As shown with white triangle D in Fig. 1.8, the readjusted salinity value is s_i and temperature value newly calculated from density and adjusted salinity is t. The obtained temperature lies within the range between the observed temperatures at just above and below the observed levels, as the temperature differences is large and the salinity difference is small.

As a summary of discussion of interpolation scheme, the whole procedure of our interpolation scheme is illustrated in Fig. 1.9. In this study, a gradient check was not conducted to test the interpolation scheme, while it was one of the process of the data quality check.

1.6 Concluding remarks

We designed a reliable interpolation scheme by selecting temperature and potential density values as independent variables, and salinity value as the dependent variable. The scheme is effective for areas of complex hydrographic structure such as the Kuroshio/Oyashio mixed water region. Also, our scheme gives almost the same results as the conventional scheme that selects temperature and salinity as independent variables, for the seas of moderate conditions such as the subtropical regions and Kuroshio Region. MIRC will adopt our scheme to create the MIRC standard depth database of temperature and salinity. In the discussion of this paper, the acceptable density inversion criterion was set as 0.001, which is strict for shallower depth. In real application, we shall use the criterion used by NODC for convenience sake.

References

Antonov, J. I., S. Levitus, T. P. Boyer, M. E. Conkright, T. D. O'Brien and C. Stephans, 1998: *World Ocean Atlas 1998, Vol. 2: temperature of the Pacific Ocean.* NOAA Atlas NESDIS 28, pp.166.

Nagata, Y., S. Iwata, T. Suzuki, S. Oguma, T. Yoshimura, J. Takeuchi and T. Miyake, 1999: Errors in oceanic data-set often generated in data processing and data management – I. Case of the Wakayama Research Center of Agriculture, Forestry and Fisheries–. *Journal of the Japan Society for Marine Surveys and Technology*, **11**, 1-10 (in Japanese).

Oguma S., T. Suzuki, Y. Nagata, H. Watanabe, H. Yamaguchi, and S. Takasugi, 1999:

Errors in oceanic data-set often generated in data processing and data management –II. Case of the Iwate Fisheries Technology Center, and treatment of duplicated data–. *Journal of the Japan Society for Marine Surveys and Technology*, **11**, 11-18 (in Japanese).

Oguma, S., and Y. Nagata, 2002: Skewed occurrence frequency of water temperature in the sea off Sanriku, Japan, and intrusion of the pure Kuroshio Water. *Journal of Oceanography*, **58**, 787-796.

Oguma, S., T. Suzuki and Y. Nagata, 2002: Seasonal variations in the sea off Sanriku Coast, Japan. *Journal of Oceanography*, **58**, 825-835.

Reiniger, R. F., and C. F. Ross, 1968: A method of interpolation with application to oceanographic data. *Deep-Sea Research*, **9**, 185-193.

Talley, L. D., Y. Nagata, M. Fujimura, T. Iwao, T. Kono, D. Inagake, M. Hirai, and K. Okuda, 1995: North Pacific Intermediate Water in the Kuroshio/Oyashio mixed water region. *Journal of Physical Oceanography*, **25**, 475-501.

UNESCO, 1991: *Processing of Oceanographic Station Data.* Imprimerie dews Presses Universitaires de France, United Nations Educational Scientific and Cultural Organization, France, pp.138.

Table 1.1: Acceptable distances (m) for defining the interior and exterior values used in the NODC scheme (Reiniger and Ross scheme) for interpolating observed levels data to standard levels (after Antonov et al., 1998).

Standard Level number	Standard depths (m)	Acceptable distances (m) for interior values	Acceptable distances (m) for exterior values
1	0	5	200
2	10	50	200
3	20	50	200
4	30	50	200
5	50	50	200
6	75	50	200
7	100	50	200
8	125	50	200
9	150	50	200
10	200	50	200
11	250	100	200
12	300	100	200
13	400	100	200
14	500	100	400
15	600	100	400
16	700	100	400
17	800	100	400
18	900	200	400
19	1000	200	400
20	1100	200	400
21	1200	200	400
22	1300	200	1000
23	1400	200	1000
24	1500	200	1000
25	1750	200	1000
26	2000	1000	1000
27	2500	1000	1000
28	3000	1000	1000
29	3500	1000	1000
30	4000	1000	1000
31	4500	1000	1000
32	5000	1000	1000
33	5500	1000	1000

Table 1.2: Typical example of the generation of unacceptable salinity values at the objective standard depth. Interpolation was conducted at 30 m depth, and its results are shown in *italics*. Results of the cubic interpolation are shown in left columns (2nd-4th columns), those of the linear interpolation in middle columns (5th-7th columns), and those of the salinity readjustment in right columns (8th-10th columns). Observation data in the case below were obtained on September 24, 1971 at 142°59′E, 39°00′N.

	cubic interpolation			linear interpolation			salinity adjustment		
depth (m)	temp.	density	salinity	temp.	density	salinity	temp.	density	salinity
10	17.70	23.865	33.065						
25	17.20	24.173	33.311	17.20	24.173	33.311			33.111
30	*15.37*	*24.501*	*33.181*	*14.47*	*24.633*	*33.104*	*15.18*	*24.633*	*33.298*
50	3.57	26.434	33.247	3.57	26.434	33.247			33.247
70	2.43	26.582	33.307						

Table 1.3: Same as in Table 2, except that an observation was not conducted at 20 m depth and that the parabolic interpolation was applied first. Observation data in the case below were obtained on November 7, 1985 at 142°4′E, 39°15′N.

	parabolic interpolation			linear interpolation			salinity adjustment		
depth (m)	temp.	density	salinity	temp.	density	salinity	temp.	density	salinity
75	16.80	24.686	33.821						
100	16.43	24.808	33.856	16.43		33.856			33.856
125	*13.31*	*25.399*	*33.749*	*11.93*	*25.634*	*33.712*	*12.47*	*25.634*	*33.844*
150	7.43	26.460	33.831	7.43		33.831			33.831

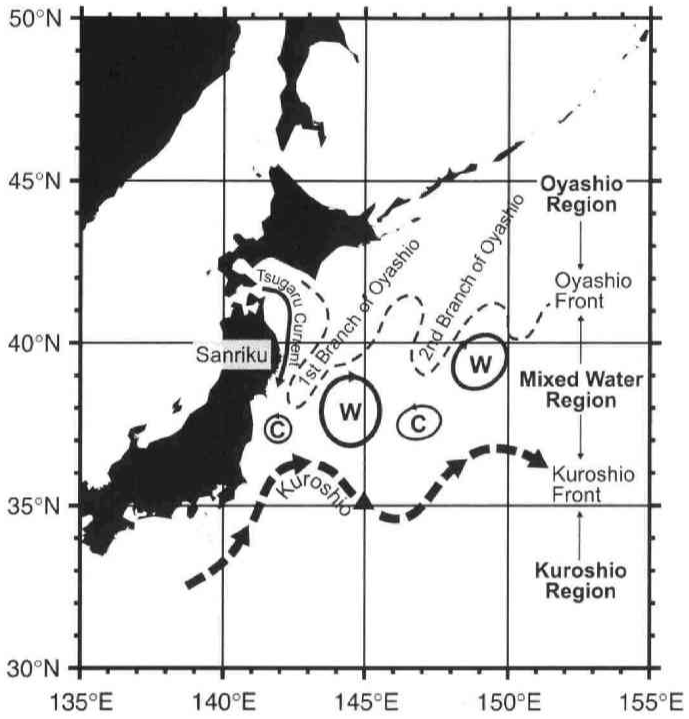

Figure 1.1: Schematic view of the Mixed Water Region between the Oyashio and Kuroshio fronts. W indicates the warm-core ring and C the cold-core ring.

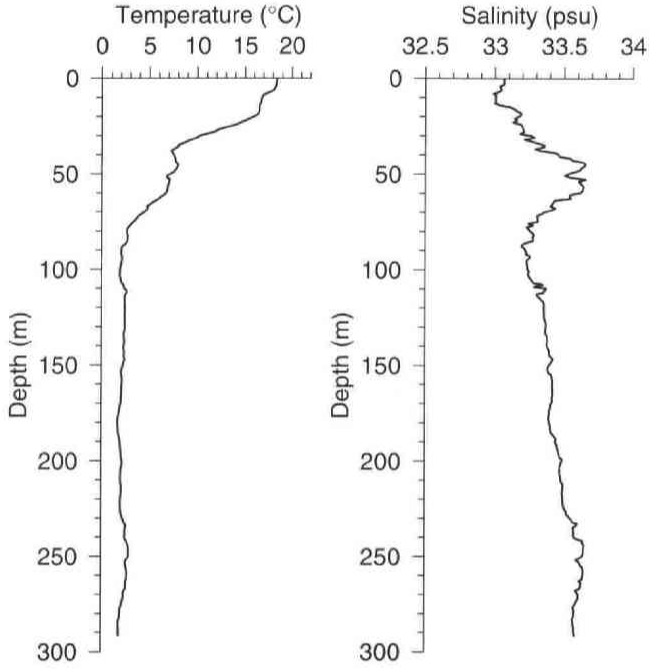

Figure 1.2: CTD profile at 143°10.95′E, 39°31.85′N on September 1, 1993, obtained by Iwate Fisheries Technology Center.

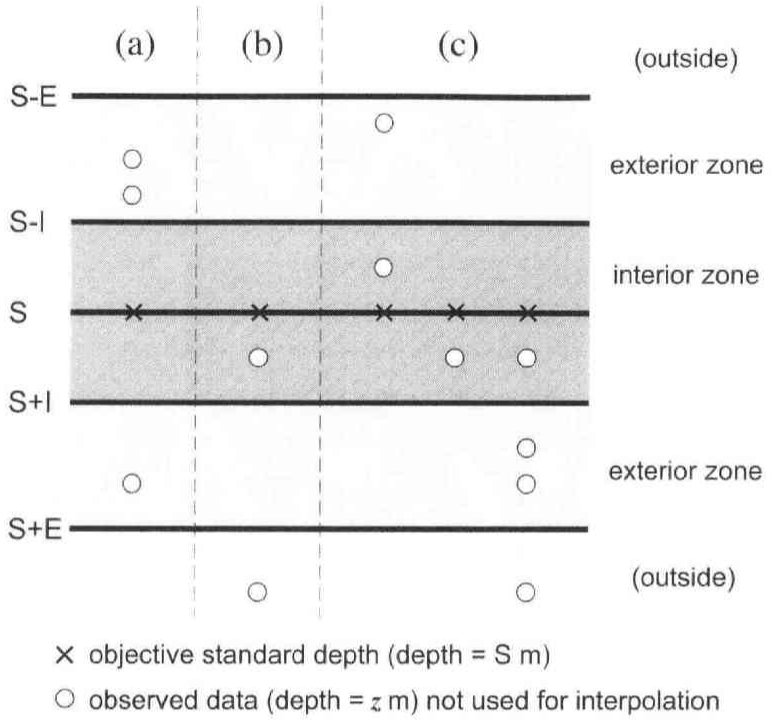

Figure 1.3: The cases in which no interpolation is made even if some data are available within the exterior domain. (a) is the case that no data is available in the interior domain, (b) is that one data is available on one side of the interior domain, but no data is available inside the exterior domain of the other side, and (c) is that data are available only on one side. White circles indicate the observed data which are not used for the interpolation procedure. S denotes the objective standard depth, I and E denote the interior and the exterior acceptable distances, respectively.

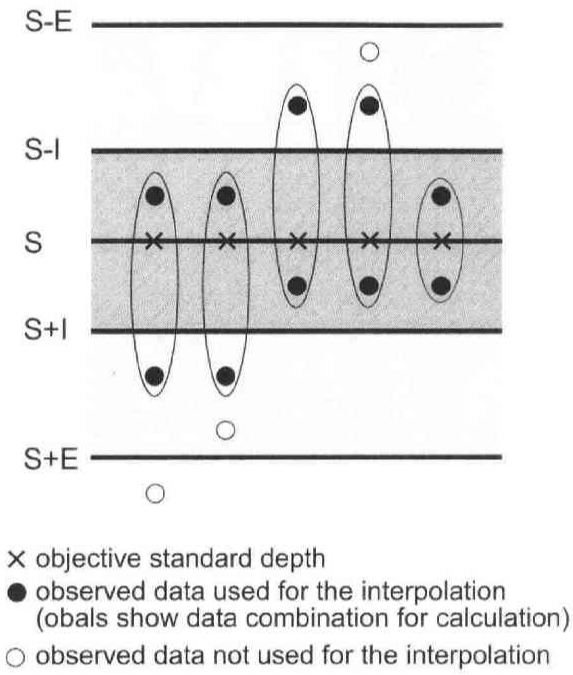

Figure 1.4: The cases in which linear interpolation is made using two values. Black circles indicate the observed data to be used in interpolation procedure. See Fig. 1.3 for other symbols.

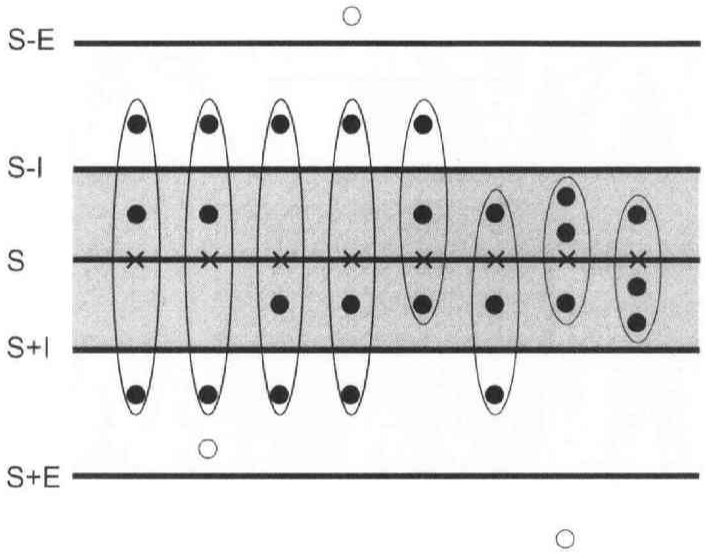

Figure 1.5: The cases in which parabolic or Lagrangian interpolation is made using three values, in the same manner as Fig. 1.4.

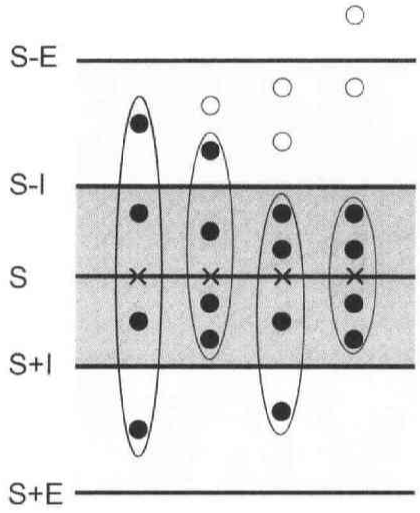

Figure 1.6: The cases in which cubic interpolation is made using four values, in the same manner as Fig. 1.4.

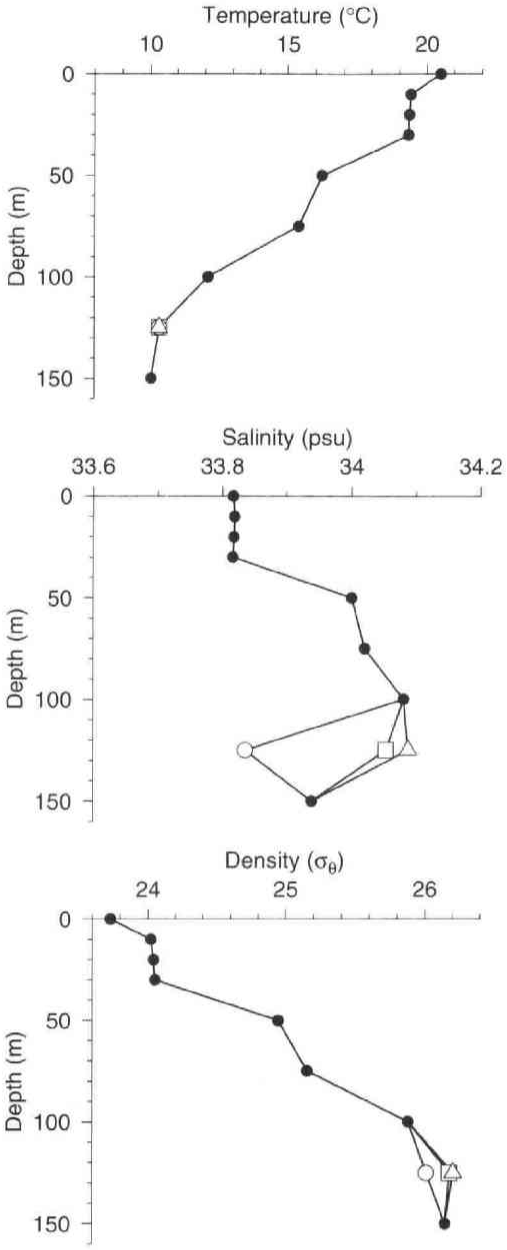

Figure 1.7: An example of the generation of a pseudo density inversion at the 125 m standard depth. The observed values are shown with black circles. The results of the parabolic interpolation applied for temperature and salinity are shown with white squares, and for temperature and density are shown with white triangles. White circles indicate data based on linear interpolation. Observation data in this case were obtained on September 5, 1986 at 142°4′E, 39°15′N.

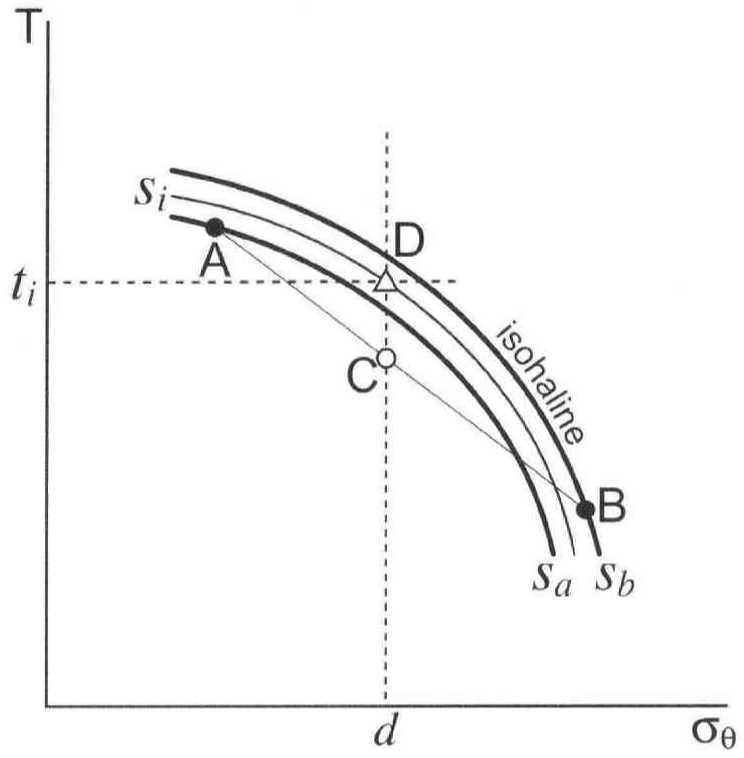

Figure 1.8: Schematic explanation of the generation of an unacceptable salinity value in the procedure of the linear interpolation of temperature and density. Curvatures in the T–σ_θ plane indicate isohalines. The observed temperature and density values at the depths directly above and below are shown with A and B in the T–σ_θ plane. Salinity values of A and B are s_a and s_b. The result of the linear interpolation of temperature and potential density is denoted with C (white circle), and its density value is denoted with d. The finally readjusted value s_i in our scheme is denoted with D (white triangle), and newly calculated temperature is t_i.

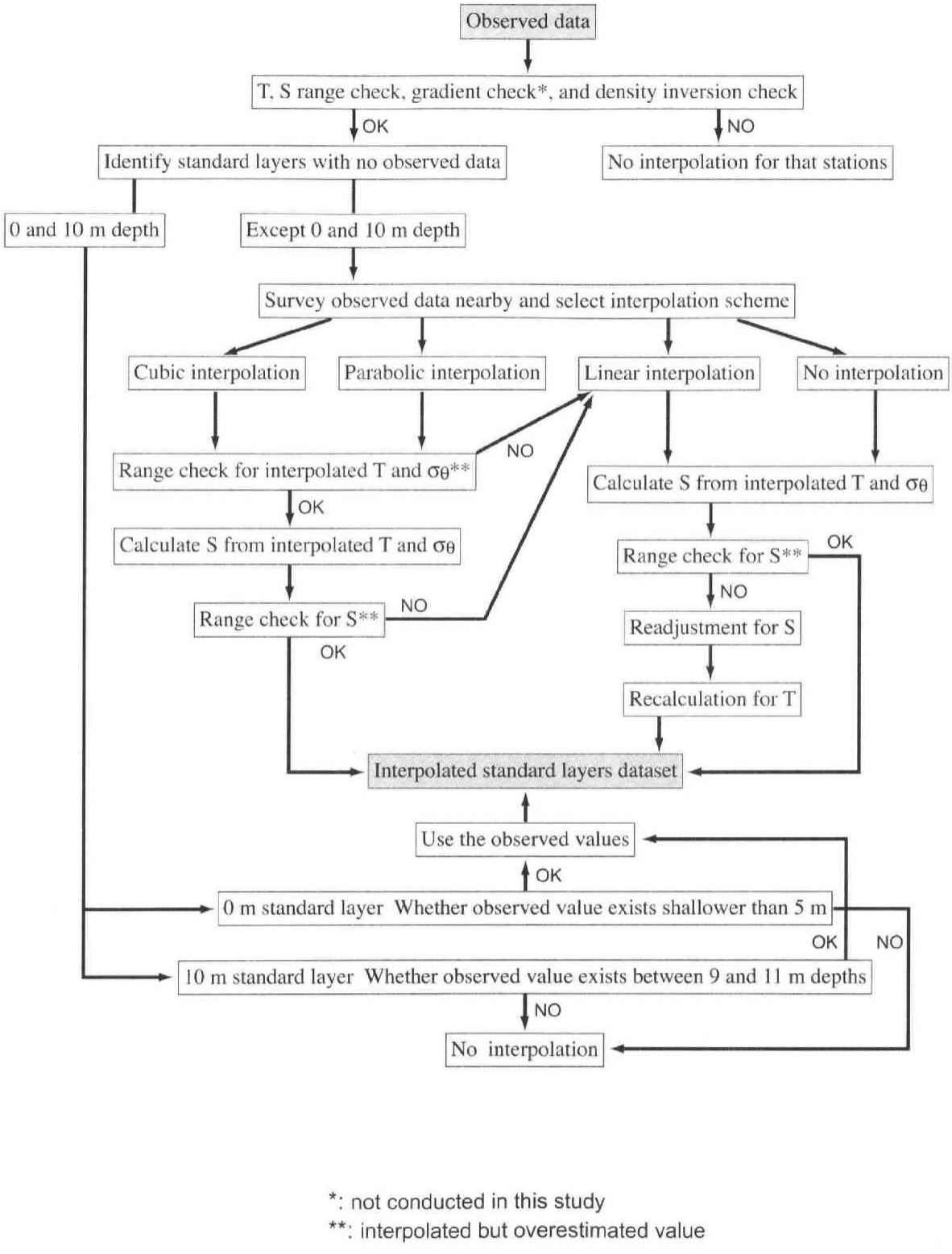

Figure 1.9: Flow diagram of the MIRC interpolation scheme. Asterisk (∗) indicates that the gradient check was not conducted in this study. Double asterisks (∗∗) mean the interpolated value which is overestimated compared to the values at just above and below layers.

2 Skewed water temperature occurrence frequency in the sea off Sanriku, Japan, and intrusion of the pure Kuroshio Water

2.1 Introduction

Checks on the range of values of temperature, salinity and their vertical gradients, and a density inversion check are very effective techniques for controlling the quality of oceanic data, and they are used by almost all data management organizations throughout the world. For example, the US National Oceanographic Data Center (NODC) conducted these checks prior to compiling World Ocean Dataset 1998 (WOD98), and the permissible ranges adopted are widely used. The Marine Information Research Center (MIRC) of the Japan Hydrographic Association also used these permissible ranges when compiling its MIRC Ocean Dataset 2001 (MODS2001).

NODC divided the world oceans into 9 sub-domains to set the permissible ranges; the whole North Pacific Ocean to the north of 10°N is considered as one sub-domain including marginal seas such as the Bering Sea and the Okhotsk Sea. Therefore, the permissible ranges of WOD98 are too wide if we seek to confine our attention to some limited area. We selected the sea off the Sanriku coast, Japan, as a test area, and analyzed the data obtained by the Iwate Fisheries Technology Center for the period from 1971 to 1995. The sea off the Sanriku is located at the westernmost portion of the Mixed Water Region between the Kuroshio and Oyashio Fronts, where many warm and cold eddies exist and where the oceanic status is most complicated in the vicinity of Japan (e.g. Kawai, 1972). It is demonstrated that the WOD98 ranges are too wide in this complicated oceanic area, and that the occurrence frequency of water temperature is very skewed so much so that the usual three sigma criterion for data quality control is hardly applicable.

2.2 Data used

Since 1963, the Iwate Fisheries Technology Center has maintained routine observation lines, called the Kurosaki Line (KR), Todogasaki Line (TD), Osaki Line (OZ) and Tsubakishima Line (TS) from north to south, as shown in Fig. 2.1. The coastal observation points, which are shown as black dots in Fig. 2.1, were occupied monthly except for the two points furthest offshore, where observations were usually not conducted in the winter season (December–March). The offshore observation points are occupied several times a year, as shown in Fig. 2.2. The observations were usually performed down to 300 m depth; data from

levels deeper than 300 m are very sparse. MIRC conducted quality checks on the database of the Japan Oceanographic Data Center (JODC), including the data taken by the Iwate Fisheries Technology Center, during the compilation of MODS2001. The quality checks used are ship speed check, range checks on temperature and salinity and their vertical gradient, and density inversion, the permissible ranges used being the same as those adopted by NODC during the compilation of WOD98 (Ocean Climate Laboratory, 1998; Marine Information Research Center, 2001). Although only the data obtained before 1993 are stored in MODS2001, the data taken by the Iwate Fisheries Technology Center in 1994 and 1995 are processed in the same manner, and are used in this analysis.

The quality of the observations improved over time, especially for salinity values after 1971, when the accurate Auto-Lab Co. salinometer was introduced (Oguma et al., 1999). We use the data taken in the period from 1971 to 1995 in the present analysis.

The Neil-Brown CTD was introduced in 1990, and the observational data obtained exactly at each standard depth were reported thereafter. The data reported before 1989 are for the observation depths, and we need to interpolate to obtain the values at each standard depth. The MIRC is preparing a standard depth database by applying a unified interpolation scheme; we have completed the interpolation for the data of the Iwate Fisheries Technology Center obtained before 1995. This interpolated standard depth dataset has also been used for the statistical analysis presented here.

2.3 Occurrence frequency distributions of temperature and salinity in the sea off Sanriku

All of the temperature and salinity values observed during routine observations of the Iwate Fisheries Technology Center in the period from 1971 to 1995 are plotted against depth in the left and right panels of Fig. 2.3, respectively. As the observed values are reported exactly for standard depths in recent observations using CTD, the data points tend to be densely distributed at the standard depths. The stepped lines in Fig. 2.3 indicate the WOD98 range. The data points lie well inside the WOD98 ranges, and it is clear that WOD98 ranges are too wide to applied in the limited area concerned here, especially in the very complicated areas like the sea off Sanriku Coast.

By using the interpolated standard depth dataset, mean value (m) and standard deviation (σ) are calculated for each standard depth, and m and $m\pm3\sigma$ are plotted in each panel of Fig. 2.3 as white triangles and white circles, respectively. The $m\pm3\sigma$ curves do not give lower and upper boundaries of the data distributions both for temperature and salinity.

No temperature data point appears below 0°C for all depths, while the $m-3\sigma$ curve runs below -3°C (lower limit of WOD98 permissible range) for depths shallower than 250 m. On the other hand, a significant number of the data points lie in the domain higher than $m+3\sigma$ below 150 m depth. A similar tendency can also be seen in the salinity data.

NODC applied 3σ criterion in the statistical analysis used to create the World Ocean Atlas 1998: *i.e.* m and σ are calculated from the raw data, and values greater than $m+3\sigma$ subsequently, or less than $m-3\sigma$ are considered to be erroneous or exceptional, and are excluded from the dataset. m and σ are recalculated by the new dataset. This procedure is repeated until m and σ converge to fixed values. This procedure would be reasonable in common cases, because, if the occurrence frequency distribution of the data can be approximated as normal or Gaussian, about 99.7% of the data lie in the $m\pm3\sigma$ range. However, this criterion would not be justified in the sea off Sanriku because a considerable number of data values lie outside the $m+3\sigma$ range, as shown in Fig. 2.3.

Temperature and salinity occurrence frequency distributions for each standard depth, which were created by using the interpolated standard depth dataset, are shown in Figs. 2.4 and 2.5, respectively. The distributions at depths shallower than 100 m are fairly symmetrical, and the 3σ criterion appears to be applicable. However, the distribution patterns at depths deeper than 200 m are very skewed, and the 3σ criterion appears not to be applicable. The distribution at 150 m depth seems to have an intermediate nature.

We calculated the mean, standard deviation, skewness and kurtosis for each standard depth. Values are shown in each panel of Figs. 2.4 and 2.5. Skewness and kurtosis are defined as:

$$\text{skewness} : \frac{\sum_{i=1}^{n}(x_i - \bar{x})^3}{(n-1)\sigma^3}, \quad \text{kurtosis} : \frac{\sum_{i=1}^{n}(x_i - \bar{x})^4}{(n-1)\sigma^4},$$

where x_i is the value of the i-th data point and n the number of data. For a normal distribution, skewness is zero and kurtosis is 3. We use excess kurtosis,

$$\frac{\sum_{i=1}^{n}(x_i - \bar{x})^4}{(n-1)\sigma^4} - 3,$$

in this paper. The mean temperature and standard variation decrease with depth, while skewness tends to increases with depth. The skewness is very small at the depths shallower than 100 m, it increases rapidly between 100 m and 200 m, and then it increases gradually to a depth of 300 m (below 400 m, the data are too sparse to draw any firm conclusion). The variation of kurtosis shows a similar tendency to that of skewness. Mean salinity shows a weak minimum near 250 m, indicating a shallow minimum salinity layer in coastal region of this area. The standard deviation of salinity distribution decreases monotonically, just as the temperature distribution. The skewness and kurtosis are small at depths shallower than 100

m, and large at depths deeper than 200 m; they tend to increase significantly with depth up to at least 300 m. The distribution patterns deeper than 200 m are quite different from those shallower than 150 m, both for temperature and salinity, and the most skewed distributions are seen at 300 m in the present analysis.

The distribution pattern of temperature at 300 m depth is reproduced in Fig. 2.6. Below the abscissa in Fig. 2.6, two kinds of standard deviation scale are shown: the upper scale is based on the mean m and standard deviation σ calculated directly from the distribution shown, and the lower the converged mean m' and standard deviation σ' resulting from the iterative procedure (for this typical case, eight iterations were needed to obtain the converged standard deviation). The maximum temperature found is 15.71°C, which corresponds to $m+5.8\sigma$ and $m'+8.9\sigma'$, respectively. (We do not use the converged values except for the present discussion.)

The position of the isotherms from 13°C to 15°C at 200 m depth roughly corresponds to the position of the current axis of the Kuroshio Extension to the east of Honshu (e.g. Nagata, 1970). The origin of the warm water, which is warmer than 15°C at 300 m depth, should be sought in the Kuroshio Extension or the subtropical regions. We have investigated the oceanic conditions in which such pure Kuroshio Water can be brought into the sea off Sanriku and we discuss this in the next section.

The sharp cut-off of the distribution at the colder side of Fig. 2.6 can be explained by the fact that water temperature cannot be below the freezing point. No sea ice formation occurs in the sea off Sanriku, and 0°C becomes the minimum temperature in the sea off Sanriku.

2.4 Intrusion of the pure Kuroshio Water into the sea off Sanriku

We surveyed the observation points and dates that a temperature higher than $m+5\sigma$ (14.14°C) was recorded during the analyzed 25-year period using the standard depth dataset. These are listed in Table 2.1, which shows that such a high temperature was found only in 1972 and 1979. However, it should be noted that only four of sixteen cases were found on coastal observation lines, with a station number of 8 or less, and that the four cases were found at the outermost two stations. As the observations on offshore lines are not frequent, as shown in Fig. 2.2, many more cases might have been found if the offshore lines had been occupied monthly. As discussed above, the highest temperature found at 300 m depth is 15.71°C. The maximum temperature value decreases to 15.13°C if we confine our attention to the data obtained at coastal observation stations only, and decreases to 12.30°C if we

confine ourselves to the data obtained in the five coastal stations along each observation line. The high temperature water would be found frequently if the observation lines were extended further eastward.

Also, if observations had been restricted to depths shallower than 300 m, the high temperature water would also have been missed. We surveyed the 250 m depth data similarly, and listed the cases when temperatures occurred higher than $m+4\sigma$ (14.48°C). However, almost all cases are related to the events shown in Table 2.1, except the case found in November 1994, when the maximum temperature found was 13.9°C at St. TS8 (see Fig. 2.1).

Hanawa and Mitsudera (1987) analyzed the data obtained by the Iwate Fisheries Technology Center in the period from 1977 to 1981, and published a conventional classification of the water masses in the sea off Sanriku. Typical Kuroshio Water would have salinity higher than 34.2 psu and density between 24.0 and 26.7 σ_t. All of the high temperature waters listed in Table 2.1 lie well inside this domain, which suggests that these high temperature waters originated in the Kuroshio, and that the water had not been modified by any influence from the Oyashio Water or other surrounding waters.

2.4.1 Case found in 1972

In 1972, the offshore observation lines were occupied four times (May, August, September and October) as shown in Fig. 2.2. The highest temperature at 300 m depth (15.71°C) in our analysis was found at TS10 in May 1972. The temperature cross-sections along four observation lines in May and August 1972 are shown in Figs. 2.7 and 2.8, respectively. The warm water mass can be recognized along the long Kurosaki and Tsubakishima Lines in both figures. The temperature sections along the short Todogasaki and Osaki Lines, also indicate that the warm water mass exists offshore. The warm water mass has a thick thermostad between 15°C and 16°C, especially along the Tsubakishima Line in May and along the Kurosaki Line in August. This structure is a typical of the warm-core rings, which persisted over one winter season after separation from the Kuroshio Extension (Tomosada, 1978). Tomosada (1978) pointed out that this warm-core ring was generated in February-March 1972, but this is hard to confirm due to lack of data in this winter season.

The center of the warm-core ring appears to be located near the southern boundary of the area under consideration in May, but near the northern boundary in August, judging from the position of the thermostad. However, the movement of the warm-core ring cannot be clarified since the observations in June and July were made only along the coastal observation lines. No signature of the warm-core ring was observed in July, but it was recognized at the

offshore end of the Todogasaki Line in June. As can be seen in Table 2.1, the warm-core ring stayed in the area under consideration during September and October 1972. Relatively warm water was recognized along coastal observation lines, but it was hard to identify as the warm-core ring from limited data.

Tomosada (1978) investigated the structure of this warm-core ring by using the detailed observations conducted in the period from July 25 to September 1, 1972. The horizontal temperature distribution at 200 m depth is cited in Fig. 2.9. The large warm-core ring is clearly seen in this figure, and the western edge of the ring approached very near to the coast.

The relatively warm water found in 1994 mentioned above can be also attributable to a warm-core ring which approached very near to the coast.

2.4.2 Case found in 1979

Water warmer than 15°C at 300 m depth was also found in July, August, and October in 1979 (Table 2.1). The temperature cross-sections along the four observation lines of the Iwate Fisheries Technology Center in July 1979 are shown in Fig. 2.10. The warm water domain is clearly shown in the Kurosaki and Tsubakishima Lines, and the existence of the warm water domain is also shown at the eastern edge of the cross-sections along other short observation lines. Mizuno and Akiyama (1980) investigated the evolution of the oceanic structure off Sanriku during February to September, 1979. The large warm-core ring, centered at 40°N, 144°E, was observed in February-March. This warm core-ring had a clear thermostad at its central part from the surface to a depth of 300 m, and the water temperature of the thermostad was warmer than the 14°C isotherm. The maximum temperature at 300 m depth exceeds 15°C. The warm-core ring moved southward, and its southern edge touched the ridge of the large Kuroshio meander, which had developed and extended northward between 143°E and 144°E. The warm-core ring was then absorbed into the Kuroshio Extension. The temperature distribution at 100 m depth and the surface current field, and the cross-sectional temperature distribution along 144°E in the period from July 2 to July 16, 1979 are plotted in the left and right panels of Fig. 2.11, respectively. Mizuno and Akiyama (1980) traced the thermostad between 13°C and 14°C isotherms as the indicator of the absorbed warm-core ring. They concluded that the absorbed warm-core ring continued to move southward, increasing its depth, and that it was located around 37°30′N and between 300 m and 600 m depth in the first half of July 1979. The thermostad can also be seen in September at about the same depth as in July.

The oceanic structure shown in the horizontal temperature distribution (Fig. 2.11), and multiple current zones appeared to exist in the eastward flowing region of the meander. In the cross-sections shown in Fig. 2.10, the eastward declining isotherms of 4°C and 6°C (also of 8°C) are commonly seen in each cross-section. The current associated with this portion was flowing northward along the coast, crossing all of the four cross-sections, and appeared to form the northern branch current in the eastward flowing region in Fig. 2.11. On the other hand, the warm water of temperature greater than 14°C, is found to the depth of 300 m in the Tsubakishima Line, but is found at depths shallower than 50 m in the Kurosaki Line. If the current axis of the Kuroshio can be approximated by the isotherm of about 14°C at 200 m depth, the main part of the Kuroshio did not reach the Kurosaki Line, turning eastward at around 39°N, as shown in Fig. 2.11.

In the case of July 1979, the Kuroshio flowed along the coast abnormally northward, and the pure Kuroshio Water was carried into the sea off Sanriku, at least crossing southern observation line (Tsubakishima Line). The relatively high temperature water found at the Kurosaki Line may be considered to be brought by the Kuroshio extending abnormally northward.

Though the warm water of temperature higher than 15°C at 300 m depth is found very seldom in the sea off Sanriku, it could be a real phenomenon, as seen in the 1972 and 1979 cases.

2.5 Concluding remarks

We have analyzed the occurrence frequency distributions in the sea off Sanriku, Japan, and found that the distribution patterns deeper than 200 m are quite different from those shallower than 150 m. Seasonal short period variations are predominant in the surface layers, and the distributions are widely spread, as shown in Fig. 2.4. Moreover, the structures of the Tsugaru Current and the First Branch of the Oyashio have shallow structure and are confined in the layer shallower than 200 m (these characteristics of the sea off Sanriku will be discussed in separate papers). This large variability would make the distributions in the shallower layers symmetric. Therefore, the distributions may be considered quasi-normal, and the data outside the range $m \pm 3\sigma$ would be assumed to be erroneous (the 3σ criterion).

However, the distributions below 200 m depth are very skewed, and sometimes higher temperature values exceeding $m+5\sigma$ are observed at 300 m depth. If such high temperature values are real, the 3σ criterion should not be applied. We have surveyed the oceanic conditions under which such abnormally high temperatures were observed. The abnormally

high temperature (and high salinity) water was shown to be the pure Kuroshio Water introduced into the region due to some special conditions, such as the abnormal approach of large warm-core ring to the Sanriku Coast or an abnormal northward extension of the Kuroshio along the coast. It happened very seldom (only twice in the 25-year period analyzed), but the abnormally high temperature observed is a real one. We need to design specific quality control techniques for the area where the temperature and salinity distributions are skewed. We are trying to conduct an area classification of the western North Pacific Ocean based on skewness of frequency distributions, in order to design a high-level data quality control scheme.

References

Hanawa, K., and H. Mitsudera (1987): Variation of water system distribution in the Sanriku coastal area. *J. Oceanogr. Soc. Japan*, 42, 435-446.

Kawai, H. (1972): Hydrography of the Kuroshio Extension. In *Kuroshio, Its Physical Aspect*, edited by K. Yoshida and H. Stommel, 235-352.

Marine Information Research Center (2001): *MIRC Ocean Dataset 2001 Documentation.* Marine Information Research Center, Japan Hydrographic Association, 169pp (in Japanese).

Mizuno, K. and M. Akiyama (1980): Hydrographic study of the Tohoku area using satellite IR imagery. *Sora to Umi*, 2, 47-55 (in Japanese).

Nagata, Y. (1970): Detailed temperature cross section of the cold-water belt along the northern edge of the Kuroshio. *Jour. Mar. Res.*, 28, 1-14.

Ocean Climate Laboratory, NODC (1998): *World Ocean Database 1998 Documentation and Quality Control Ver.2.0.* National Oceanographic Data Center Internal Report 14, Ocean Climate Laboratory, National Oceanographic Data Center, Silver Spring, MD, 113pp.

Oguma, S., T. Suzuki and Y. Nagata (1999): Errors in oceanic dataset often generated in data processing and in data a management - II. Case of the Iwate Fisheries Technology Center, and treatment of duplicated data. *Jour. Japan Soc. Mar. Surv. Tech.*, 11 (2), 11-18 (in Japanese with English captions).

Tomosada, A. (1978): A large warm eddy detached from the Kuroshio east of Japan. *Bull. Tokai. Fish. Res. Lab.*, 94, 59-103.

Table 2.1: Observation points and dates that temperatures exceeding $m+5\sigma$ (14.14°C) were found in the period 1971–1995. Dates, stations, their locations, temperature (°C), salinity (psu) and density (σ_t) are given from left to right. KR, TD and TS in the station name indicate Kurosaki Line, Todogasaki Line and Tsubakishima Line, respectively. The number attached indicates the station number counted from the coast offshore along each observation line. A number greater than 8 indicates that the station is taken on the offshore line. TS7-8 indicates that this observation was conducted at the mid-point between TS7 and TS8 (see Fig. 2.1 for the locations of observation lines and observation points).

Year	Month	Day	St.name	lon.	lat	Temperature	Salinity	Density
1972	5	17	TS7-8	143.000	39.000	14.966	34.655	25.820
	5	17	TS10	144.033	39.000	15.709	34.737	25.725
	5	18	TS11	144.500	38.967	15.053	34.659	25.805
	6	20	TD7	143.167	39.550	14.970	34.650	25.815
	8	20	KR9	144.033	40.000	15.590	34.740	25.753
	8	20	KR8	143.500	40.033	15.382	34.704	25.770
	9	26	TS9	143.500	39.000	14.408	34.591	25.886
	9	27	TS10	144.000	38.983	15.384	34.729	25.789
	10	18	TS9	143.500	38.983	15.301	34.606	25.711
	10	18	TS10	144.000	38.983	14.422	34.473	25.792
1979	7	7	TS10	144.000	39.000	15.260	34.649	25.753
	7	7	TS11	144.500	39.000	14.143	34.551	25.910
	8	2	TS8	143.250	38.933	14.591	34.616	25.868
	10	7	TS14	145.800	39.050	14.263	34.587	25.913
	10	9	KR12	145.500	40.000	14.879	34.638	25.825
	10	9	KR11	145.000	40.000	14.441	34.619	25.901

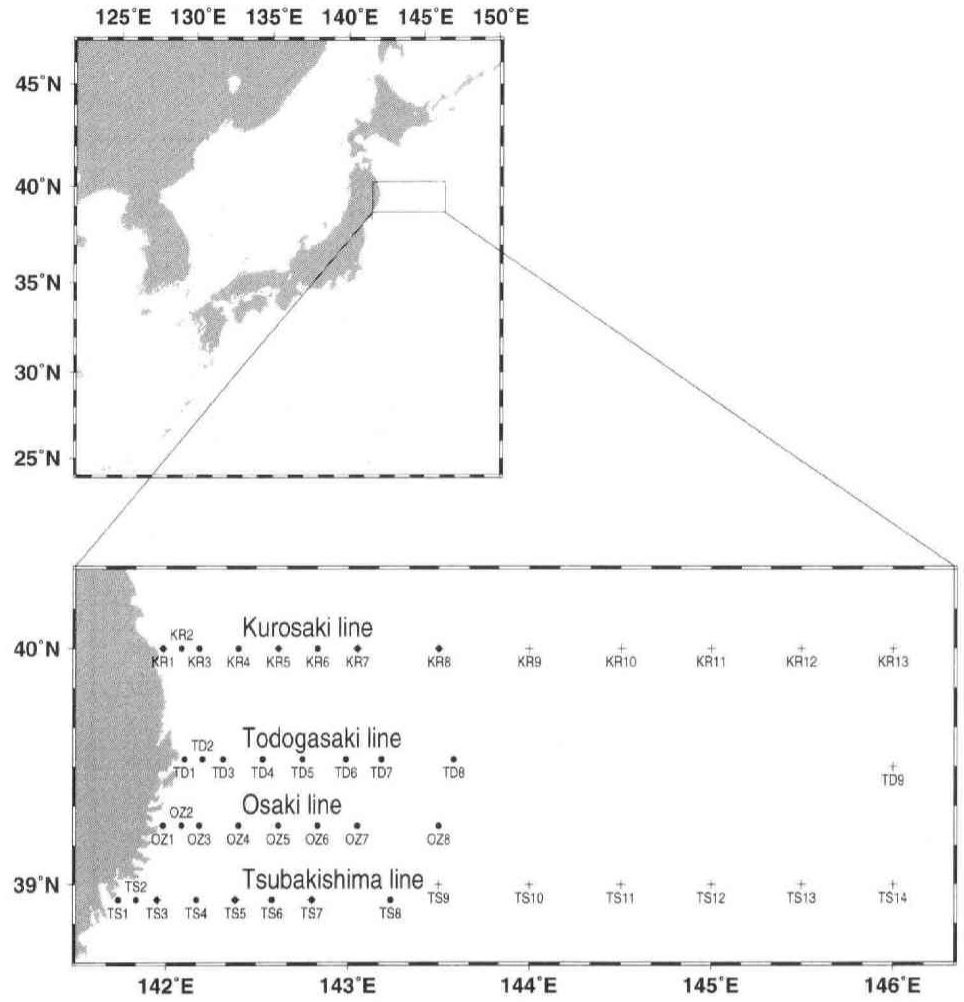

Figure 2.1: Routine observation stations occupied by the Iwate Fisheries Technology Center: bullets indicate coastal observation stations where observation is done once a month (observations at easternmost station of each line are usually not conducted in winter season from December to March), and plus marks indicate offshore observation stations where the observation is done several times per year (see Fig. 2.2). Observation lines are called as Kurosaki Line (KR), Todogasaki Line (TD), Osaki Line (OZ) and Tsubakishima Line (TS) from north to south. For convenience, station number is attached from coast to offshore: 1 through 8 are the coastal observation points, and 9 through 14 are offshore observation points.

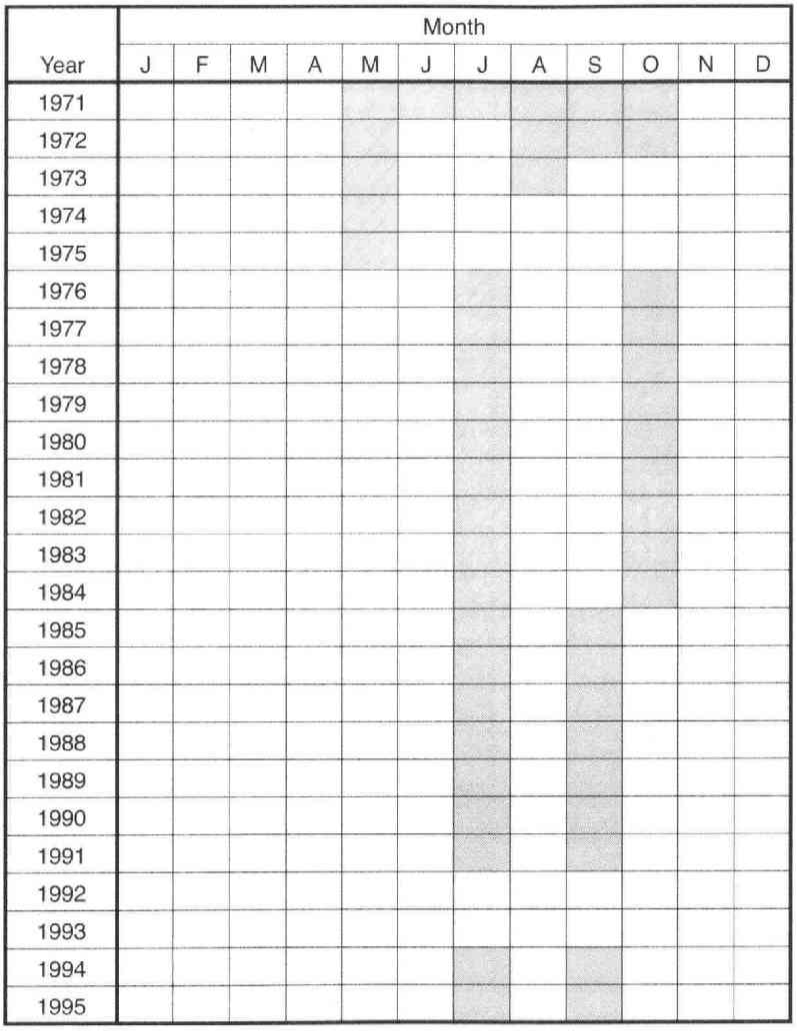

Figure 2.2: Observation months of the offshore observation lines in the period 1971–1995.

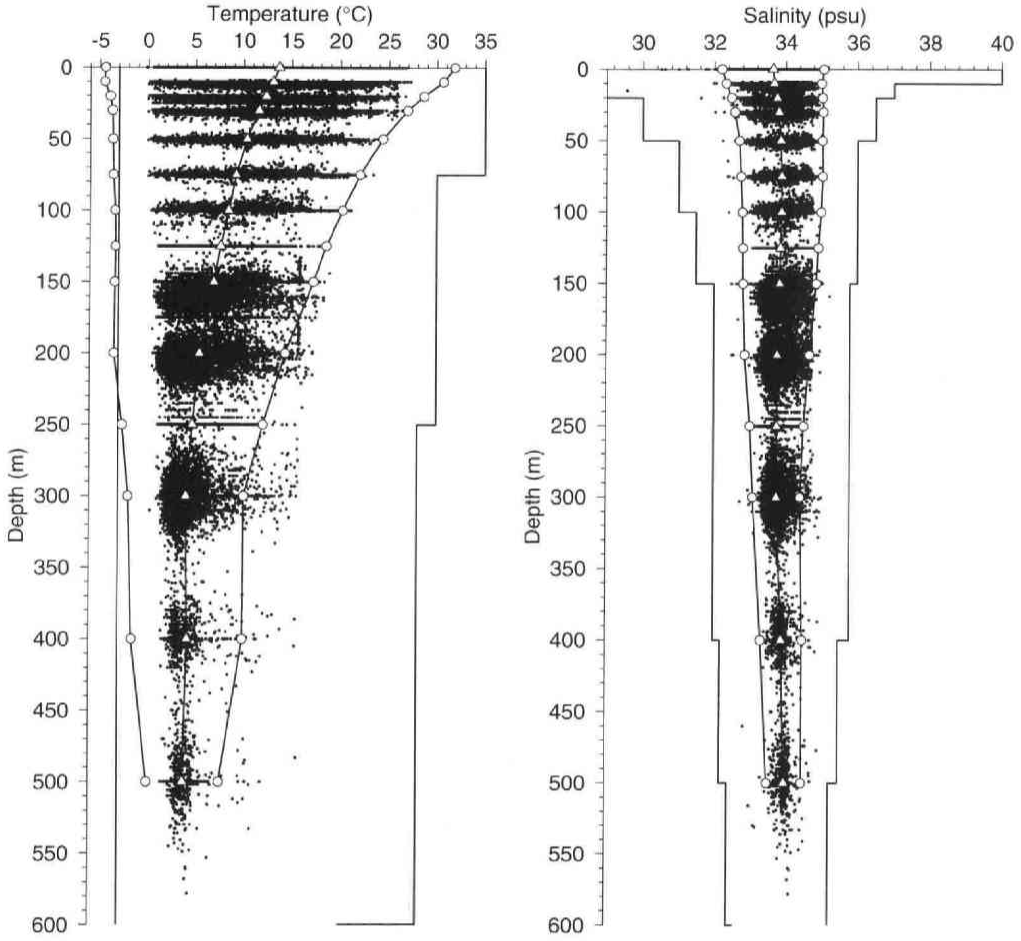

Figure 2.3: Distributions of observed temperature (left) and salinity (right) measured along the routine lines (see Fig. 2.1) by the Iwate Fisheries Technology Center in the period 1971–1995. The stepwise lines drawn in both figures indicate the ranges of normal or permissible values (Ocean Climate Laboratory, 1998). White triangles and white circles indicate mean (m) and mean $\pm$ three times standard deviation ($m \pm 3\sigma$), which were calculated using the interpolated standard depth dataset.

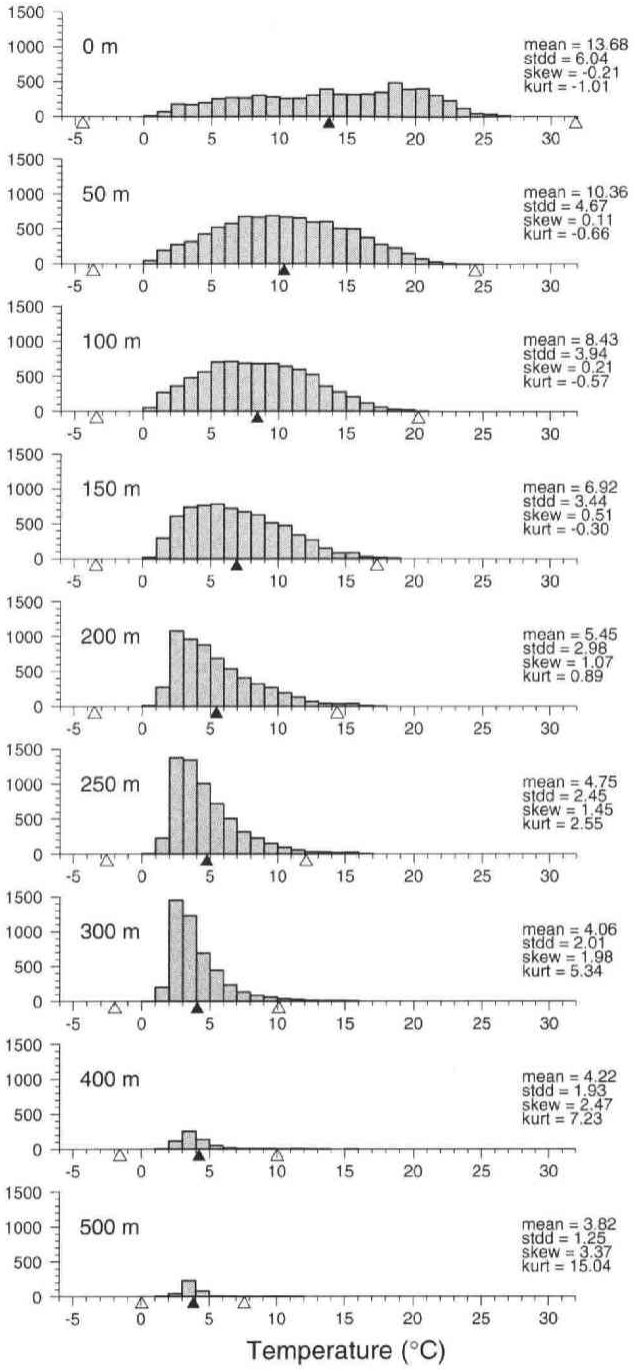

Figure 2.4: Variation of the occurrence frequency distribution of temperature with depth. The interpolated standard depth dataset was used. Black triangles and white triangles attached to abscissa indicate m and $m \pm 3\sigma$, respectively. Values of mean, standard deviation, skewness, and kurtosis are shown for each standard depth.

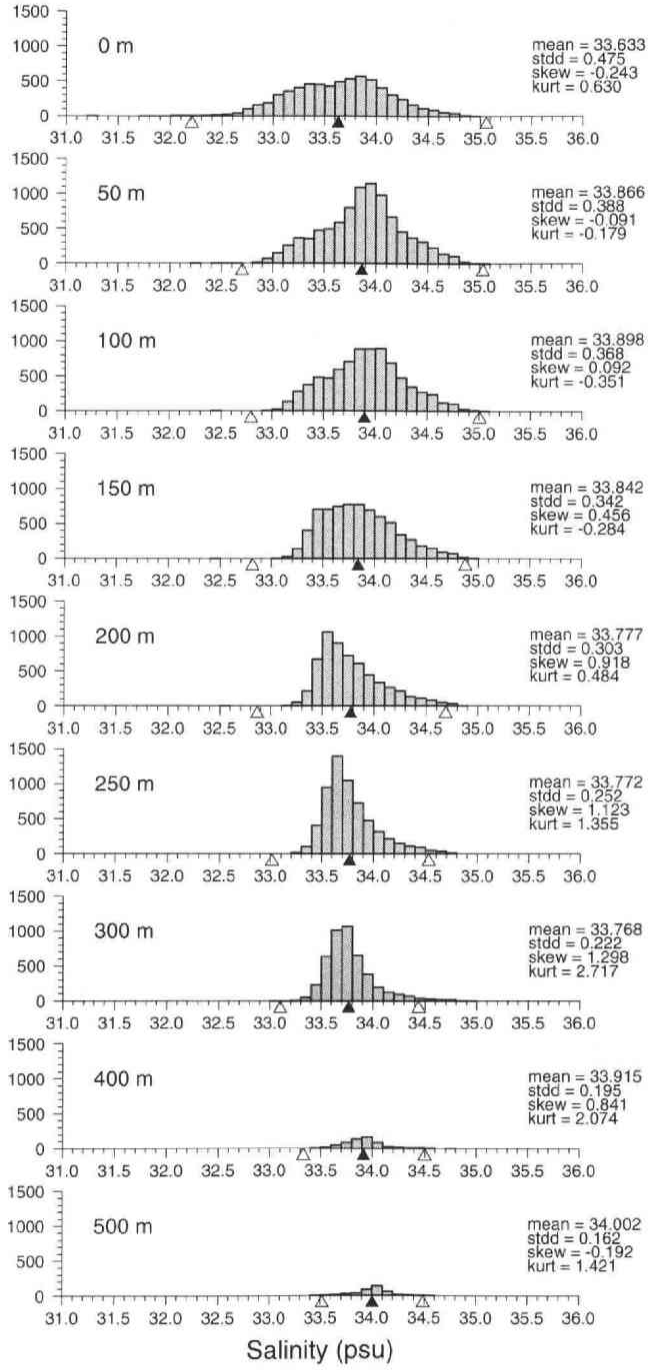

Figure 2.5: As Fig. 2.4, except for frequency distribution for salinity.

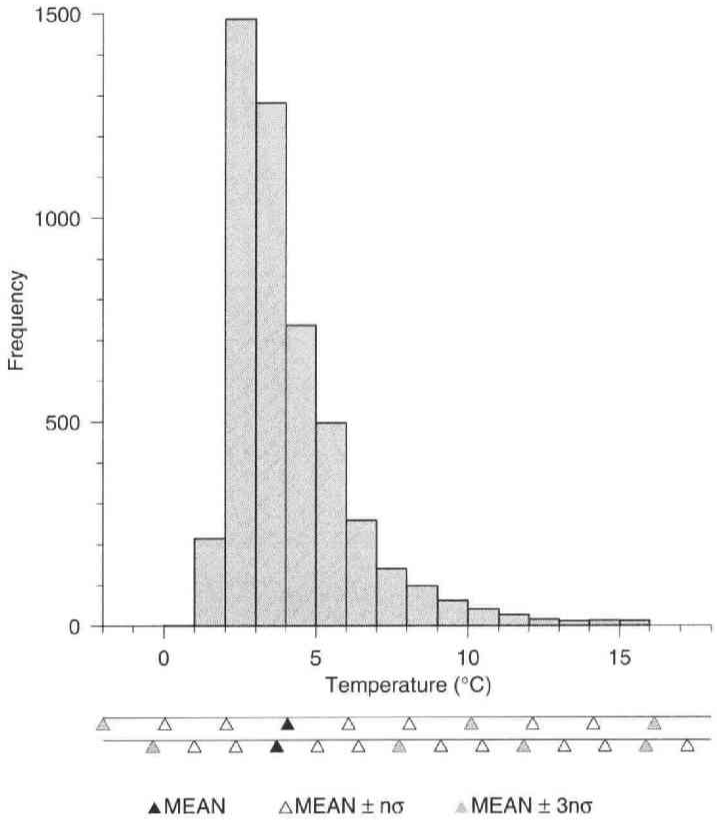

Figure 2.6: Occurrence frequency distribution of temperature at 300 m depth. Below the abscissa, the two kinds of standard deviation scale are shown: the upper scale is based on the standard deviation calculated directly from the distribution shown, and the lower based on the converged standard deviation, which was obtained by iterative procedure in which data lying outside $m \pm 3\sigma$ are omitted, and m and σ are recalculated using remaining data.

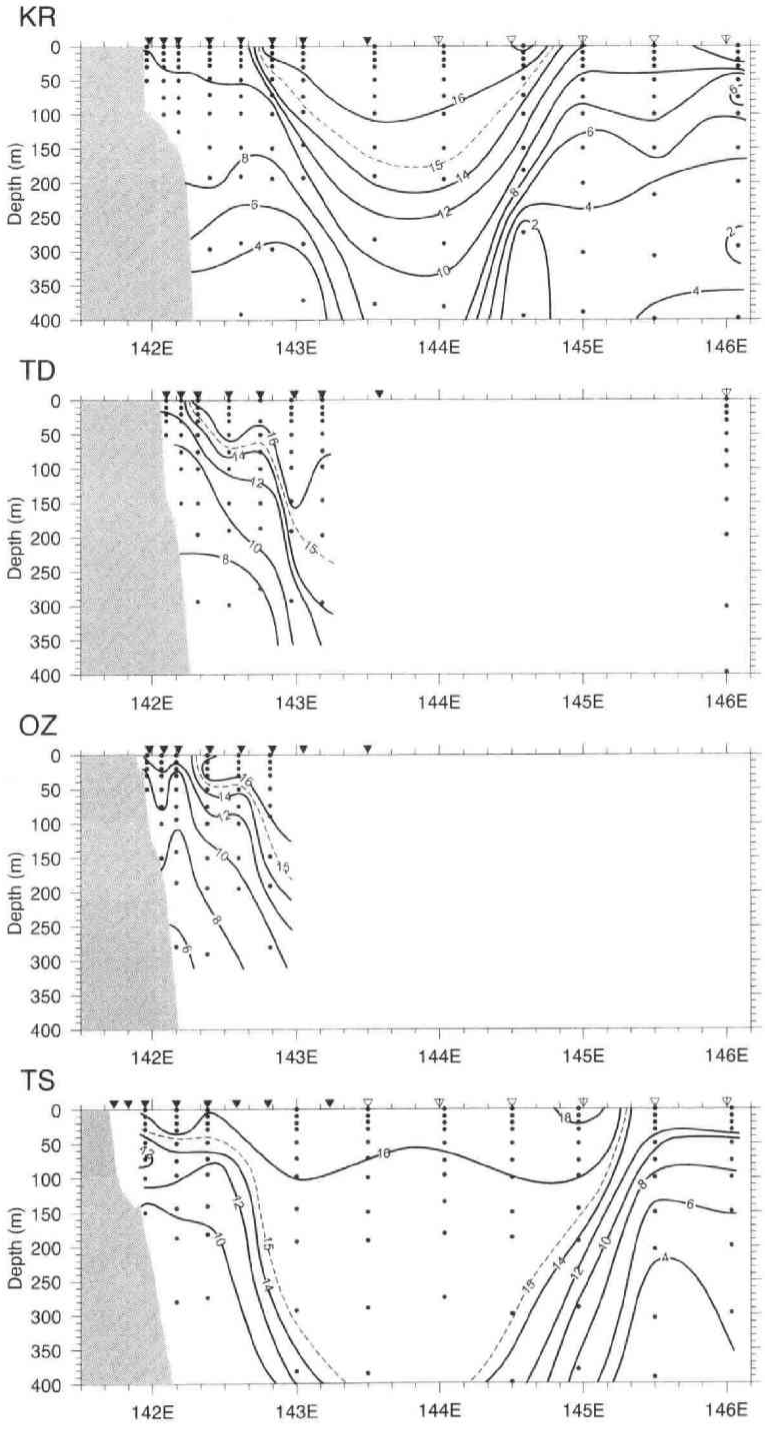

Figure 2.7: Cross-sectional temperature (°C) distributions along the four routine observation lines of the Iwate Fisheries Technology Center (KR: Kurosaki Line, TD: Todogasaki Line, OZ: Osaki Line, and TS: Tsubakishima Line). The observations were conducted in the period May 17–May 22, 1972. Observation points are shown with triangles above the figure: black triangles indicate the coastal line stations, and white triangles the offshore line stations. Black dots in the figure indicate the location of the observed data used. Raw data at observed depths were used to draw the figure (we ignored error flag of density inversion here). Isotherms are drawn at 2°C interval, but additional isotherm of 15°C is added with dashed line.

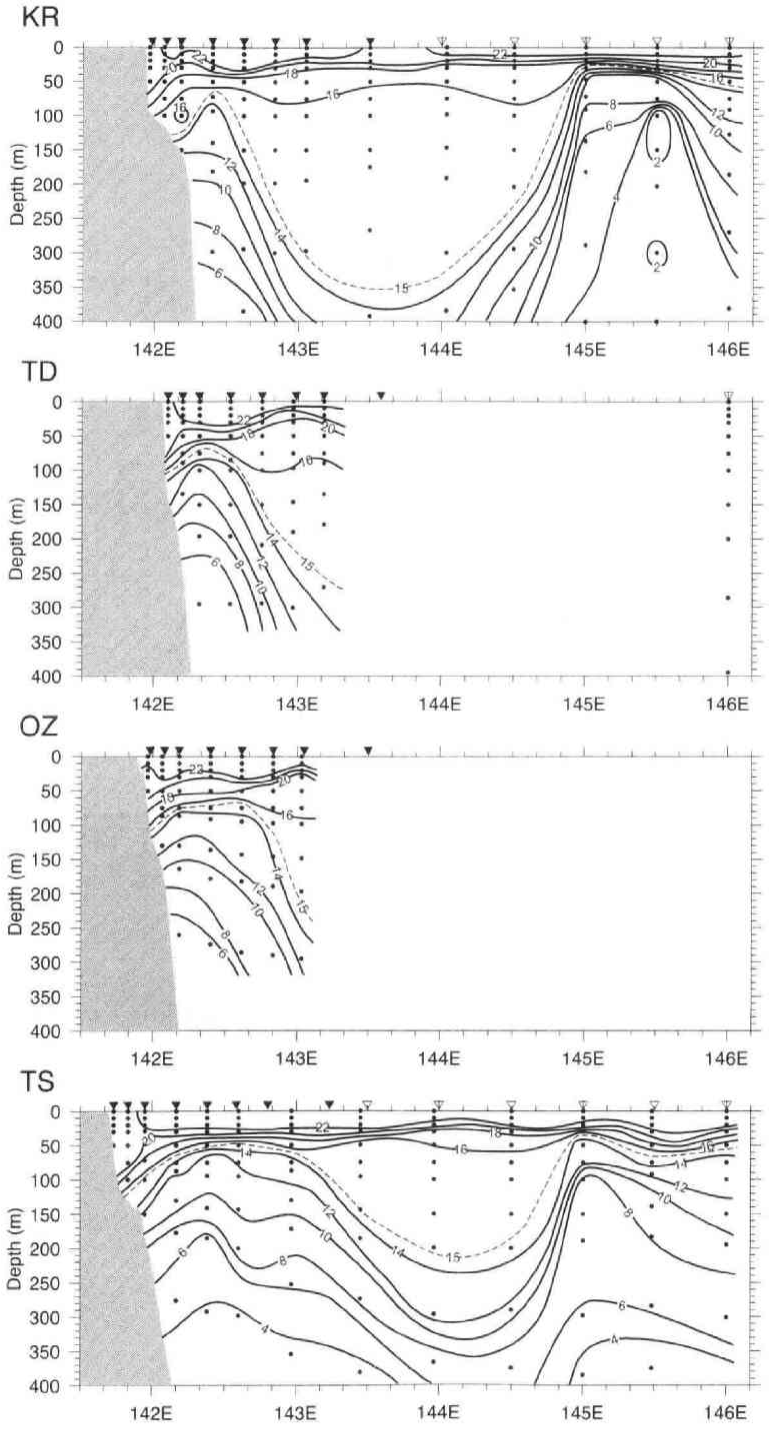

Figure 2.8: As Fig. 2.7, except for the observation period August 18–August 23, 1972.

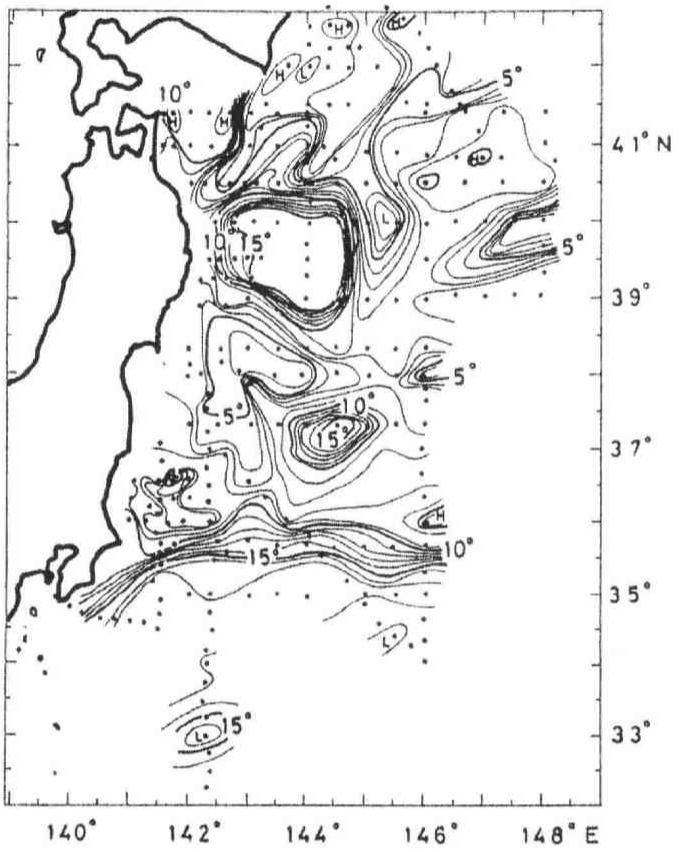

Figure 2.9: Horizontal temperature distribution (°C) at 200 m depth in the period July 25–September 1, 1972 (after Tomosada, 1978).

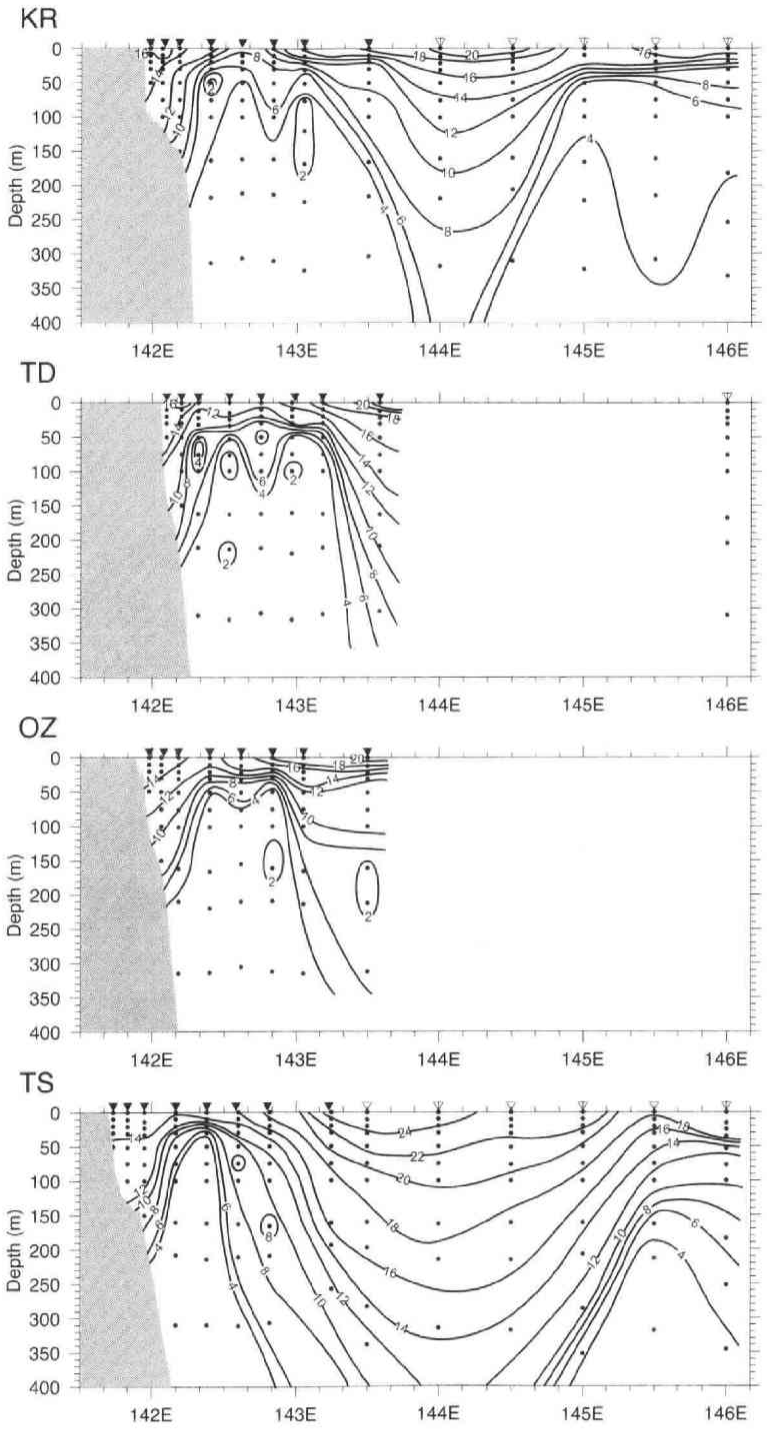

Figure 2.10: As Fig. 2.7, except for the period July 6–July 10, 1979. The supplemental isotherm of 15°C is not given.

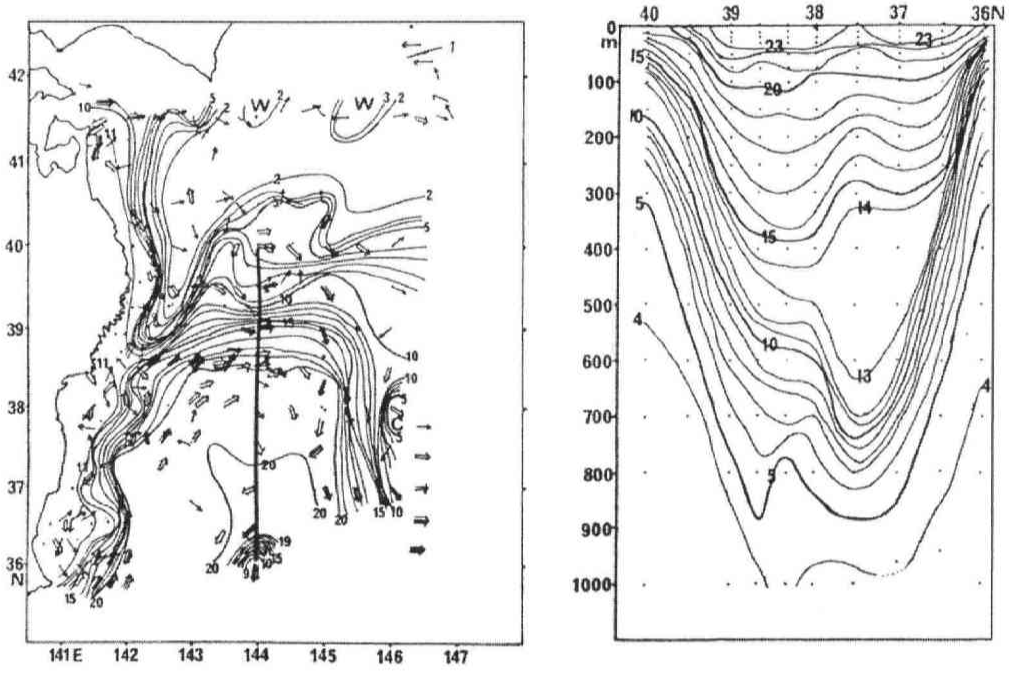

Figure 2.11: Temperature (°C) distribution at 100 m depth and surface current field (left) in the period July 2–July 16, 1979, and temperature cross-section along 144°E (right). Position of the cross-section is shown in the left figure (after Mizuno and Akiyama, 1980).

3 Seasonal variations in the sea off Sanriku Coast, Japan

3.1 Introduction

The broad Mixed Water Region lies between the Oyashio Front and Kuroshio Front to the east of Honshu, Japan as shown in Fig. 3.1 (e.g., Kawai, 1972 and Talley et al., 1995). The oceanic conditions in this region are very complicated, and warm and cold eddies originating from Kuroshio and Oyashio are found there. The sea off Sanriku, Japan, is the westernmost area of the Mixed Water Region. The Tsugaru Current, which originates from the Tsushima Current in the Japan Sea and runs out into the Pacific Ocean through the Tsugaru Strait, flows southward along the Sanriku Coast. Thus, the sea off Sanriku Coast has a relatively complicated structure under the influence of three water masses: the Tsugaru Current water, the Oyashio water, and the Kuroshio water.

The oceanic condition of the sea off Sanriku Coast exhibits considerable seasonal variation: the Tsugaru Current water clearly appears in summer and in autumn but almost disappears in winter, and then the Tsugaru Current water, the Oyashio water, and the Kuroshio water occupy this area alternatively. Temperature and salinity distributions at 100 m depth have often been used to discuss the complicated distributions of these three waters. Many investigators analyzed the variability of the Oyashio strength using the data of the southernmost position of the First Branch of the Oyashio, which is characterized by the position of the 5°C isotherm at 100 m depth (e.g., Okuda, 1986 and Sekine, 1988). Mizuno (1984) applied EOF analysis by using temperature distributions at 100 m depth to discuss the variability near and in the Mixed Water Region. Muto et al. (1969) discussed the hydrographical condition of this region using temperature, salinity, and current fields at 100 m depth during the period from 1964 to 1968. Takasugi (1992) described seasonal variation in the coastal area of this region, focusing on the Tsugaru Current water and the Oyashio water, with monthly mean temperature and salinity at 100 m depth during the period from 1963 to 1990. However, there has been scarcely any discussion of why the oceanic structure at 100 m depth is useful to describe the oceanic structure off the Sanriku Coast and in the Mixed Water Region.

Hanawa and Mitsudera (1986) discussed seasonal variations of water type distribution in the sea off Sanriku using the data obtained by the Iwate Fisheries Technology Center in the period from 1977 to 1981, and attempted water type classification in a T-S diagram. The Marine Information Research Center (MIRC) of the Hydrographic Association conducted quality control on the data obtained by prefectural fisheries experimental stations in cooperation with the National Research Institute of Fisheries Science. Using this new dataset,

we re-analyzed seasonal variations of water type distribution in a T-S diagram. Seasonal variations of the horizontal temperature and salinity distributions in the sea off the Sanriku Coast are also discussed with an emphasis on 100 m and 200 m depth surfaces.

3.2 Data used

The Iwate Fisheries Technology Center has maintained routine Coastal Observation Lines off Sanriku Coast as shown in Fig. 3.2. The observation was initiated in 1963, and has been conducted on a monthly basis, whereas the most offshore station of each observation line is usually not occupied in winter season from December to March. The observations have been usually performed close to a depth of 300 m. The Iwate Fisheries Technology Center has also maintained Offshore Observation Lines as offshore extensions of the Kurosaki and Tsubakishima Lines. However, these lines are occupied only few times per year, and seasonal coverage is deficient. For this reason, the data along the Offshore Observation Line were not used in this analysis. We conducted quality-control on the data obtained by Iwate Fisheries Technology Center prior to 1995. Error data were checked by comparison with the field book, and were corrected. The quality-control procedure used is described in MIRC (2001). It was shown that the data quality is improved considerably after 1971 (Oguma et al., 1999), so we used the data obtained for the 25 years from 1971 to 1995. The recent data obtained by CTD are reported exactly at the standard depths (0, 10, 20, 30, 50, 75, 100, 125, 150, 200, 250, and 300 m). For the previous serial observation data, we interpolated to obtain the standard depth dataset. Basically we used the standard depth data for this analysis.

The observation dates are shown in Fig. 3.3 for the period analyzed. The observation cruises were conducted regularly for each month, as shown in the figure, but the cruise dates change year by year, and the cruise period is sometimes extended over two calendar months. For convenience' sake, we divided the calendar year into 12 periods from I to XII as shown in Table 3.1, so as to include almost all observations in each corresponding month. The starting date of each period is shown with vertical dashed lines in Fig. 3.3. As seen in Fig. 3.3, one cruise is included in one of the newly defined periods, except in the periods from February to April, 1975. We call the periods from I to XII January to December in this paper.

3.3 Seasonal variation of the water type distribution in T-S diagram

All of the observed raw data in the period from 1971 to 1995 are plotted on T-S diagrams for corresponding months, and shown in Fig. 3.4 in just the same way as was used

by Hanawa and Mitsudera (1986). Hanawa and Mitsudera (1986) tried to classify water types found off Sanriku Coast into Kuroshio water (K), Tsugaru Current water (T), Oyashio water (O), Coastal Oyashio water (C), surface layer water (S), and deeper layer water (D). These water types are also shown in Fig. 3.4, separated by thick full lines. Although the number of data is increased in the present analysis, the distribution patterns of the water types and their seasonal variations are almost identical to those given by Hanawa and Mitsudera (1986). As the oceanic structure appears to be very changeable year by year, it should be noted that the distribution patterns are not widened even though the analyzed period was increased by a factor five from their study.

The most prominent seasonal variation shown in Fig. 3.4 occurs near and in the domain T (Tsugaru Current water) defined by Hanawa and Mitsudera (1986). The water types in domain S (surface water) just on the fresher side of domain T can be the Tsugaru Current water modified by coastal fresh water, which would be seen in shallow surface layers. To see the seasonal variation of the Tsugaru Current water, we selected the second and third stations of each observation line (the water depth of the first station is shallower than 100 m). Since the Tsugaru Current water basically distributes along the coast, the three coastal stations along each observation line are included in the Tsugaru Current zone where the clear Tsugaru Current water can be found at least in the summer season. Fig. 3.5 shows the water types observed at 100 m depth and at 200 m depth at these stations. The plot of water type observed at 100 m depth exhibits clear seasonal variation mainly inside the domain T. Fig. 3.4 suggests that the water types in domain S (surface water) are often modified by surface warming and cooling or by mixing with coastal waters. Fig. 3.5, however, indicates that the Tsugaru Current water at 100 m depth seems to be less influenced by such modification. On the other hand, the water types observed at 200 m depth show much smaller seasonal variations, and remain in the lower part of the domain T throughout the year. It should be noted that the water types at 200 m depth lie straight, connecting the water types in the domain K and in the domain O.

In the following sections we analyze the seasonal variations of the oceanic structures at 100 m and at 200 m depth.

3.4 Seasonal variations of horizontal distributions of temperature and salinity at 100 m depth

The oceanic condition in the sea off Sanriku Coast is very changeable month-by-month and year-by-year. On this account, some part of seasonal variation might be masked by short-

period fluctuations, if we pay attention to a specified year. However, as seen in Figs. 3.4 and 3.5, the seasonal variability in the Tsugaru Current zone is very dominant, and the horizontal variability of temperature and salinity is clearly small in the winter season. Here, we inspect the gross features of the seasonal variation using monthly averaged fields for the 25 years analyzed.

The monthly averaged temperature and salinity fields at 100 m depth are shown in Figs. 3.6 and 3.7, respectively. The relatively warm and saline water is found along the Sanriku Coast throughout year, corresponding to Tsugaru Current water. The temperature and salinity fronts between the Tsugaru Current water and the Oyashio water gradually disappear in January through April, appear again in May, then become clearest in September. The clear fronts in summer can be recognized in the fields in individual months. The signature corresponding to the Tsugaru Current water can be seen weakly even in the winter season from January to April in the averaged fields, while this does not mean that the Tsugaru Current water always exists in these months. As one example of the non-observation of the Tsugaru Current water in winter, the temperature fields in January 1980 through in April 1980 are shown in Fig. 3.8. The Tsugaru Current water was hardly seen in the winter of 1980.

The colder and fresher water tends to stretch southward in the middle of the area analyzed, where stations 4 to 6 exist along each observation line. This water corresponds to the First Branch of the Oyashio, though its structure is blurred in the field averaged for 25 years. The area of the Coastal Observation Lines, to the east of the offshore-most station along each observation line, seems to be determined so as to cover the area of the First Branch of the Oyashio.

We set sub-groups, two coastal stations (stations 2 and 3), two middle stations (stations 4 and 5) and two offshore stations (stations 6 and 7), and calculated the monthly average temperatures and salinities. (The water depth of station 1 along each line is shallower than 100 m, and few observations are made at station 8 of each line in winter.) The seasonal variations of the averaged temperature and salinity values at 100 m depth are shown for each sub-group in Fig. 3.9. The seasonal variation pattern can be more clearly seen in this figure. The minima of temperature and salinity appear in April, and the maximum temperature appears in November or December for all sub-groups. However, the maximum salinity occurs in September for all of the coastal sub-groups, and in October for the middle sub-group on Tsubakishima Line (TS St.4-5), while it occurs in November or December in other middle and offshore groups. The seasonal variations of coastal sub-groups in Fig. 3.9 seem to agree with the findings of previous studies (e.g., Muto et al., 1969 and Takasugi, 1992). This difference of

variation between temperature and salinity in the period from September to December means that the signature of the Tsugaru Current water is less clear in the salinity field (Fig. 3.7) than in the temperature field (Fig. 3.6). The difference of the time of occurrence between the maximum of temperature and that of salinity in the coastal sub-groups can be related to seasonal variation of the Tsushima Current water, which is the source of the Tsugaru Current water. Amano (1986) reported that the maximum salinity value is found in August and the maximum temperature value is found in November at 75 m depth in the Tsushima Current region off Aomori Prefecture.

If the variable nature of the coastal sub-groups is typical of the current region of the Tsugaru Current, the middle sub-group on Tsubakishima Line (TS St.4-5) could be considered to be influenced by the Tsugaru Current water. It is possible that some of the Tsugaru Current water is carried eastward along the northern margin of the Kuroshio Extension near the Tsubakishima Line, though the fate of the Tsugaru Current passing by Sanriku Coast has not yet be well documented.

3.5 Seasonal variations of horizontal distributions of temperature and salinity at 200 m depth

The monthly averaged temperature and salinity fields at 200 m depth are shown in Figs. 3.10 and 3.11, respectively. The distribution patterns of temperature and salinity at 200 m are quite different from those at 100 m. In the temperature and salinity distributions shown in Figs. 3.10 and 3.11, relatively high temperature and high salinity water tends to appear in the coastal and offshore region. The water near the coast reflects a sporadic influence of the Tsugaru Current water having a deep structure, and in the offshore region this suggests Kuroshio water or water strongly influenced by the Kuroshio water. Nonetheless, there is no systematic pattern in both fields.

The temperature and salinity fields at 100 m depth and at 200 m depth in July 1979 are shown in Fig. 3.12. At 100 m depth three typical water masses are seen: the Tsugaru Current water along the coast, the Kuroshio water on the south-eastern corner of the area analyzed, and the Oyashio water extending southward from the northern margin of the area. By contrast, at 200 m depth, no clear front can be seen between the Tsugaru Current water and the Oyashio water. The isotherms and isohalines are dense only at the margin of the Kuroshio water or the water strongly influenced by Kuroshio water. This indicates that the structure of the Tsugaru Current is shallow and does not often reach to 200 m depth. Another example is shown in Fig. 3.13, the case of August 1980. The three typical water

masses are obvious at 100 m depth. These three waters are also recognizable at 200 m depth in this case, but the front between the Tsugaru Current water and the Oyashio water seems to be ambiguous. These two examples suggest the reason why the temperature structure at 100 m depth is often used to describe the Tsugaru Current and the First Branch of the Oyashio.

The seasonal variations of averaged temperature and salinity for each sub-group are given in Fig. 3.14. The seasonal variations of temperature and salinity are also suggested at 200 m depth, but the variation pattern is very different from that at 100 m depth in Fig. 3.9. Both the maximum temperature and salinity appear in the period from November to January with the minimum temperature and salinity appearing in the period from April to August. No remarkable difference can be seen among the sub-groups.

3.6 Concluding remarks

Seasonal variations of the sea off Sanriku were investigated using the data obtained along the routine Coastal Observation Lines of the Iwate Fisheries Technology Center during the period from 1971 to 1995. The mean temperature and salinity fields at 100 m depth display clear seasonal variations. The Tsugaru Current water is clearly shown in temperature and salinity fields at 100 m depth in the summer-to-autumn season, but its signature is weakened or disappears in winter to spring. By contrast, the Tsugaru Current water is hardly seen in the mean temperature and salinity fields at 200 m depth, suggesting that the structure of the Tsugaru Current is mainly confined to the surface layer shallower than 200 m. The seasonal variations of temperature and salinity at 100 m depth seem to depend partly on those of the Tsushima Current water, from which the Tsugaru Current water originates.

We need to investigate the seasonal variations of the Tsugaru Current water together with those of the source waters, such as Tsushima Current water. Also, current fields of the sea off Sanriku should be discussed to understand the transport of the water masses in this region. These problems remain for future investigations. MIRC is now archiving and processing the ADCP data in the vicinity of Japan, the main data source of which is the patrol vessels of Japan Coast Guard. We plan to analyze these data to clarify the seasonal variation of the current fields in the sea off Sanriku.

References

Amano, K. (1986): Study on variations of oceanic structure in the sea off Aomori Prefecture-II. Data book published by Aomori Prefectural Fisheries Station, 364pp. (in Japanese)

Hanawa, K., and H. Mitsudera (1986): Variation of water system distribution in the Sanriku coastal area. J. Oceanogr. Soc. Japan, 42, 435-446.

Kawai, H. (1972): Hydrography of the Kuroshio Extension. In: Kuroshio, its physical aspect, ed. H. Stommel and K. Yoshida, Chap. 8, 235-352, Univ. of Tokyo Press.

MIRC (2001): MIRC Ocean Dataset 2001. MIRC Technical Report No. 1.

Mizuno, K. (1984): Notes on the hydrographic variability in the vicinity of the east coast of Japan. Bull. Tohoku Reg. Fish. Res. Lab., 46, 61-80 (in Japanese with English abstract).

Muto, S., T. Sano, M. Hirai, H. Kudo, K. Yao, and Y. Yamamura (1969): The hydrographical study in the coastal sea region off Sanriku. Bull. Tohoku Reg. Fish. Res. Lab., 29, 93-123 (in Japanese with English abstract).

Oguma, S., T. Suzuki, Y. Nagata, H. Watanabe, H. Yamaguchi, and S. Takasugi (1999): Errors in oceanic dataset often generated in data processing and in data management -II Case of the Iwate Fisheries Technology Center and treatment of duplicated data. J. Japan Soc. Marine Sur. and Tech., 11, 11-18 (in Japanese with English abstract)

Okuda, K. (1986): Occurrence of extremely low temperature in the coastal region of the Tohoku area associated with interannual variation of the Oyashio. Bull. Tohoku Reg. Fish. Res. Lab. 48, 87-96 (in Japanese with English abstract).

Sekine, Y. (1988): Anomalous intrusion of the Oyashio east of Japan. 1. Influence of the interannual and seasonal variation in the wind stress over the North Pacific. J. Geophy. Res., 93, 2247-2277.

Takasugi, S. (1992): Distribution of Tsugaru Warm Current Water in the Iwate coastal area and their influence to the sea surface temperature at coastal hydrographic station. Fish. Oceanogr., 56, 434-448 (in Japanese with English abstract).

Talley, D. L., Y. Nagata, T. Iwao, T. Kono, D. Inagake, M. Hirai, and K. Okuda (1995): North Pacific Intermediate Water in the Kuroshio/Oyashio Mixed Water Region. J. Phys. Oceanogr., 25, 475-501.

Table 3.1: Definition of the sub-periods I to XII, which are used as calendar months from January to December in this paper. Each sub-period is defined so as to include almost all observations in each corresponding month, and the length of sub-period is thus changeable.

Sub-period	Dates
I	Jan. 1∼Jan. 26
II	Jan. 27∼Feb. 23
III	Feb. 24∼Mar. 23
IV	Mar. 24∼Apr. 23
V	Apr. 24∼May 27
VI	May 28∼Jun. 23
VII	Jun. 24∼Jul. 21
VIII	Jul. 22∼Aug. 25
IX	Aug. 26∼Sep. 26
X	Sep. 27∼Oct. 26
XI	Oct. 27∼Nov. 28
XII	Nov. 29∼Dec. 31

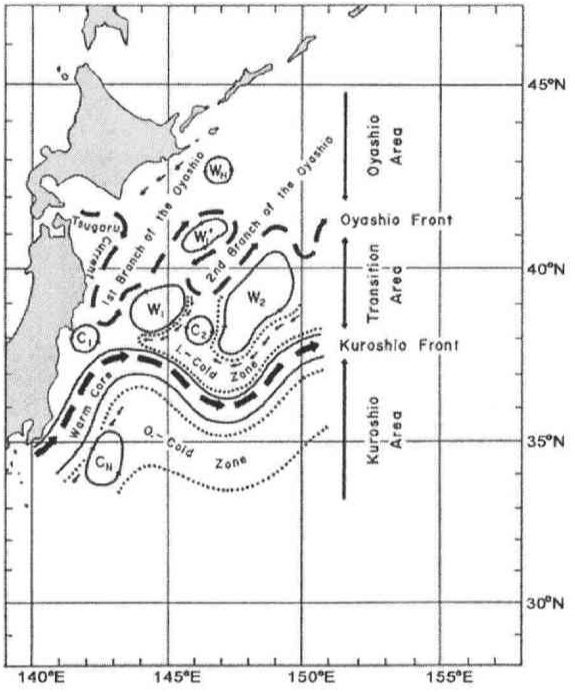

Figure 3.1: Schematic view of the Mixed Water Region between the Oyashio and Kuroshio Fronts (Kawai, 1972). The Mixed Water Region is called by various names by different authors: Transition Area, Confluence Zone, Perturbed Area, etc. W indicates the warm-core ring and C the cold-core ring.

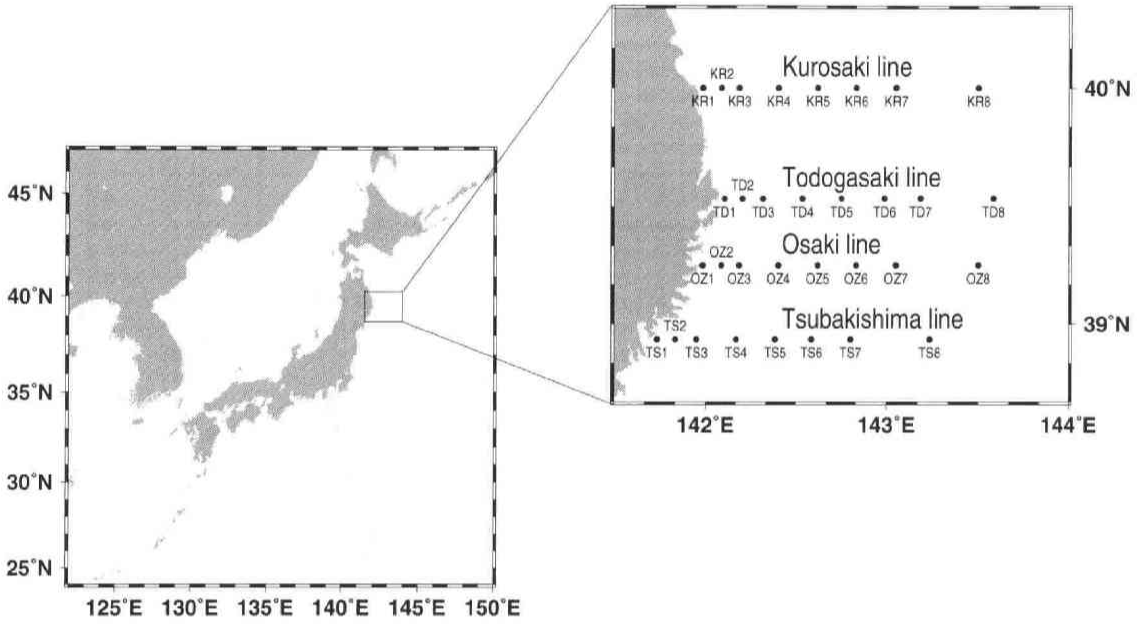

Figure 3.2: Distribution of the observation points along the routine Coastal Observation Lines of the Iwate Fisheries Technology Center. The observations are conducted almost monthly from 1963. The lines are called Kurosaki Line, Todogasaki Line, Osaki Line and Tsubakishima Line from north to south. No observation at the most offshore point of each line is usually conducted in the winter season.

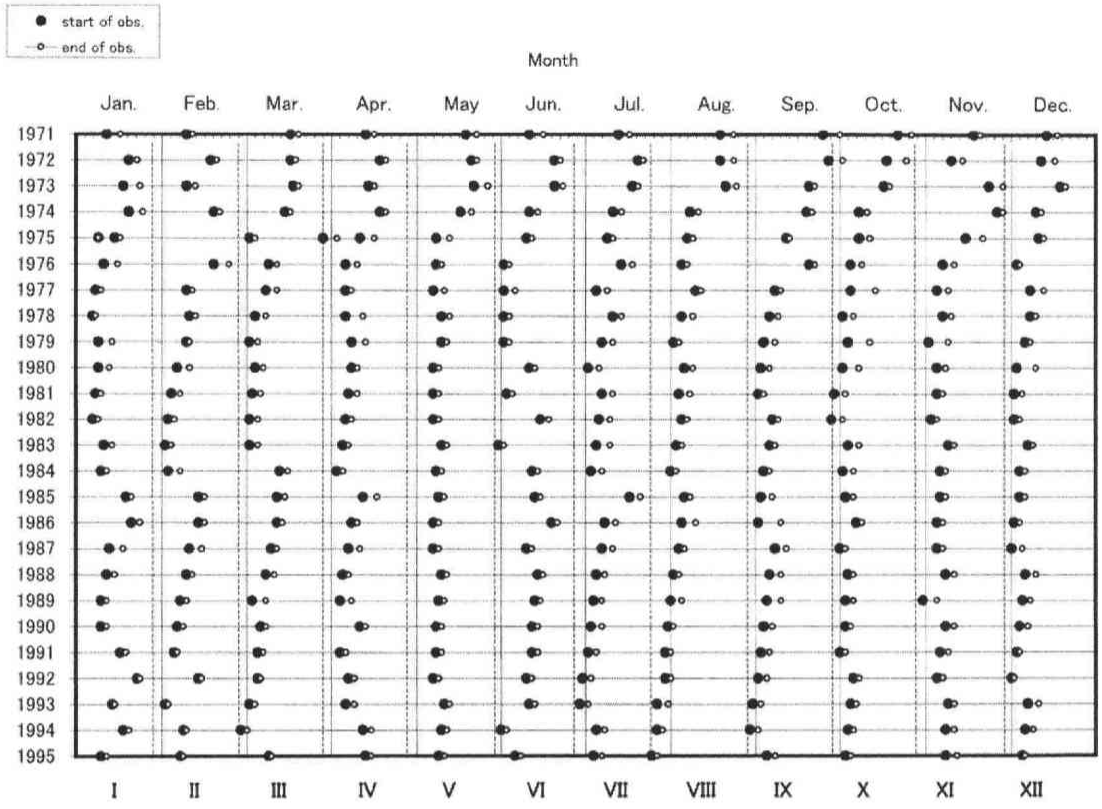

Figure 3.3: Cruise periods conducted by the Iwate Fisheries Technology Center from 1971 to 1995. Black and white circles indicate the start date and the end date of each cruise. Cruise period can be classified into 12 sub-periods separated by dashed vertical lines, except from February to April, 1975. These sub-periods I to XII are used as calendar months from January to December in this paper. See Table 3.1 for exact date range of each sub-period.

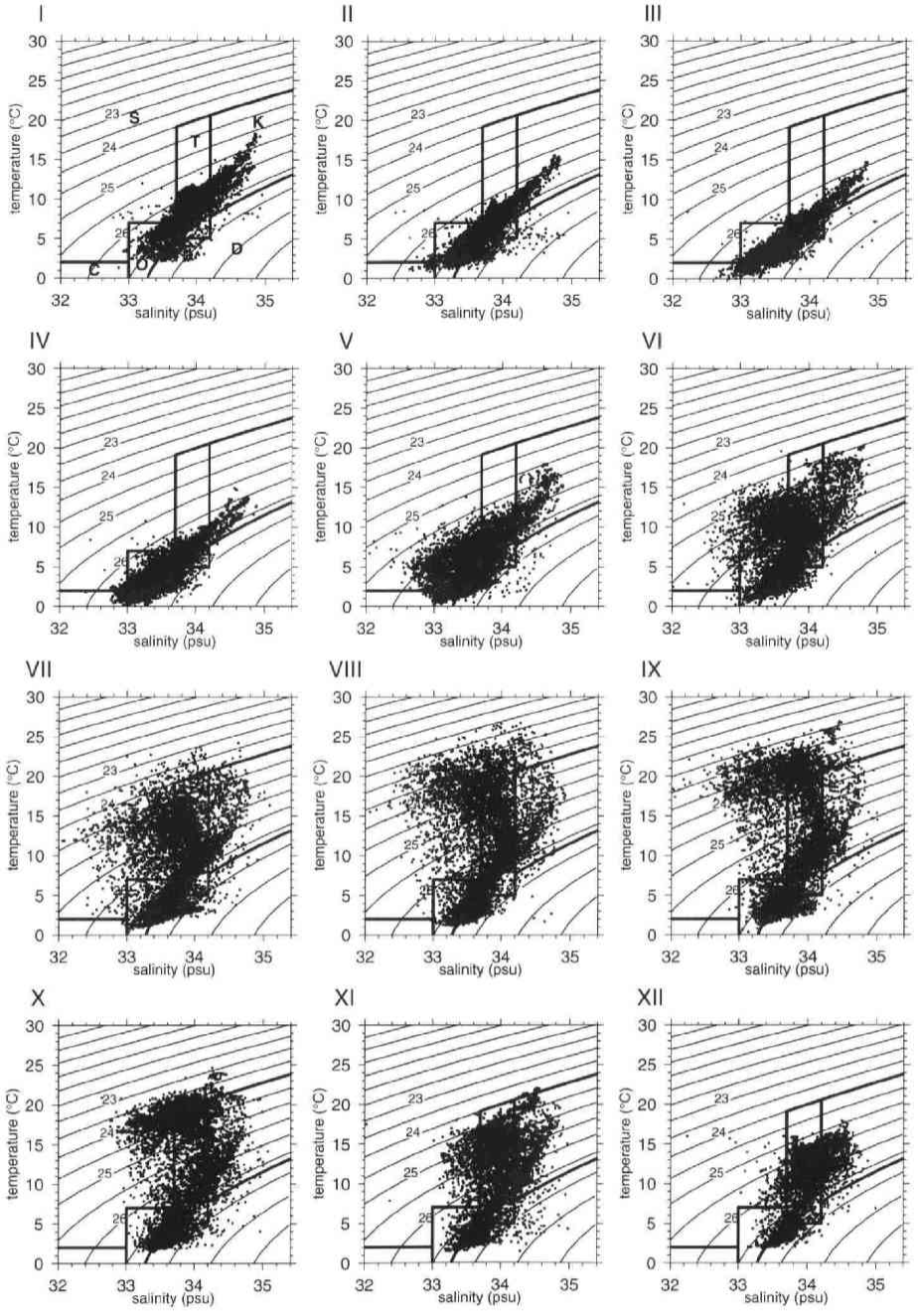

Figure 3.4: T-S diagrams of the water types for each month, observed off Sanriku Coast. All plotted data were observed in the period from 1971 to 1995. See Table 1 for the definition of months I to XII. The domains separated by thick lines show the conventional water type classification by Hanawa and Mitsudera (1986). The identification of water types is given in the diagram of month I: Tsugaru Current water (T), Oyashio water (O), Kuroshio water (K), Coastal Oyashio water (C), the surface layer water (S), and the deeper layer water (D).

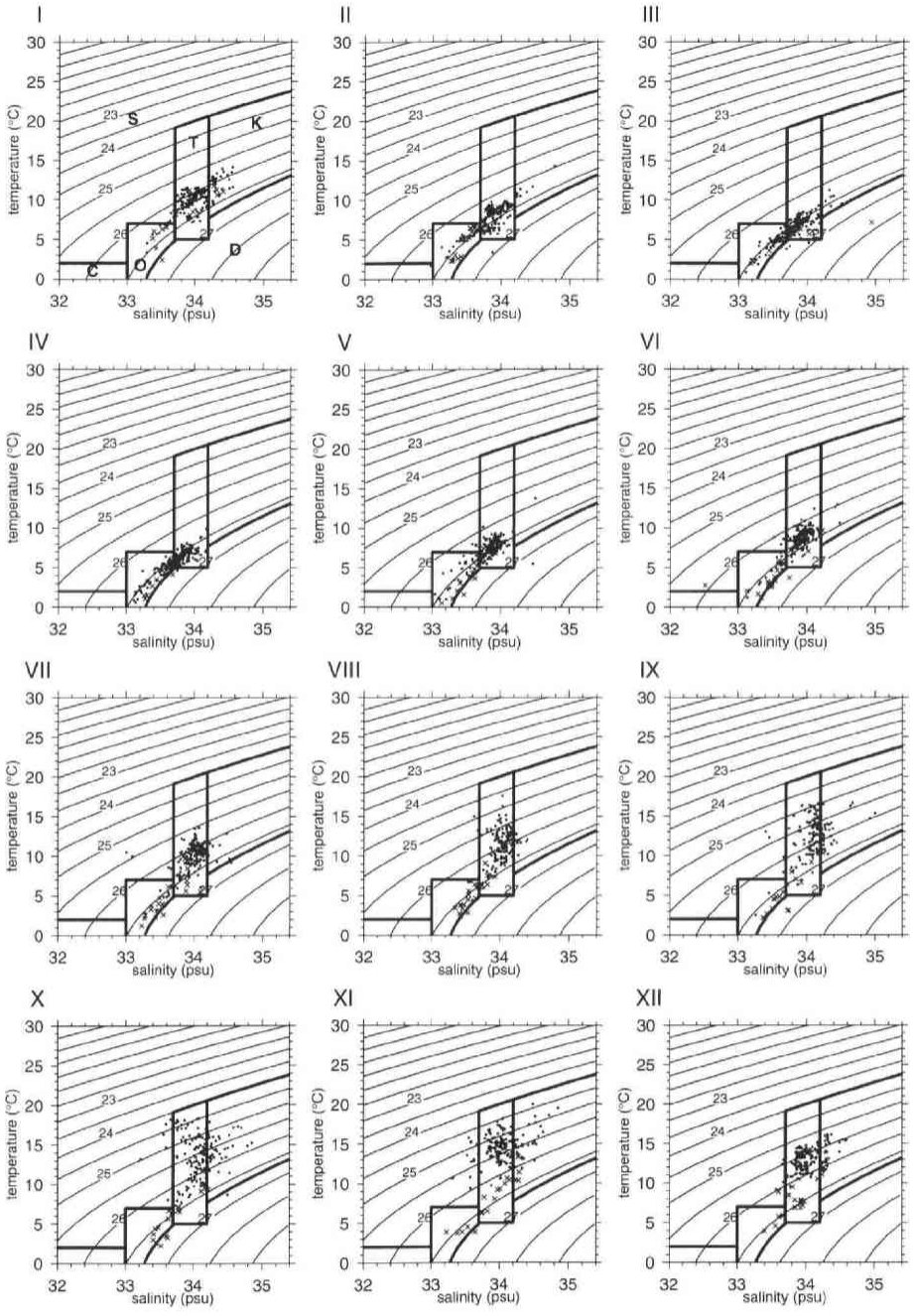

Figure 3.5: T-S diagrams of the water types at 100 m depth (•) and at 200 m depth (×) for each month. The data taken at the coastal second and third stations along each observation lines are plotted.

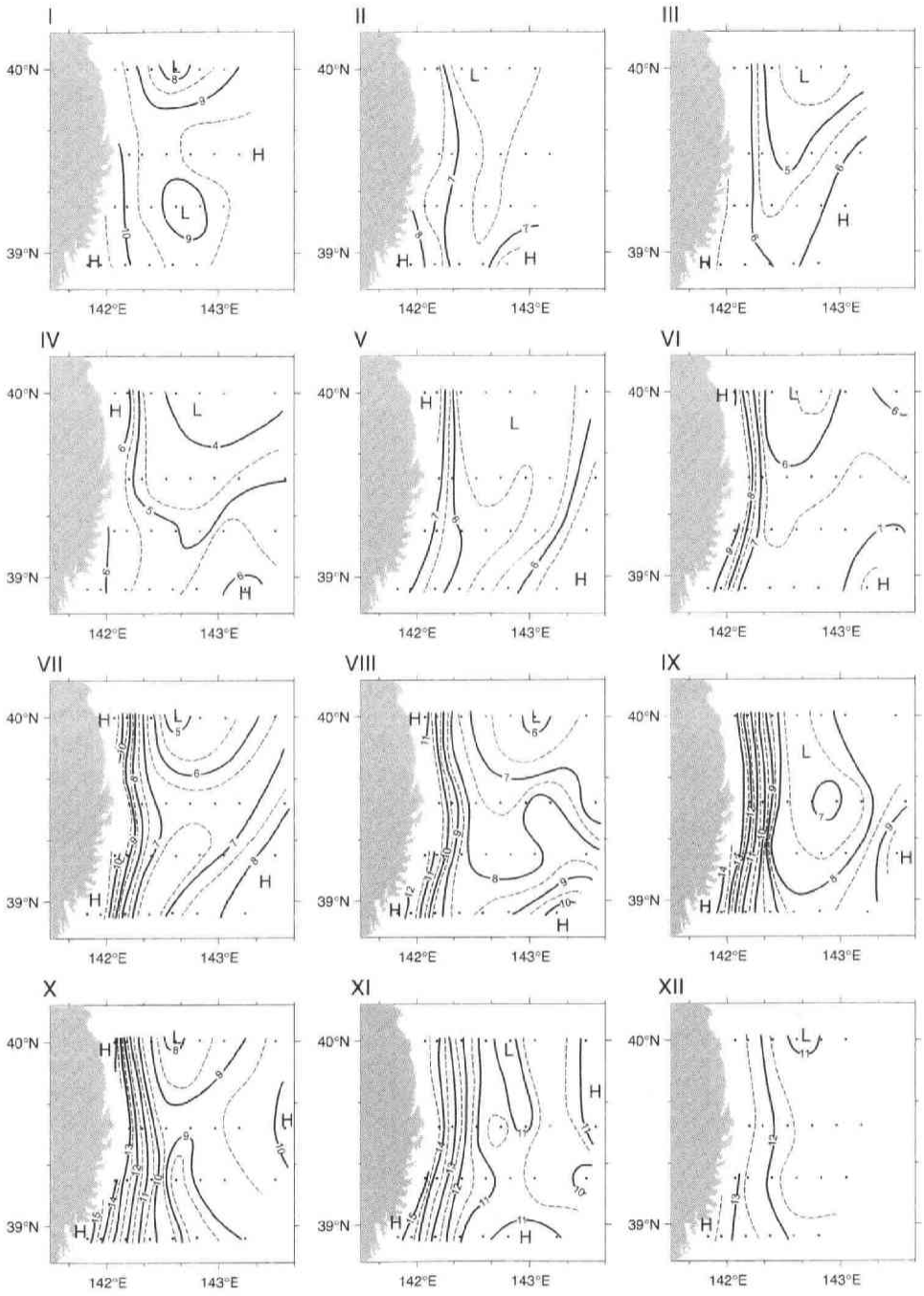

Figure 3.6: Seasonal variations of the temperature distributions at 100 m depth in the sea off Sanriku. Monthly mean values averaged for 25 years period from 1971 to 1995 are shown. I to XII correspond roughly to January, February, March etc. (see Table 1 for exact definition). Isotherms are shown with full lines at interval of 1°C, and auxiliary isotherms with dashed line at interval of 0.5°C.

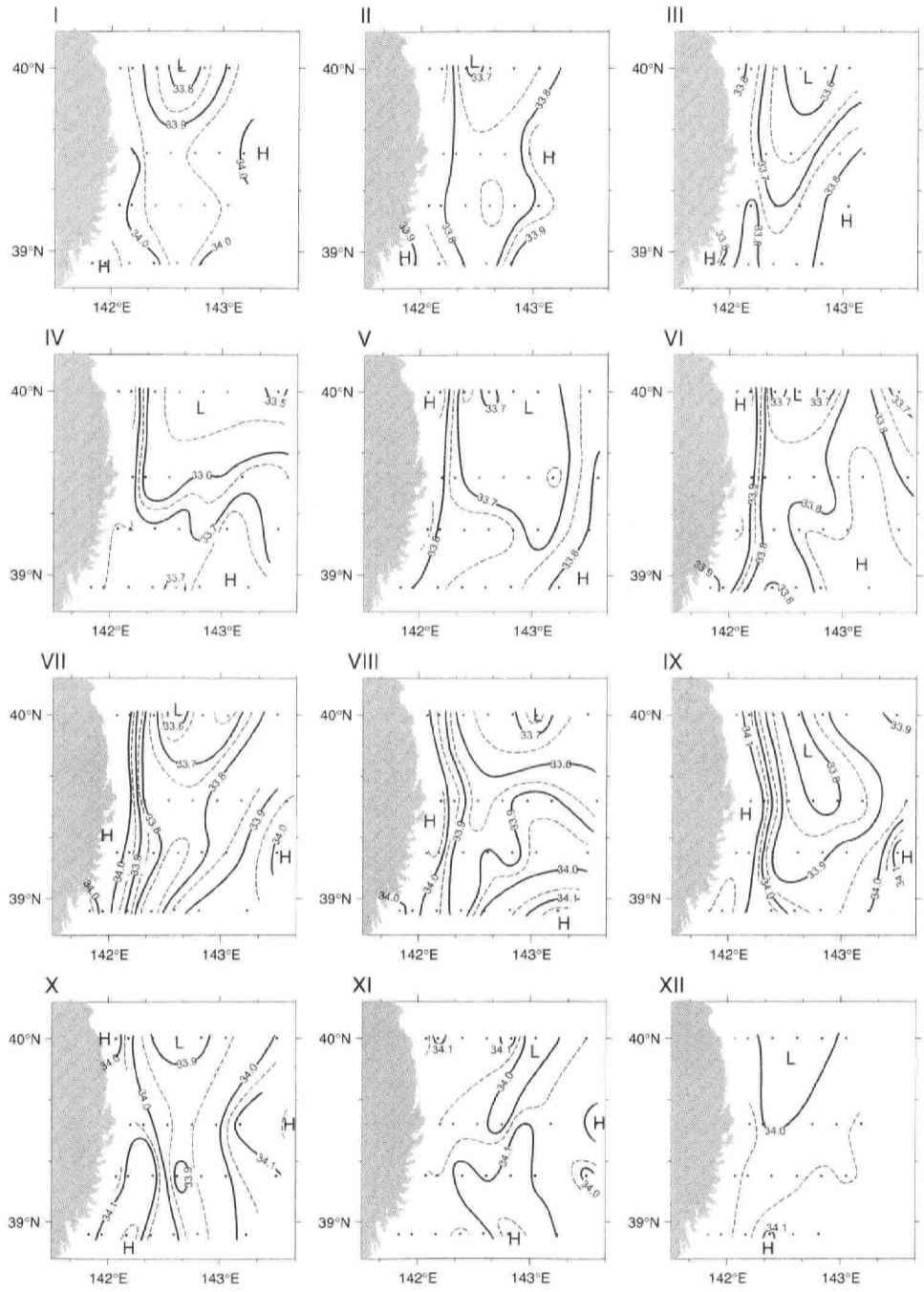

Figure 3.7: As Fig. 3.6, except for the salinity distribution. Isohalines are shown with full lines at interval of 0.1 psu, and auxiliary isohalines with dashed line at interval of 0.05 psu.

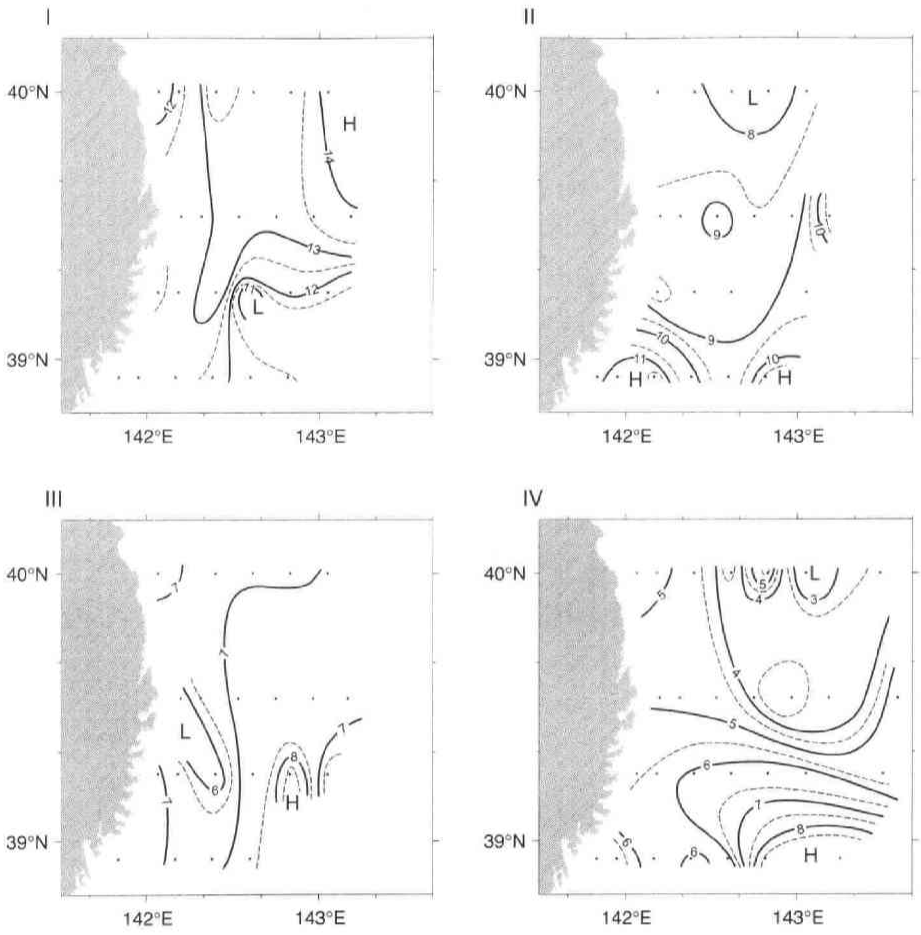

Figure 3.8: Temperature fields at 100 m depth in January, February, March and April, 1980. Isotherms are shown with full lines at interval of 1°C, and auxiliary isotherms with dashed line at interval of 0.5°C.

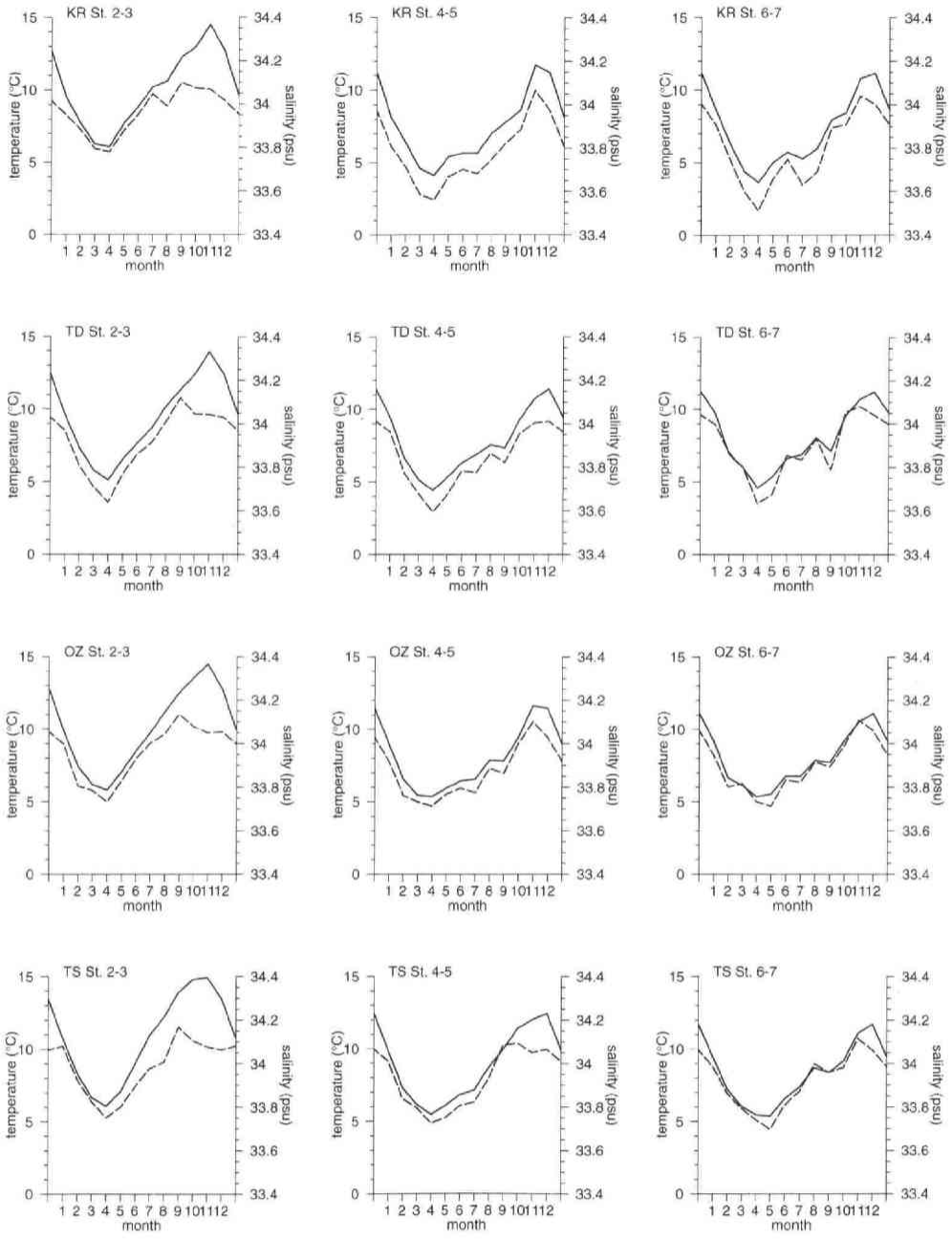

Figure 3.9: Seasonal variations of monthly averaged temperature (full line) and salinity (dashed line) for each sub-group. Sub-groups comprise of the two coastal stations (Sts. 2 and 3), the two middle stations (Sts. 4 and 5) and two offshore stations (Sts. 6 and 7) along each line. KR denotes the Kurosaki Line, TD the Todogasaki Line, OZ the Osaki Line and TS the Tsubakishima Line.

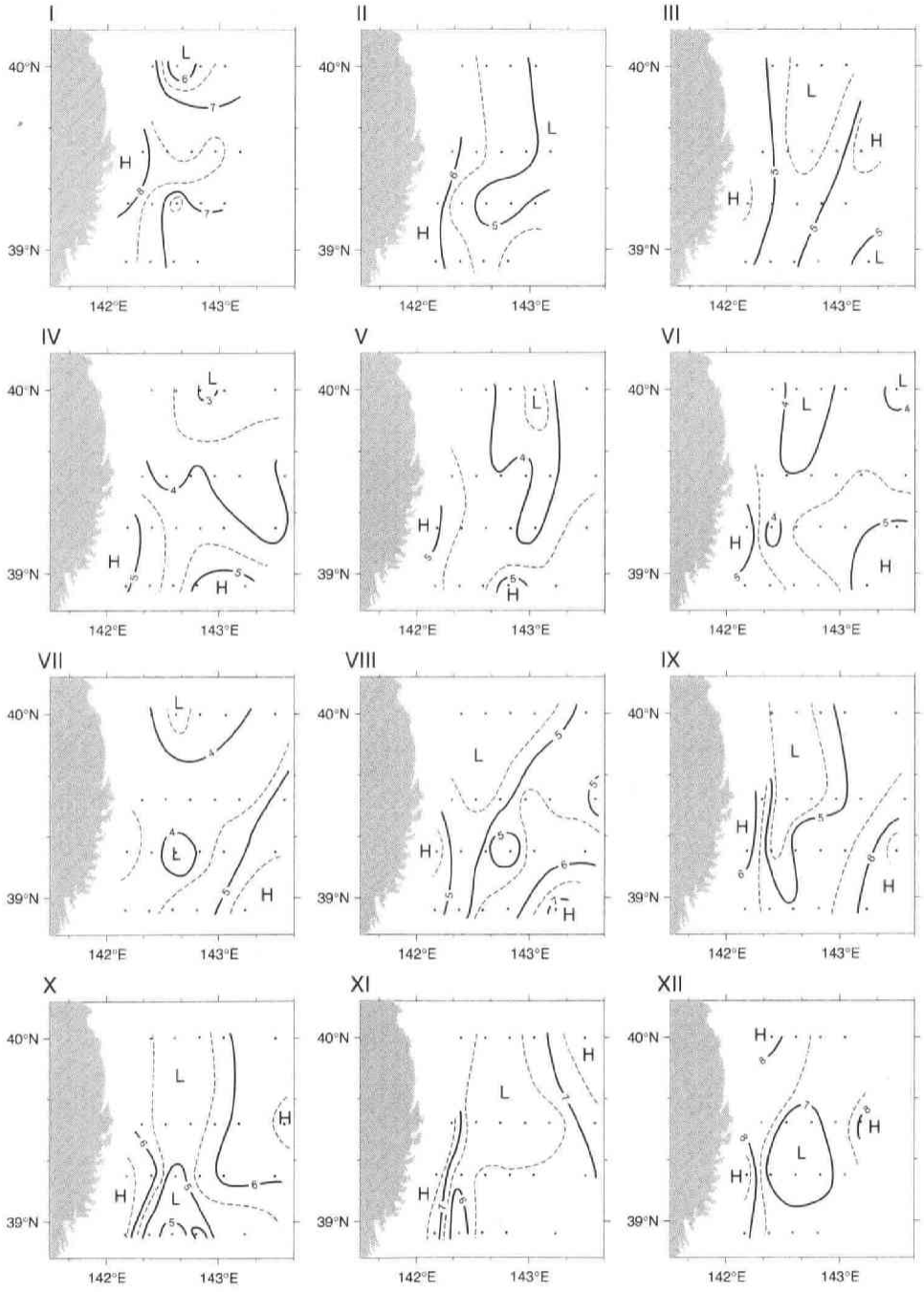

Figure 3.10: As Fig. 3.6 except at 200 m depth.

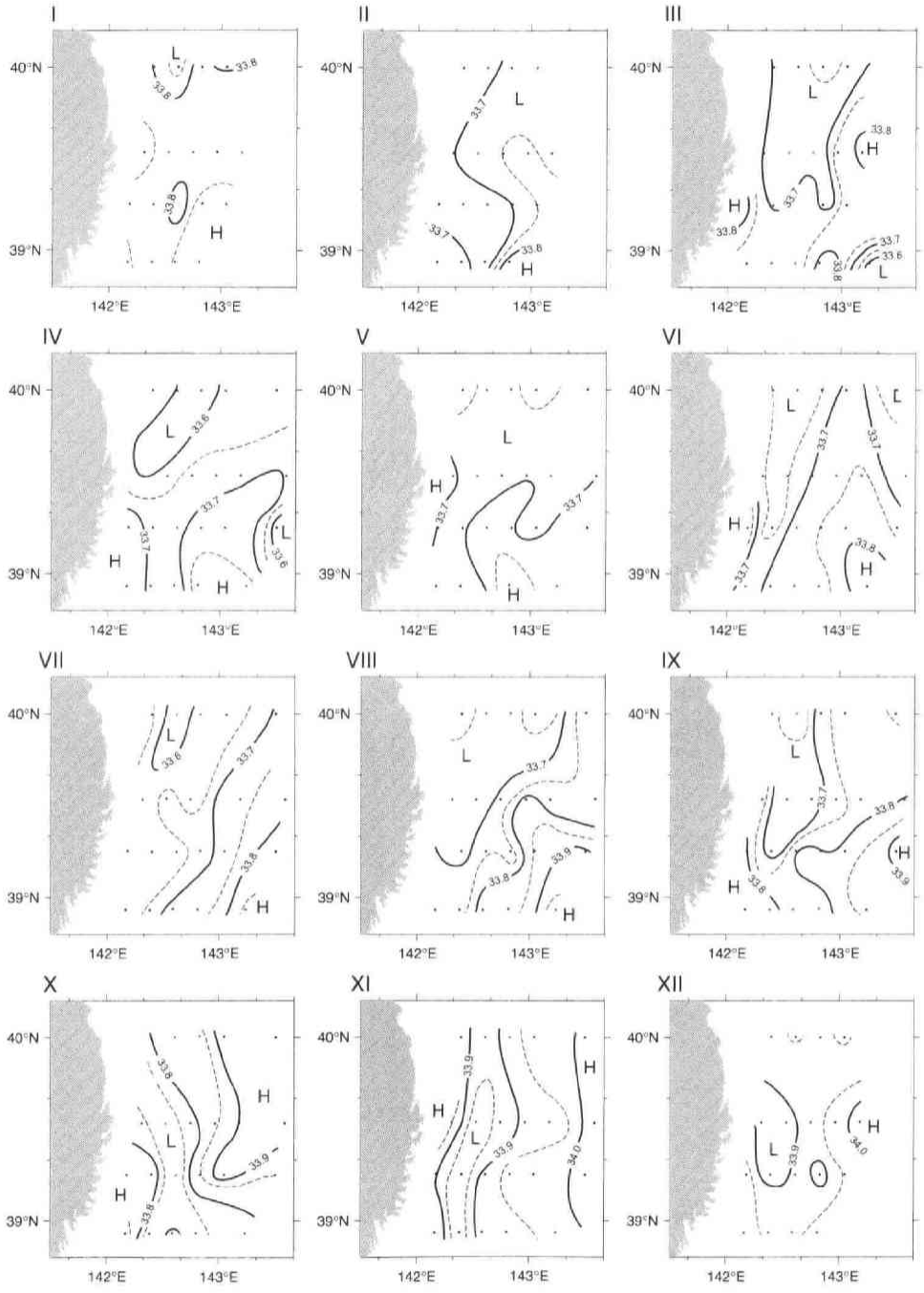

Figure 3.11: As Fig. 3.7 except at 200 m depth.

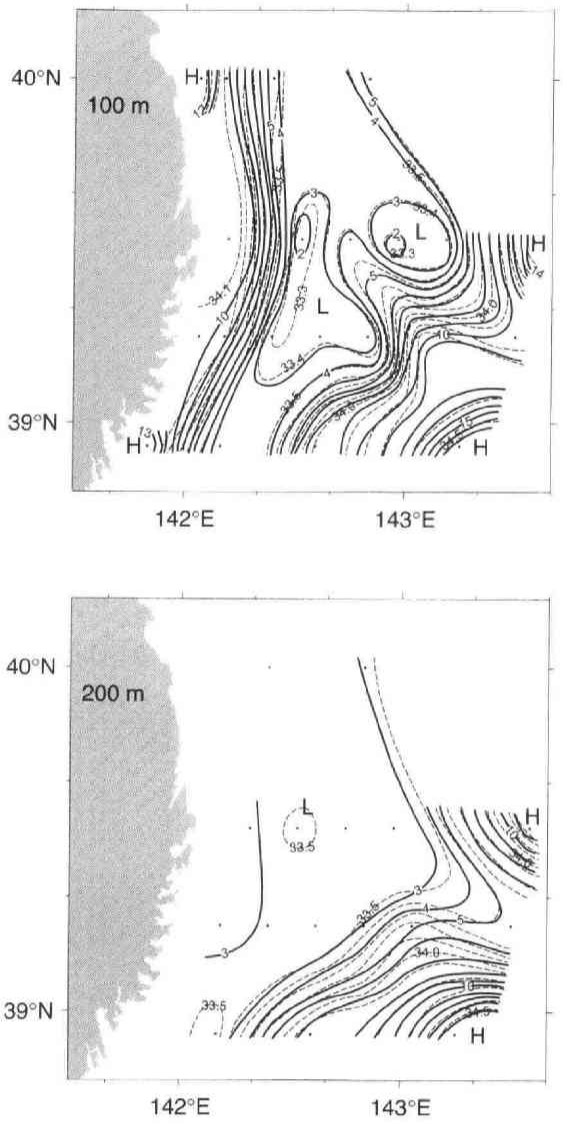

Figure 3.12: Temperature and salinity fields at 100 m depth (upper figure) and at 200 m depth (lower figure) in July 1979. Isotherms (full line) and isohalines (dashed line) are given at interval of 1°C and 0.1 psu, respectively.

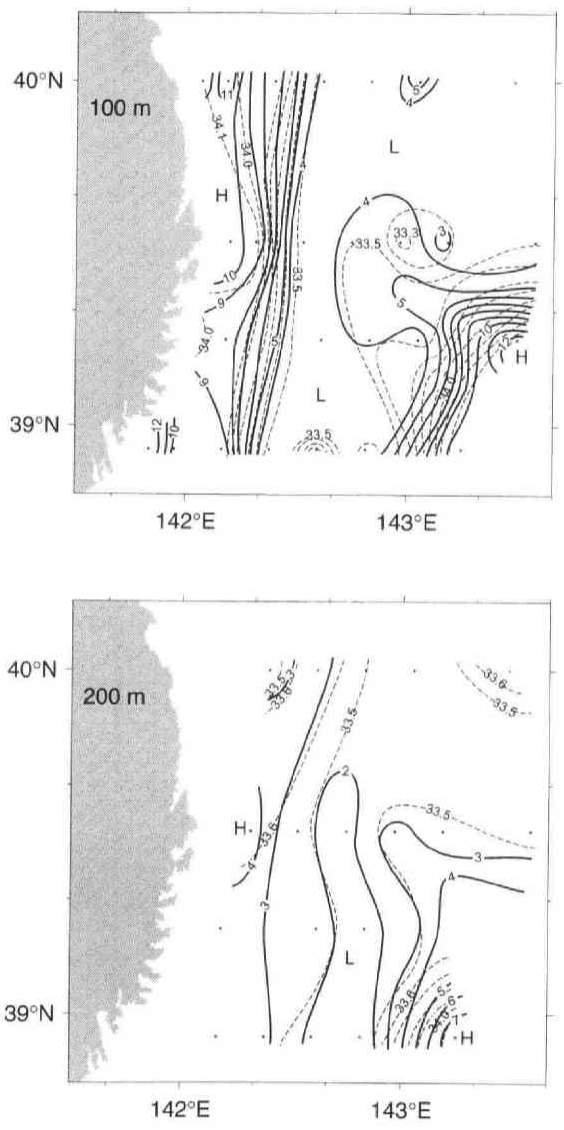

Figure 3.13: As Fig. 3.12 except in August 1980.

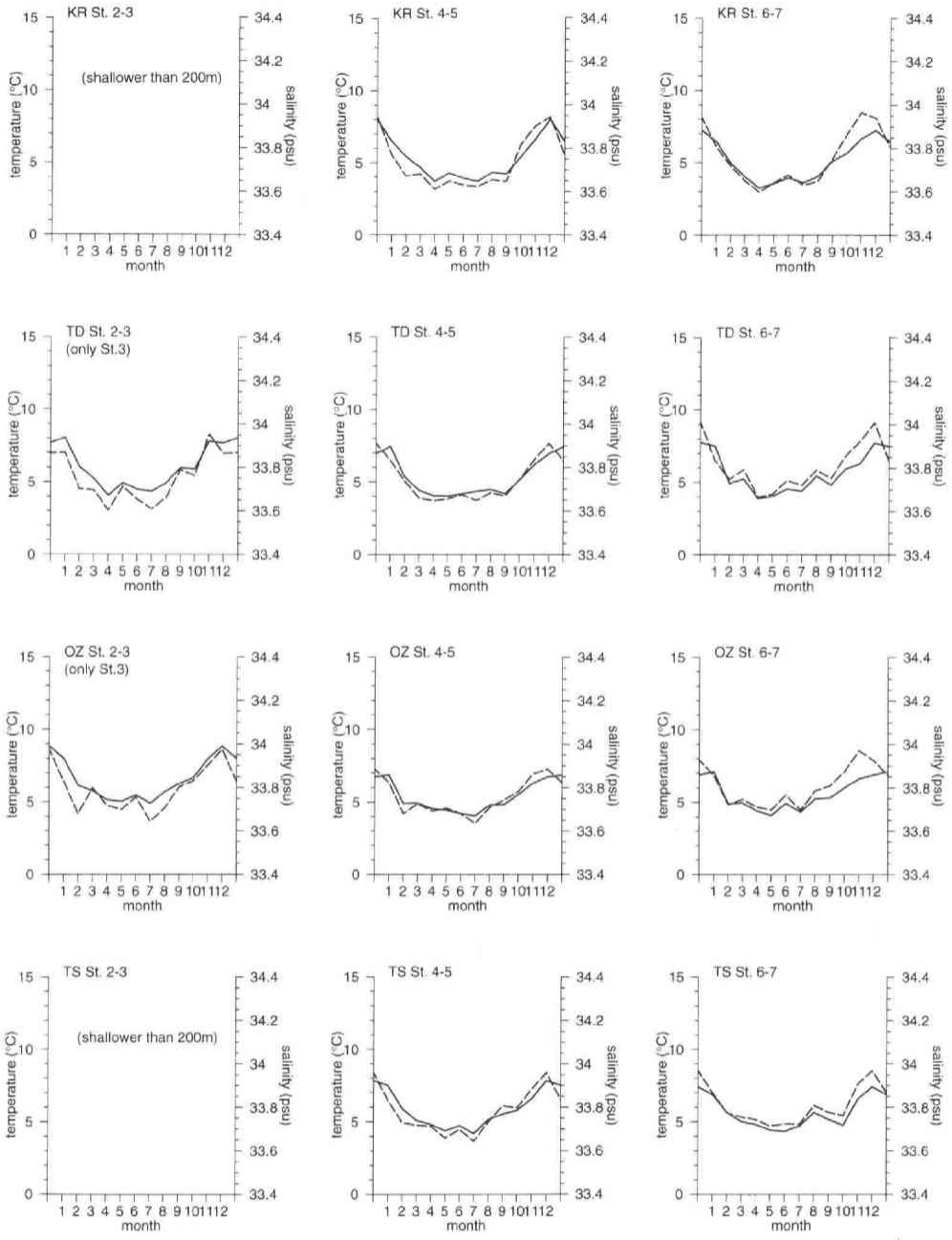

Figure 3.14: As Fig. 3.9 except at 200 m depth. Water depths at sub-groups KR St. 2-3, and TS St. 2-3 are shallower 200 m, and water depths at Sts. 2 on TD and OZ are also shallower than 200 m.

4 Seasonal variation of the vertical structure of the Tsugaru Current off Sanriku Coast, and appearance of the forerunner of Tsugaru Current

4.1 Introduction

The Tsushima Current in the Japan Sea flows through Soya Strait into the Okhotsk Sea, and forms the Soya Current. Between the subtropical water of the Soya Current and the subarctic water in the Okhotsk, a conspicuous front having large temperature and salinity gradients is formed. In summer, the differences of temperature and salinity across the front exceed 10°C and 0.8 psu as shown in Fig. 4.1. The seasonal variation of the nature of the Soya Current is generally much larger than the Tsugaru Current, however, high temperature and high salinity signatures of the Soya Current are completely disappeared in mid winter (e.g. Aota, 1971, 1975). Due to its high salinity, the Soya Current water tends to subside beneath the surrounding water having much less salinity, especially in low temperature circumstance.

Especially in November through December before its disappearance, and in March through May after its revival, the warm Soya Current water is found on the shelf bottom as shown in Fig 4.2. Takizawa (1982) investigated seasonal variation of the characteristics of the Soya Current water, and pointed out that salinity value of water after its revival in spring is about 34 psu, which corresponds to that of typical Soya Current water in other seasons, but its temperature is much lower than those in other seasons. Takizawa (1982) defined this water as the forerunner of the Soya Current.

In the case of the Tsugaru Current water, it also originates from the Tsushima Current, however, it does not show such conspicuous contrast with surrounding water as the Soya Current does, and subsidence of warmer water beneath colder water can be found not so frequently. Ueno and Yamazaki (1987) analyzed the data along Todogasaki Line obtained by the Iwate Fisheries Technology Center in the period from 1976 to 1985 (see Fig. 4.3 for the location of the observation line), and gave monthly mean fields of temperature and salinity along this cross-section. The subsurface warm water can be seen above the continental shelf in their cross-sectional temperature field in spring time, typically in March and April. It is found on the bottom in the mean fields, but it appears at mid-depths in the sections in individual months. The subsurface water has temperature value warmer than 5°C and has salinity higher than 33.6 psu. It is accompanied by conspicuous temperature inversion in its upper portion, but its density profile is stable. The subsurface warm water found in spring would correspond to the forerunner of the Soya Current, and may be called as "the forerunner of the Tsugaru Current". In order to clarify the nature of the forerunner of

the Tsugaru Current, we shall analyze the data obtained by the Iwate Fisheries Technology Center in the period from 1971 to 1995 (the data is the same as used in Oguma et al. (2002).

4.2 Data used

The Iwate Fisheries Technology Center has conducted oceanographic observations for each month since 1963 along four coastal observation lines as shown in Fig. 4.3. From 1971, when high precision salinometer was introduced, data precision became higher than before. Position data was also improved in about the same period (Oguma et al., 1999). In this study, dataset obtained by the Iwate Fisheries Technology Center from 1971 to 1995 is used after data quality control (MIRC, 2001). In addition, the analysis of occurrence of the forerunner was extended up to 2001 by using "the Coastal Lines Observation Result" published monthly by the Iwate Fisheries Technology Center.

4.3 Seasonal variations of cross-sectional fields of monthly mean temperature and salinity off Sanriku Coast

Cross-sectional distributions of monthly mean temperature and salinity of 25-years along four observation lines of the Iwate Fisheries Technology Center (Fig. 4.3) are shown in Figs. 4.4 and 4.5, respectively. For each month, the monthly mean temperature distributions along four lines resemble to each other. The seasonal variations are more eminent in the monthly mean distributions. In addition to a warm and saline Tsugaru Current water near the coast, a dome-shape upheaval of cold and less saline water can be seen in the middle part of the cross-section in general. This upheaval corresponds to the First Branch of the Oyashio.

Oguma et al. (2002) discussed about seasonal variations of monthly mean horizontal distributions at 100m depth and 200m depth of temperature and salinity, and pointed out that the lowest temperature appears in April at 100m depth, and that the temperature at 200 m depth also appears in April but this low temperature is maintained until August or September. This tendency can be recognized also in Fig. 4.4.

In the temperature distributions (Fig. 4.4), isotherms slope down coastward from sea surface to the shelf bottom and warm water region is formed near the coast at each observation line in each month. The salinity distributions (Fig. 4.5) are rather complicated, but the warm water region is generally corresponds to high salinity region. It suggests that the warm and saline water mass corresponding to the Tsugaru Current water is found in the monthly mean

fields even in mid winter. Although the warm and saline Tsugaru Current water disappears often in mid winter in the temperature and salinity distributions in individual months, the monthly mean fields indicate that the Tsugaru Current is maintained even in winter in many of years. The temperature front formed offshore of the warm Tsugaru Current water is much clearer from June through October. In Fig. 4.4, the position of temperature front of the Tsugaru Current along southernmost Tsubakishima Line is located offshoreward and the width the Tsugaru Current is widened, in comparison with those along the northern lines. This supports the suggestion by Oguma et al. (2002) that the Tsugaru Current may flow to offshore along the northern edge of the Kuroshio Extension.

Monthly mean temperature of the flow region of the Tsugaru Current tends to increase southward in the region to the south of Todogasaki Line. This tendency can be seen in horizontal temperature distributions in Figs. 6 and 10 of Oguma et al. (2002). This tendency is seen even at 200 m depth, and it could not be warmed by atmospheric heating. Presumably, it would be understood that the southern near-shore region is often influenced by warm water originated from south. When high temperature and high salinity water is observed at Tsubakishima Line, it is often described in "the Coastal Lines Observation Result" that the high temperature and high salinity water is brought by northward intrusion of Kuroshio. It has never observed that the Kuroshio water flows northward directly along the coast. However, if the Tsugaru Current water is carried to offshore direction near Tsubakishima Line, the northward intrusion of the high temperature and high salinity water strongly influenced by Kuroshio water would occur. We need much more detailed analysis in this region.

In the monthly mean temperature distributions in March and April (Fig. 4.4), relatively high temperature water can be found on the bottom of the continental shelf. except in the distribution along Tsubakishima Line in April (Weaker but similar tendency is also seen in some of February distributions). This is the same as subsurface warm water found by Ueno and Yamazaki (1987) in their 10 years mean distributions. We shall discuss this water in the next section as a forerunner of the Tsugaru Current.

The cross-sectional distributions of salinity are more complicated than those of temperature distribution. Except the distributions for January when the vertical mixing due to surface cooling is very active, a thin layer of low salinity water is often found near sea surface. These low salinity waters appear to be generated by fresh water discharge or by rainfall. Very low salinity water of the Coastal Oyashio (Ohtani, 1971) originated from sea ice of Okhotsk Sea might be one of the generation mechanism. The temperature of this thin surface layer is usually higher than below, and no temperature maximum layer is accompanied. However, it is somewhat difficult to define the forerunner of the Tsugaru Current

from the salinity distributions. Another salinity maximum layer is often observed in mid-layer from 50m depth to 100m depth. This salinity maximum layer appears to have a large extent from near-coast to outside of the area under consideration, though it has sometimes interrupted by the First Branch of the Oyashio. The temperature maximum layer of large extent is sometimes generated with associated to such salinity maximum layer of large extent in individual cross-sections. It is seldom to appear in the monthly mean distribution, but the situation in the distribution along Kurosaki Line in March would give an example. In the discussion in the next section, we shall pay our attention to subsurface high temperature water only above the continental shelf, and define the forerunner.

4.4 The forerunner of the Tsugaru Current

4.4.1 Occurrence frequency of the forerunner

Firstly, we checked "the Coastal Lines Observation Result" published monthly from 1971 to 2001, and searched frequency of appearance of warm water layer above the bottom of shelf slope. Not only the warm water layer, which touches to the bottom, but also that found in mid-depths and accompanied with considerable temperature inversion in its upper part are considered. Clear warm water layer appears usually in March and April, but it is not found in every year. The subsurface warm water is found most frequently in April. If it is found in March, it is also found in April cross-section in the same year. Therefore, cross-sectional temperature distributions in April were focused.

We constructed the cross-sectional distributions in April (and adjacent months if necessary) using MODS2001. We focused our attention to the Tsugaru Current region (the continental shelf region or near-shore 4 observation points along each observation lines), and made survey whether the forerunner of the Tsugaru Current, namely the subsurface warm water, is found or not. However, the configuration of the subsurface warm water cannot be well defined as in the case of the forerunner of the Soya Current, and sometimes it is hard to identify. So we defined three cases (1) the forerunner clearly exists, (2) it is not clear but the forerunner appears to exist, and (3) the forerunner is not recognized. The results are summarized in Table 4.1, and the three cases are shown by white circle, white triangle and cross mark, respectively.

As seen in Table 4.1, the forerunner of the Tsugaru Current does not appear every year like that of the Soya Current. Among analyzed 31 years, the forerunner was not observed along any of the observation lines in six years of 1977, 1979, 1980, 1983, 1990 and 1999. The forerunner was clearly observed along all of the observation lines in three years of 1974, 1986,

and 1989. The forerunner of the Tsugaru Current is not observed in every year along every observation lines. On the other hand, the forerunner of the Soya Current is observed every year, and along long extent of the Okhotsk coast of Hokkaido.

The occurrence of the case (1) that the forerunner is observed clearly is 14 times at Kurosaki Line, 16 times at Todogasaki Line, 10 times at Osaki Line, and 4 times at Tsubakishima Line, respectively. If we include the ambiguous case (2), it becomes 18, 18, 16, 7 times, respectively. Appearance frequency is considerably smaller along the southernmost Tsubakishima Line in comparison with the other northern three lines. It declines in the south side of Todogasaki Line, at where width of shelf slope becomes the narrowest and oceanic condition slightly changes. However, appearance period does not delay over one month in each case.

4.4.2 The case of the forerunner clearly observed at all four observation lines

In this subsection, we shall investigate the structure of the forerunner of the Tsugaru Current in three years of 1974, 1986 and 1989 when the forerunner was clearly observed at all four observation lines. In Fig. 4.6, the temperature distributions in the cross-section along each observation in April are given for these three years. The forerunner is seen on the bottom of the continental shelf along the four observation lines in April 1986. In 1974 and 1989, the region of the forerunner is more confined, but its warmest core appears at mid-depth. The core temperature of the forerunner is the highest in 1974, and exceeds 7°C along Kurosaki and Osaki Lines. However, the temperature is almost comparative in the other lines. In general, the configuration of the forerunner is changeable cross-section by cross-section, but the core temperature is almost identical for all four lines in each year. As discussed before, the monthly temperature tends to increase southward along the coast, suggesting intrusion of the warm water influenced by the Kuroshio water. The fact that the core temperature of the forerunner is constant in each year appears to indicate that the forerunner water had been carried from north. However, any time lag among four lines cannot be detected due to the observation interval about one month.

In the case of 1989, the core of the forerunner shifts gradually offshore from Todogasaki Line through Tsubakishima Line. In the cross-section of Tsubakishima Line, the western edge of the subsurface warm water can be seen still on the shelf bottom, but the main body of the forerunner is found offshore. This may indicate that the Tsugaru Current leave the coast near the southernmost Tsubakishima Line. Using monthly mean temperature distributions, Oguma et al. (2002) suggested that the Tsugaru Current may turn to the east in some

occasion. The situation in April 1889 would give an example of such behavior of the Tsugaru Current.

4.4.3 The case of the forerunner disappeared

The forerunner of the Tsugaru Current was not observed even in April along any of observation lines for seven years during 31 analyzed years (Table 4.1). Namely, the forerunner is almost not observed for about 39% of years. This would be a reason why the forerunner of the Tsugaru Current has not been investigated before.

An example of temperature distributions of when no forerunner was seen is shown along four observation lines are shown for April, 1990 in Fig. 4.7. The Tsugaru Current was always observed in the winter from 1989 to 1990. No forerunner tends to be formed after the winter that the conspicuous Tsugaru Current is observed, but there are some exceptions as discussed in the following sub-section.

4.4.4 An example of change of oceanic condition in spring

The structure of the Tsugaru Current is very changeable, and it is usually hard to follow the changes between succeeded months. The temporal variation of the structure in the cross-sectional temperature distribution is shown in Fig. 4.8 for Kurosaki Line from January to June in 1981. The situation in February is somewhat similar to that in January, and significant warm water corresponding to the Tsugaru Current exists subsurface of coastal region for these months. However The temperature of the subsurface warm water decreases about 2°C from January to February. The forerunner of the Tsugaru Current appears in the distribution of March and April. However, the core temperature of the forerunner in April is increased about 1°C than that in March. The temperature of the water on the bottom increases continuously through May and June. These distributions indicate that the warm water in the Tsugaru Current region is always renewed, and its properties may be not the same as that of the previous month. This is one of the cases that the subsurface warm water can be found as the forerunner even if a significant Tsugaru Current is observed in mid-winter. From the variation of the structure shown in Fig. 4.8, the subsurface warm water seems to be formed by intrusion of the Oyashio water or the First Branch of the Oyashio water to the surface layer. However, the water of the forerunner is not the same as that of the Tsugaru Current in the previous months. At this point, the situation shown in March and April distributions can be understood as the intrusion of the Tsugaru Current water submerged underneath of the environmental cold and less saline water. In order to clarify

the formation mechanism or the evolution of the forerunner of the Tsugaru Current, we need to conduct much more detailed and frequent observations in the region under consideration.

4.5 Concluding remarks

In this study, seasonal variations of monthly mean distributions of temperature and salinity along the cross-section along four observation lines of the Iwate Fisheries Technology Center were analyzed.

The subsurface water in the Tsugaru Current region is clearly seen in March and in April, in the distributions averaged over 25 years from 1971 to 1995, as shown by Ueno and Yamazaki (1987). We call this subsurface warm water as the forerunner of the Tsugaru Current, as it has somewhat similar nature to the forerunner of the Soya Current discussed by Takizawa (1982). The forerunner of the Tsugaru Current does not necessarily appear every year, while that of the Soya Current appears in every year. Also, the forerunner of the Tsugaru Current may appear in mid-depths, but that of the Soya Current appears on the bottom of the shelf slope.

On T-S diagram, isopycnal curve tends to be parallel with temperature axis at lower temperatures, and salinity mainly controls water density. Oguma et al. (2002) showed that the water temperature in the region of the Tsugaru Current becomes minimum values at 100 m depth in March or in April. This would give the reason why the forerunner of the Tsugaru Current appears in March or in April. If the water mass is saline than surrounding Oyashio water, it could sink to subsurface layer and form temperature maximum layer in low temperature conditions.

The oceanic structure off Sanriku Coast is very complicated and very changeable. It shows considerable seasonal variations, but it is hard to show typical seasonal variations from individual time series of temperature and salinity fields of individual months. As discussed in this paper and Oguma et al. (2002), seasonal variations can be discussed only in monthly mean fields. The forerunner of the Tsugaru Current is exceptional phenomena that occurs in fixed months in early spring. The results of this study may give a reference to investigate the variations of the Tsugaru Current region and its adjacent region.

References

Aota, M. (1971): Study of the variation of oceanographic condition north-east off Hokkaido in the Sea of Okhotsk III. Low Temp. Sci. A29:213-224 (in Japanese).

Aota, M. (1975): Studies on the Soya Warm Current. Low Temp. Sci. A33:151-172 (in Japanese).

Motoi, T., N. Ono and M. Aota (1982): Cold water masses appeared in the Okhotsk Sea near Hokkaido in summer. Low Temp. Sci, A41:199-206 (in Japanese).

MIRC (2001): MIRC Ocean Dataset 2001 – Documentation. MIRC Technical Report No. 1, pp.169.

Ohtani, K. (1971): Studies on the change of the hydrographic conditions in the Funka Bay – II. Characteristics of the waters occupying the Funka Bay. Mem. Fish. Hokkaido Univ., 22, 58-66 (in Japanese).

Oguma, S., T. Suzuki, Y. Nagata, H. Watanabe, H. Yamaguchi and S. Takasugi (1999): Errors in oceanic dataset often generated in data processing and in data management – II Case of the Iwate Fisheries Technology Center, and treatment of duplicated data –. Jour. Japan Soc. Mar. Surv. Tech., 11(2), 11-18 (in Japanese).

Oguma, S., T. Suzuki, and Y. Nagata (2002): Seasonal Variations in the sea off Sanriku Coast, Japan. J. Oceanogr., 58, 825-835.

Takizawa, T. (1982): Characteristics of the Soya Warm Curent in the Okhotsk Sea. J. Oceanogr. Soc. Japan, 38, 281-282.

Ueno, Y. and M. Yamazaki (1987): Some features of seasonal changes in the Tsugaru Warm Current along the Sanriku-Coast. Bull. Tohoku Reg. Fish. Res. Lab., 49, 111-123 (in Japanese).

Wakatsuchi, M., K. I. Oshima (1990): Observations of ice-ocean eddy streets in the Sea of Okhotsk off Hokkaido Coast using radar images. J. Phys. Oceanogr., 20, 595-594.

Table 4.1: Occurrence of the forerunner of the Tsugaru Current along four observation lines in April in the period from 1971 to 2001. Circles indicate that clear subsurface warm and saline layer appeared, triangles that some signature is observed and crosses that no subsurface warm layer is recognized over the continental shelf region.

	Kurosaki line	Todogasaki line	Osaki line	Tsubakishima line
1971	○	○	○	×
1972	△	×	×	×
1973	○	○	×	×
1974	○	○	○	○
1975	△	×	×	×
1976	○	○	○	×
1977	×	×	×	×
1978	△	○	△	×
1979	×	×	×	×
1980	×	×	×	×
1981	○	○	○	×
1982	○	○	△	×
1983	×	×	×	×
1984	×	×	△	×
1985	○	○	×	○
1986	○	○	○	○
1987	○	○	○	×
1988	×	△	×	×
1989	○	○	○	○
1990	×	×	×	×
1991	×	×	△	×
1992	×	○	×	△
1993	×	×	×	×
1994	×	○	×	×
1995	○	○	○	×
1996	○	○	○	×
1997	×	×	△	△
1998	○	×	△	△
1999	×	×	×	×
2000	△	○	×	×
2001	○	△	○	×

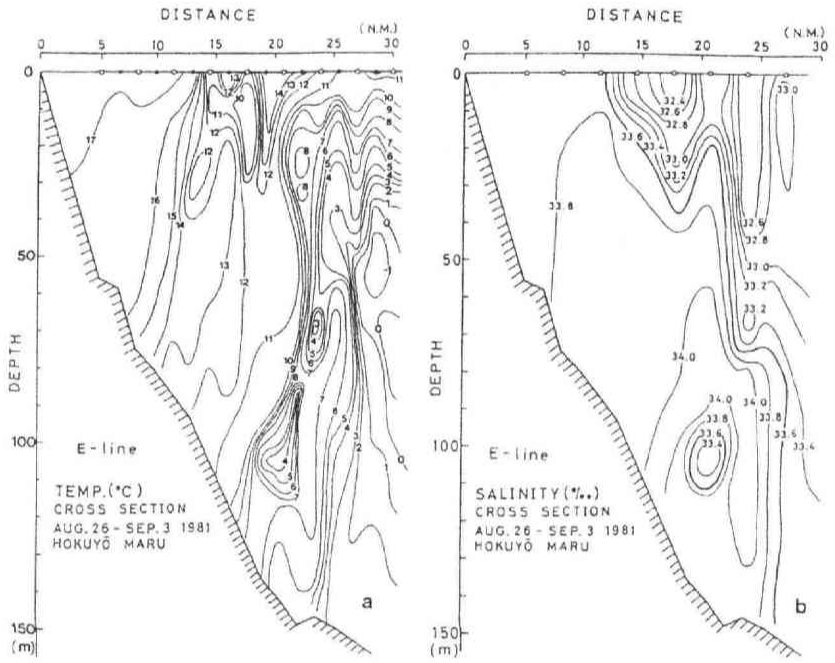

Figure 4.1: Cross-sectional distributions of temperature (°C: left) and salinity (psu: right) along the lone extending northeast off Mombetsu on 26 August-3 September, 1981 (Motoi et al., 1982).

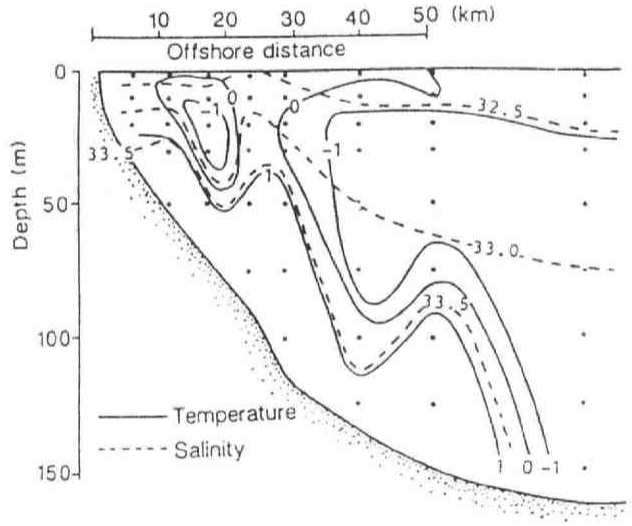

Figure 4.2: Cross-sectional distribution of temperature (°C: full line) and salinity (psu: dashed line) along the line extending northeast off Mombetsu in late April, 1984 (Wakatsuchi and Oshima, 1990). Forerunner of the Soya Current can be seen on the bottom slope.

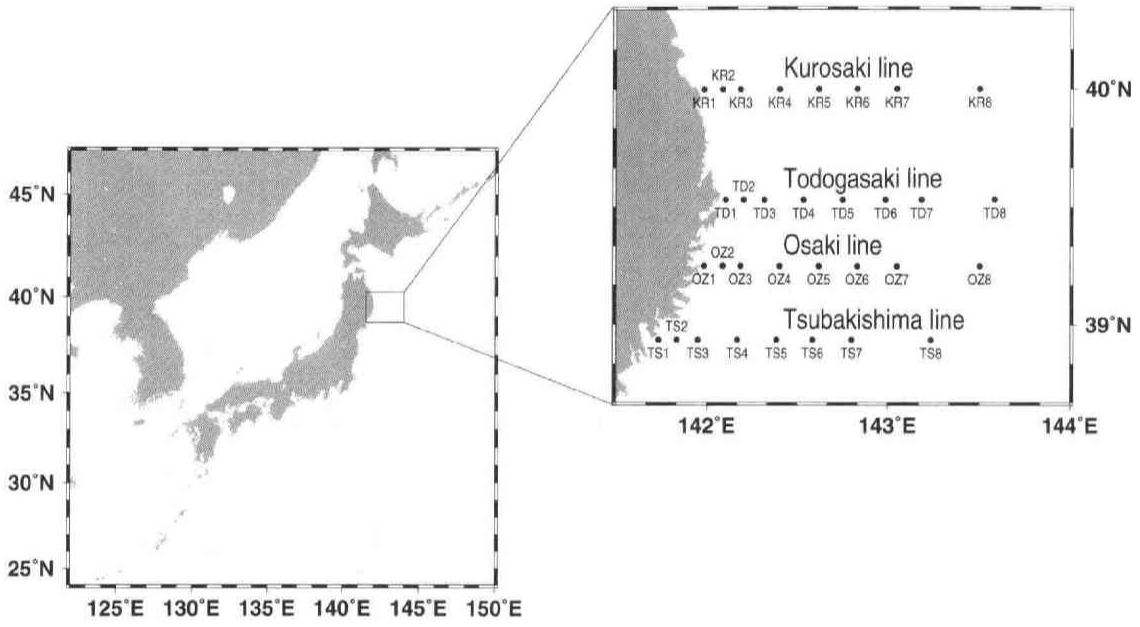

Figure 4.3: Distribution of the observation points along routine Coastal Observation Lines of the Iwate Fisheries Technology Center. The lines are called Kurosaki Line, Todogasaki Line, Osaki Line and Tsubakishima Line from north to south.

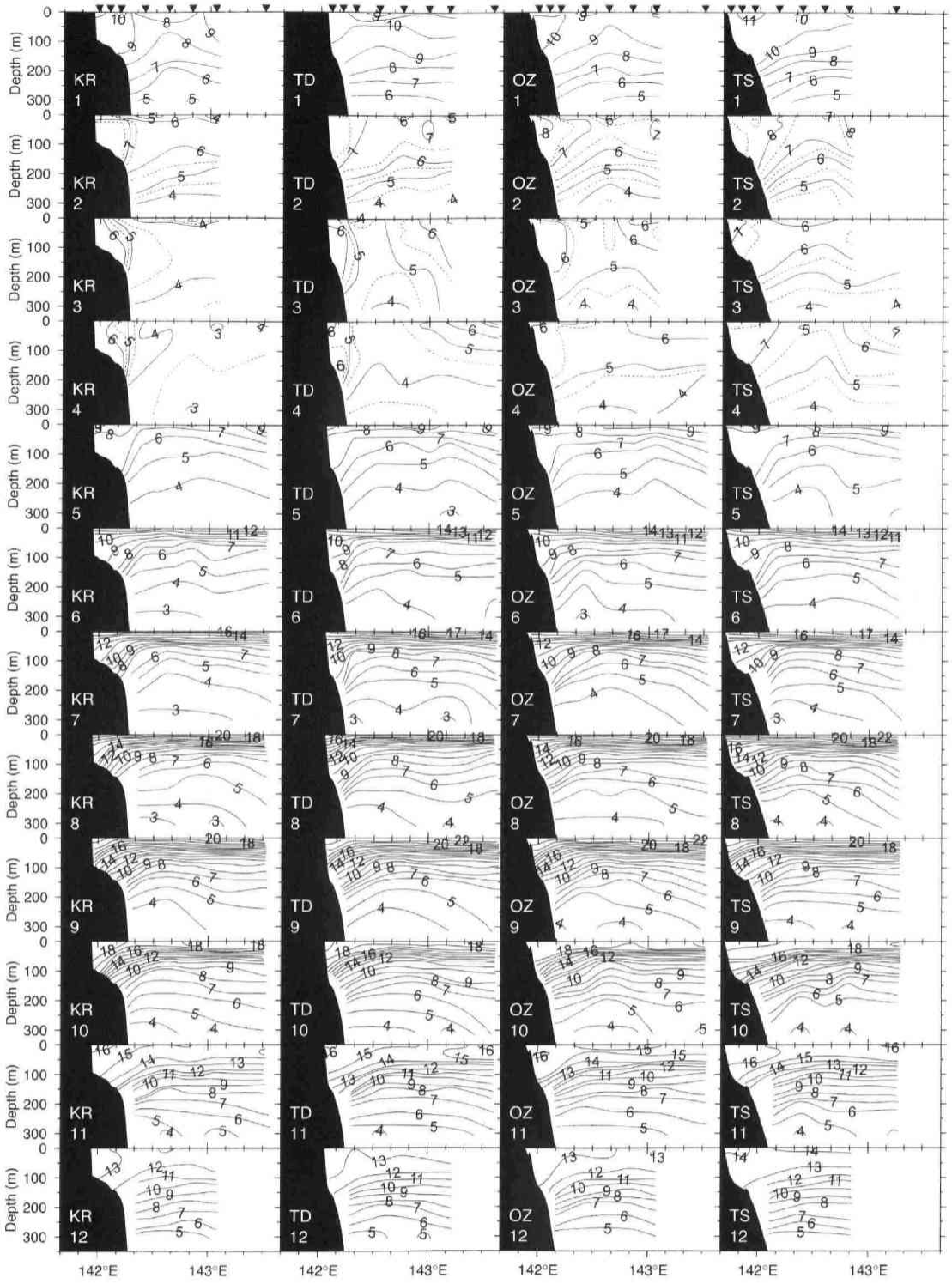

Figure 4.4: The monthly averaged temperature fields along Kurosaki Line (leftmost figure), Todogasaki Line (left middle figure), Osaki Line (right middle), and Tsubakishima Line (rightmost figure). The fields are given from January to December downward from top. Numerals attached to isotherms indicate temperature in °C (supplementary isotherm of 5.5 °C is given for the field in April).

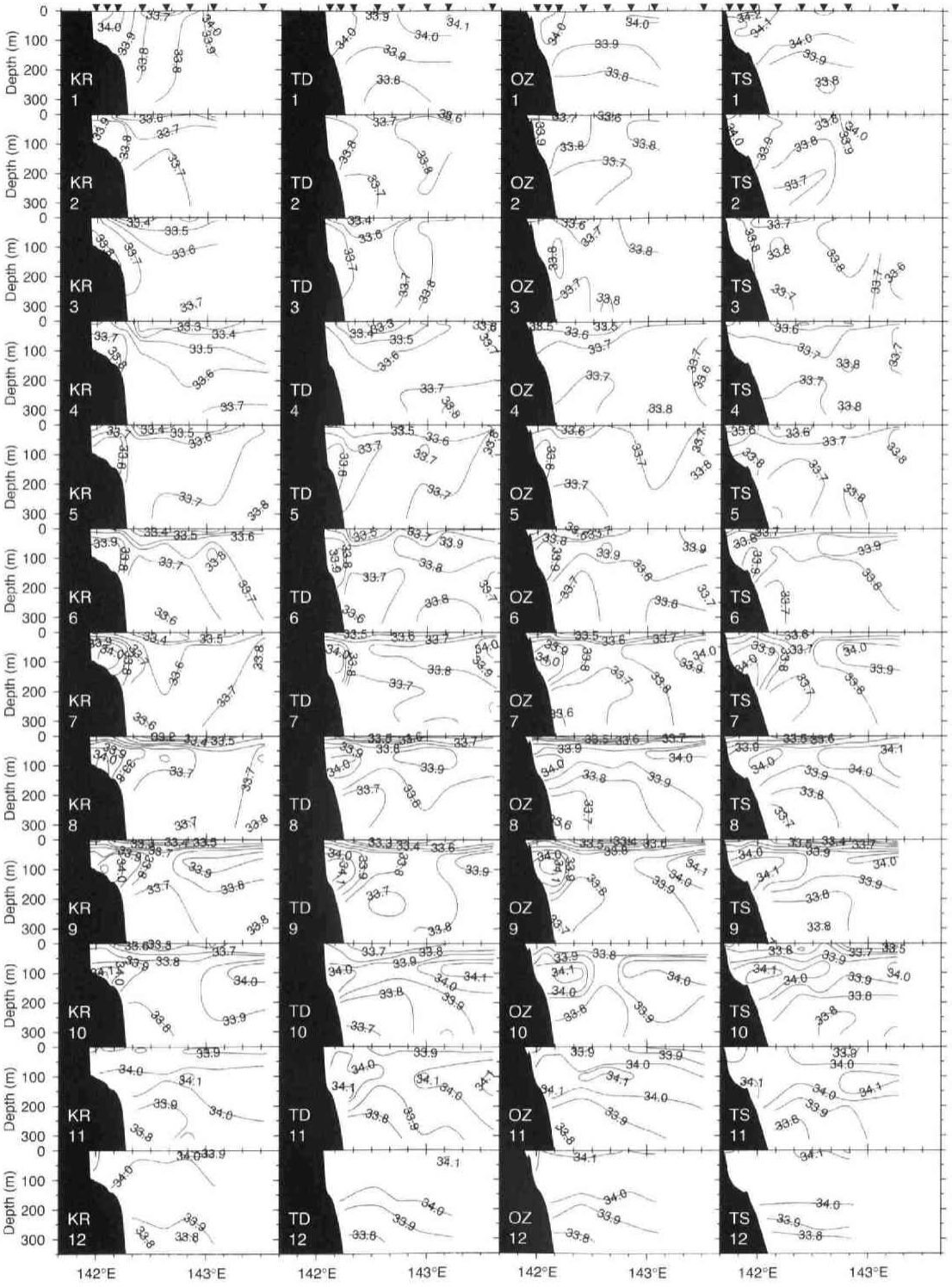

Figure 4.5: Same as in Fig. 4 except for isohalines in psu.

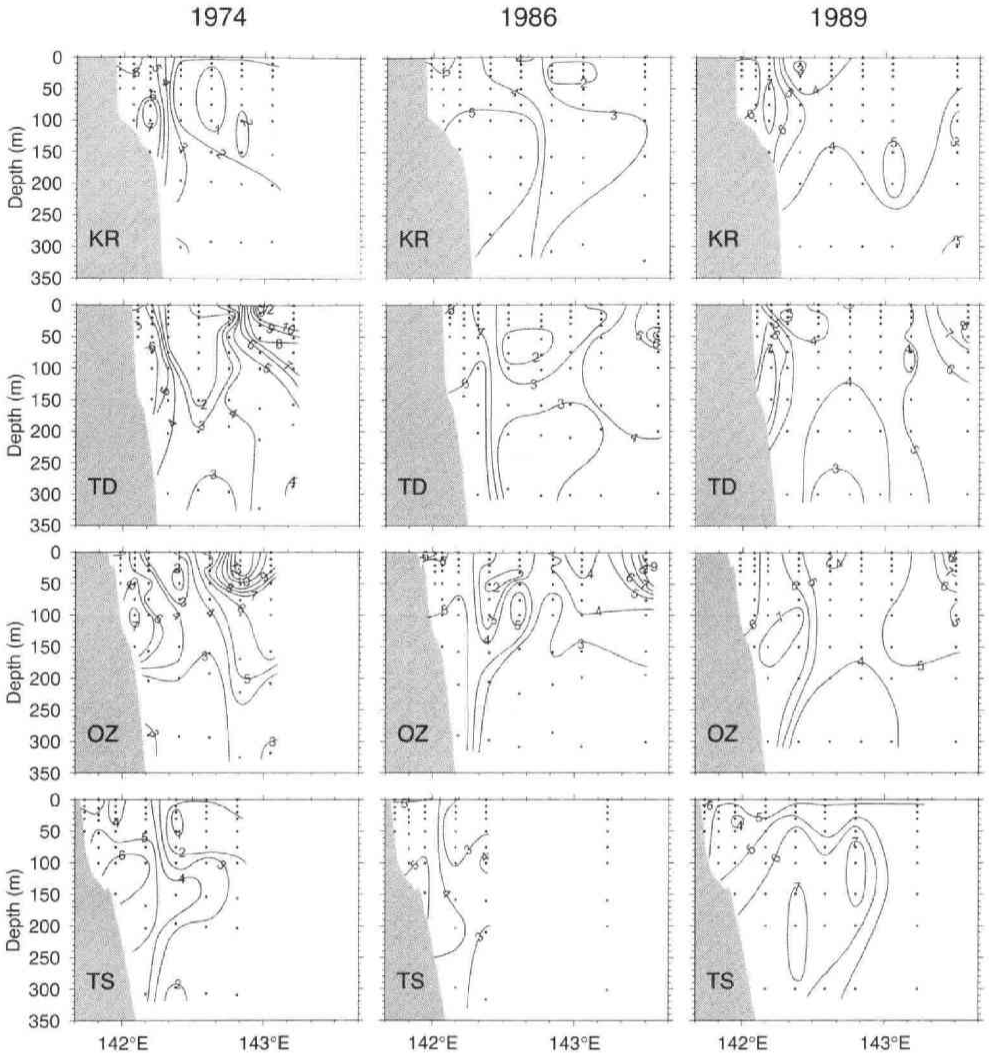

Figure 4.6: Cross-sectional temperature distributions along Kurosaki Line (KR: the first rows), along Todogasaki Line (TD: the second row), along Osaki Line (OZ: the third row) and along Tsubakishima Line (TS: the fourth row) in April 1974 (left figures), April 1986 (middle figures), and April 1989 (right figures). Isotherms are given at 1 °C interval. Numerals attached to isotherm indicate temperature in °C.

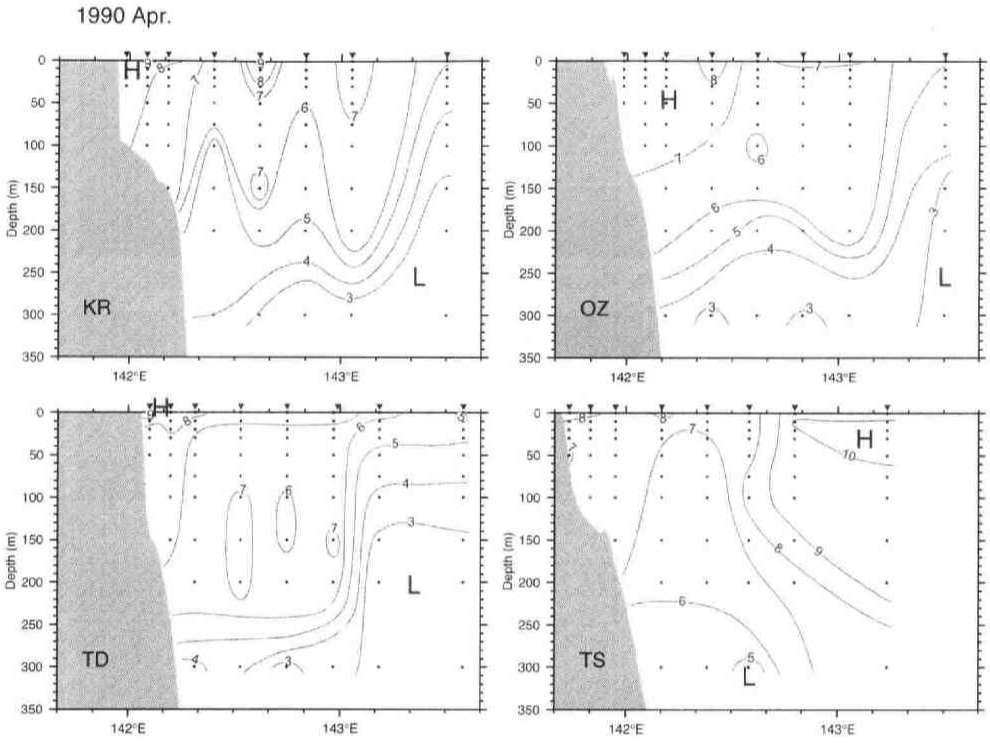

Figure 4.7: Cross-sectional temperature distributions along Kurosaki Line (KR: upper left), along Todogasaki Line (TD: lower left), along Osaki Line (OZ: upper right) and along Tsubakishima Line (TS: lower right) in April 1990. No forerunner can be seen in this year.

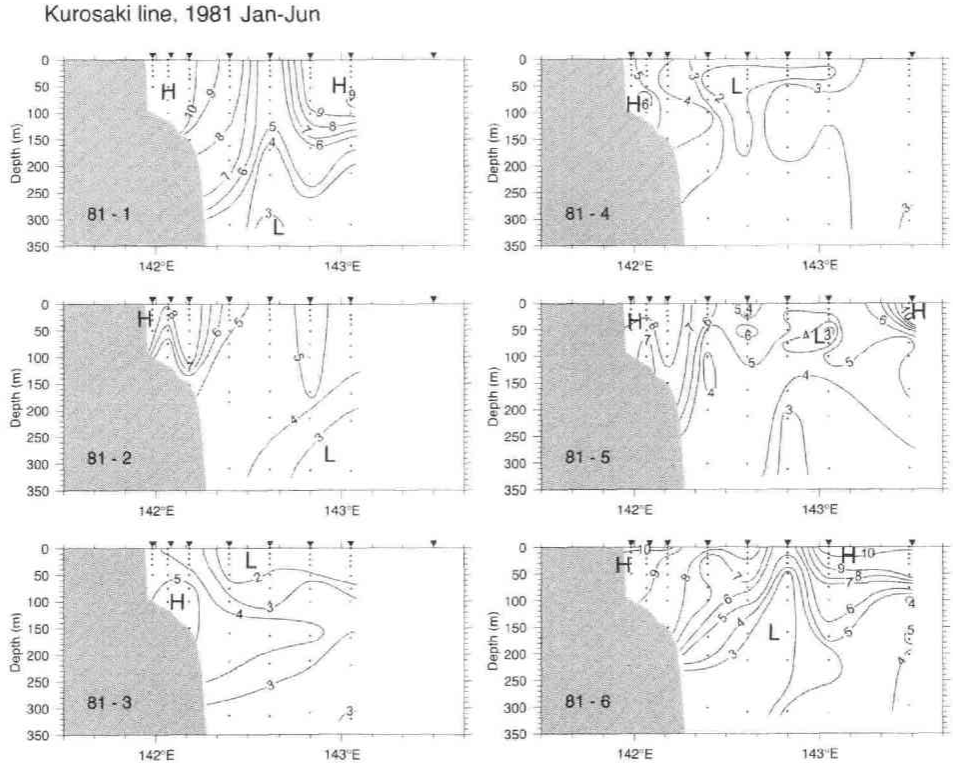

Figure 4.8: Temporal variation of the cross-sectional temperature distribution along Kurosaki Line from January to June 1981.

General Conclusion

In the present study, the dataset of temperature and salinity obtained by the Iwate Fisheries Technology Center from 1971 to 1995 was analyzed, in order to point out an importance of discussion for data interpolation and oceanic condition, and to indicate the seasonal variations of mean fields of temperature and salinity in the sea off Sanriku.

In chapter 1, a new reliable data interpolation scheme was designed to produce standard depth dataset, using temperature and potential density values as independent variables. This scheme could avoid pseudo density inversion effectively in areas with complex hydrographic structure such as the sea off Sanriku. It gave almost the same results as the conventional scheme, in which temperature and salinity as independent variables are used, in the seas of moderate conditions such as the subtropical regions. Standard depth dataset used in this study was produced using this new interpolation scheme.

In chapter 2, occurrence frequency distributions of temperature were investigated, in order to check extreme values for the sea off Sanriku. It was shown that the temperature distribution patterns deeper than 150 m depth were considerably skewed. Especially at 300 m depth, frequency distribution was so slanted to lower temperature value that highest temperature value was exceeding $m+5\sigma$ (m: mean value and σ: standard deviation). The extremely high temperature (and high salinity) values were revealed as the pure Kuroshio Water intruded into the region owing to an abnormal approach of large warm-core ring to the Sanriku Coast, or an abnormal northward extension of the Kuroshio along the coast. It happened very seldom (only twice in the 25-year period analyzed), but the extremely high temperature observed was real. As an applied study of this chapter, "skewness" of occurrence frequency of temperature in the North Western Pacific and the North Atlantic was investigated. Large skewness value of occurrence frequency of temperature was found not only in the western North Pacific area including the sea of Sanriku, but also around Gulf Stream region in the North Atlantic. Results of this applied study were summarized in appendix. Application of skewness value of occurrence frequency may be useful analysis method for studies on infrequent phenomena. Large skewness suggests an existence of extremely high value such as over five times of standard deviation from mean value. This means that temperature, for example, in the targeted area usually changes in small deviation, but extremely warm water mass is brought as an exceptional case by infrequent phenomena. The infrequent phenomena can make oceanic condition much complicated in each individual case. As shown in appendix, skewness of temperature or salinity in the sea off Sanriku is considerably greater than other regions. This point agrees with previous studies, which suggested complexity of water mass

distributions in the sea off Sanriku.

After the case studies of extreme values in the dataset, seasonal variations of the sea off Sanriku were investigated in chapter 3. The 25-year mean temperature and salinity fields at 100 m depth displayed clear seasonal variations of distributions of Tsugaru Current Water, Oyashio Water and Kuroshio Water. The front between the Tsugaru Current and the first branch of Oyashio was clearly shown in temperature and salinity fields at 100 m depth in the summer-to-autumn season. Its signature became clearest in September, but was weakened or disappeared in winter to spring. The Tsugaru Current was seen all the year in the mean fields, while it was thought that the Tsugaru Current disappeared in winter season. Although there were many differences among temperature and salinity distributions of each individual month, however, monthly mean fields could show typical seasonal variations. On the contrary, at 200 m depth, the seasonal variations of typical water masses were hardly seen in the mean fields of both temperature and salinity. This result may suggest a reason why 100 m depth distributions were mainly used in the previous studies of the sea off Sanriku.

Finally in chapter 4, seasonal variations of monthly mean distributions of the vertical cross-section along four coastal observation lines were discussed. Subsurface maxima of temperature and salinity were clearly seen in March and April in the mean fields in mid-depths or on the bottom in the shelf slope. In the present study, this subsurface warm saline water in spring was named the forerunner of the Tsugaru Current, since it had somewhat similar nature to the forerunner of the Soya Current. Although the forerunner of the Tsugaru Current was not observed in every year along every observation lines, appearance frequency was higher at the northern three observation lines. To be called as "forerunner", the maxima of temperature and salinity should be once disappeared before their appearance. However, there was an example in 1981 that the Tsugaru Current was recognized in winter and its forerunner was found in the proceeding months. This example suggested that more detailed and frequent observations were needed to chase the change of the forerunner.

The oceanic structure off Sanriku Coast is very complicated and very changeable as shown in the present study. It shows considerably large seasonal variations, but it is difficult to indicate typical seasonal variations from individual time series of temperature and salinity fields in individual months. However, seasonal variations could be discussed in monthly mean fields in this study. The existence of forerunner of the Tsugaru Current was also suggested as exceptional phenomena that occur in fixed months in early spring. The results of this study may provide a reference to the seasonal variations of the sea off Sanriku.

Acknowledgment

It is great pleasure to acknowledge the contribution of Professors Kimio Hanawa, Toshio Suga, Shoichi Kizu, Hiroshi Kawamura, Futoki Sakaida and Takakiyo Nakazawa of Tohoku University for their valuable advice.

I would like to thank Drs. Yutaka Nagata and Akira Tomosada of Marine Information Research Center for their comments and encouragement. This study would not be accomplished without their continuous support.

I would like to express my great thanks to the Iwate Fisheries Technology Center for giving permission to use valuable observation dataset and publications. I wish to thank Mr. Satoru Takasugi of the Miyako Regional Development Bureau, Mr. Kiyoshi Nozawa of Iwate Prefectural Government, Dr. Hidetoshi Watanabe and Ms. Hatsuyo Yamaguchi of Sanyo Techno Marine, Inc., for their contributions to the data analysis.

This work was partly supported by the Nippon Foundation and the Ministry of Education, Culture, Sports, Science and Technology (International Cooperative Experiments on North Pacific Subarctic Gyre and Climate Change: SAGE).

Finally, I would like to deeply acknowledge Dr. Toru Suzuki, my parents and brother for their sufficiently kind supports.

Appendix

A Skewed occurrence frequency of water temperature and salinity in the subarctic regions

A.1 Introduction

During data analysis of dataset obtained by the Iwate Fisheries Technology Center in the sea off Sanriku Coast, Japan, we found that frequency distributions of observed temperature and salinity in the Mixed Water Region range between the Oyashio and Kuroshio Fronts are very skewed, and usual techniques of quality control such as range check are hard to apply (Oguma and Nagata, 2002). For example, some of the temperature values observed at 300 m depth exceed $m+5\sigma$ (m: mean and σ: standard deviation) as shown in Fig. 6 of Oguma and Nagata (2002). Although the frequency of high temperature values is low, they are real, and show that pure Kuroshio ater intrudes into the region due to very specific events such as approach of Large Warm Eddies or the abnormal northward intrusion of the Kuroshio Extension along the Sanriku Coast. So, if we apply a 3σ criterion and erase the data which lie outside of the range $m\pm3\sigma$, lots of the real data will be lost.

We represent the non-normal nature of observed frequency distributions by using skewness and kurtosis, and expand our analysis region to the subarctic North Pacific and subarctic North Atlantic Oceans and their surrounding areas.

A.2 Data used and representation of skewed nature of frequency distributions

The Marine Information Research Center (MIRC) of the Japan Hydrographic Association conducted detailed quality checks for the oceanic data mainly distributed in the Northwestern North Pacific, and compiled MIRC Ocean Dataset 2001 (MODS2001: MIRC, 2001). This dataset was used for the analysis in the northern North Pacific. World Ocean Database 2001 (WOD01: Ocean Climate Laboratory, NODC, 2002) was used for the in North Atlantic Ocean. We used data interpolated to standard depths. In WOD01, before the interpolation procedure, range check was made using a 3σ criterion. Since this check was made for 5×5 degree subregions, some of data lie outside of the range $m\pm3\sigma$ calculated newly for 1×1 degree subregion, if we re-analyze these data for 1×1 degree subregions. As WOD01 dataset has various data sources, this process is quite useful to eliminate possible erroneous data.

Analyzed area was divided into subregions of 1×1 degree mesh. In the case of the North Atlantic, we shall try to discuss the occurrence frequency in subregions of 5×5 degree

mesh at depths below 400 m. Since the number of data below 400 m is small in the subarctic Pacific Ocean, the results at there depths were used for the purpose of check.

While there are various methods to represent skewed nature of distribution, we adopted here moments of higher orders, skewness and kurtosis. Skewness is defined by

$$\frac{\sum_{i=1}^{n}(x_i - \bar{x})^3}{(n-1)\sigma^3},$$

and kurtosis by

$$\frac{\sum_{i=1}^{n}(x_i - \bar{x})^4}{(n-1)\sigma^4},$$

where x_i is the value of the i-th data and n the number of data. m is the mean

$$m = \frac{\sum x_i}{n},$$

and σ the standard deviation

$$\sigma = \frac{\sum(x_i - m)}{n-1}.$$

For normal distribution, skewness becomes zero, and kurtosis becomes 3. We use excess of kurtosis,

$$\frac{\sum_{i=1}^{n}(x_i - \bar{x})^4}{(n-1)\sigma^4} - 3,$$

in this paper.

A.3 Mean temperature fields and standard deviation fields in the Western North Pacific

Mean temperature fields in the Western North Pacific for 100 m, 200 m and 300 m depths are shown in Fig. A.2. The mean temperature decreases monotonically from south to north, and the high gradient zone corresponds to the Mixed Water Region between the Kuroshio and Oyashio Fronts. The densest isotherms are seen at the northern edge of the Mixed Water Region at 100 m depth, and its position shifts southward as the depth increase.

Standard deviation fields in the Western North Pacific for 100 m, 200 m and 300 m depths are shown in Fig. A.3. The standard deviation shows high value band extending east-west direction, which corresponds to the highest gradient zone in temperature fields in each depth. This high standard deviation values are thought to be generated by the current path fluctuation of the Kuroshio Extension. The value tends to decrease eastward as north-south temperature gradient is weakened eastward.

A.4 Skewness and kurtosis fields in the Western North Pacific

Skewness and kurtosis fields in the Western North Pacific are shown in Figs. A.4 and A.5, respectively. Kurtosis distribution is a little simpler than skewness distribution in general, but high kurtosis values are generated in the area where high absolute values of skewness occur. This means that the distribution is not only skewed but also has sharp peak and/or long tails.

Peak area in the Mixed Water Region

The temperature distribution at 300 m depth has a high positive value region extending from off Sanriku Coast (39°N, 140°E) toward east-north-east. This high skewness region is not observed in the distributions at 100 m depth. The distribution at 200 m depth shows relatively high values in the corresponding region, but it is masked by another high value region to the south of Kuril Islands. We selected the 1×1 subregion centered at 40°N, 143°E as a representative region, and show frequency distributions of temperature and salinity for various depths ranging from 0 to 500 m in Fig. A.6. The distributions are very skewed below 200 m. It appears that the distributions below 400 m are rather symmetric, but available data are very limited for these deeper depths. The vertical change of the distribution patterns are very similar to those in the sea off Sanriku Coast discussed by Oguma and Nagata (2002) (see Fig. 4 of their paper). Therefore, this skewed nature can be interpreted as a sporadic intrusion of warm eddies ejected by the breaking of meanders of the Kuroshio Extension. The high value region extends eastward to about 155°E near the position of the Shatsky Rise.

Peak area to the south of the Kuroshio Extension

Negative high value regions extending east-west between 30°N and 35°N are seen in the skewness distributions at 200 m depth and at 300 m depth. Some signature can be seen also in the distribution at 100 m depth. We selected the 1×1 subregion centered at 33°N, 144°E, and show the frequency distribution of temperature at 0 m, 100 m, 200 m and 300 m depths in Fig. A.7. The distribution pattern is a mirror of the distributions observed in the Mixed Water Region. This skewness is thought to be generated by sporadic ejection of cold water eddies caused by the southward breaking of meanders of the Kuroshio Extension.

Peak area in shallow layers to the south of the Kuril Islands

In the skewness distributions at 100 m and 200 m depths, there is a high value region extending in east-west direction to the south of the Kuril Islands. However, no corresponding

region can be seen in the distribution at 300 m depth. We selected the 1×1 subregion centered at 43°N, 150°E, and show the frequency distribution of temperature at 0 m, 50 m, 100 m and 200 m depths in Fig. A.8. There can be seen considerably warm water at sea surface, which were mainly observed in summer season. This warm water is confined in the thin surface layer. The maximum temperature value is considerably decreased and its frequency becomes low at 50 m depth. However, some influence of the surface warm water can be seen down to 200 m depth, and the distribution pattern has a tail on higher temperature side, resulting in high positive skewness values up to this depth. This penetration of the warm water may be caused by sporadic surface mixing due to storms, internal waves (and their breaking) and so on. The first two cases are usually associated with high temperature and salinity contrasts in the horizontal direction, but this case with high contrast in the vertical direction.

Another high value region is seen inside the Japan Sea. There are warm and saline water influenced by the Tsushima Current in the surface layer, and very homogeneous Japan Sea Proper Water below it. The interface between two waters is generally sharp, and the high skewness and kurtosis values are due to similar mechanism in the region south of the Kuril Islands.

A.5 Skewness and kurtosis fields in the Western North Atlantic

Skewness and kurtosis distributions in the Western North Atlantic are calculated for subregions of 1×1 degree mesh, and the distributions are shown in Figs. A.9 and A.10 for 100 m and 300 m depths.

The skewness and kurtosis values at 100m depth (Fig. A.9) are small except in the region southeast of Newfoundland Island where the Labrador Current Water encounters the Gulf Stream Water.

At 300 m depth (Fig. A.10), the high north-south gradient zone corresponds to the average position of the Gulf Stream, and the sign of the skewness changes from positive to negative crossing the stream from north to south. The situation is similar to the case crossing the Kuroshio Extension (see Fig. A.4). However, the positive ridge along the north edge of the Gulf Stream is not as conspicuous compared with the corresponding ridge in the North Pacific. The warm rings ejected northward from the Gulf Stream are generally flowed westwards and are re-absorbed into the Gulf Stream, and have a relatively short life-time. Most of the warm eddies ejected from the Kuroshio Extension have larger scales and move northward, and are observed for several years. This result would occur in the difference between the Atlantic and the Pacific. Since the eastern coast of North America runs rather

in the east-west direction to the north of the Gulf Stream, it seems to be not enough space to generate the conspicuous mixed water zone.

The high negative skewness band along the southern edge of the Gulf Stream is strong and comparable to that along the Kuroshio Extension. Ejection of cold eddies southward from the meander of the Gulf Stream is often observed similar to the case of the Kuroshio Extension. This high skewness band extends to about 45°W.

Another large region of negative skewness appears near the Florida Current Region in the 300 m distribution. There are two peaks centered at 31°N, 78°W (Subregion A) and at 27°N, 76°W (Subregion B). The occurrence frequency distributions at 300 m depth are shown in the upper row of Fig. A.11 for these two subregions. Two temperature data lie well below the $m-3\sigma$ in the distribution for Subregion A, both of which were observed on September 7, 1966 (observed temperature are 12.330 and 15.892°C). The distributions at 500 m are shown in the lower row in Fig A.11. In addition to abnormally low temperature values, the vertical temperature gradients between 300 m and 500 m are abnormally high. In Subregion B, the abnormally low temperature value was observed at 300 m depth on February 23, 1970 (temperature value is 6.100°C). This data also shows an abnormally large temperature gradient between 300 and 500 m depths. These data are well isolated from other data in the distributions, and we feel that these data are erroneous, though more elaborate analysis is necessary to verify this. If we omit these data, the skewness would change its sign in these subregions.

Both on the 100 m and 300 m depth surface, the kurtosis distribution is similar to that of the absolute values of skewness. Variations of the occurrence frequency distribution pattern with depth are discussed in the next section.

A.6 Dependence of subregion scale on occurrence frequency distribution

As seen in Fig. A.6, number of available data is considerably decreased with depth, and the detailed nature of the distribution nature is hard to discuss below 500 m in the Western North Pacific. At first, we adopted broader subregions of 5×5 degree mesh for the analysis on 500 m depth surface in the North Atlantic, and found conspicuous bi-modal distribution in the vicinity of the Gulf Stream System. As one of the examples, variations of occurrence frequency distribution of temperature and salinity with depth are shown in Fig. A.12 for the 5×5 degree subregion centered at 37.5°N, 70°W. Both the temperature and salinity distributions show bi-modal feature below 100 m.

In order to understand why such bi-modal structure occurred, we selected two repre-

sentative subregions of 1×1 degree mesh to the north of the Gulf Stream centered at 39°N, 70°W and to the south of the Gulf Stream centered at 37°N, 70°W, respectively. The occurrence frequency distributions of temperature in these subregions are shown in Fig. A.13 for various depths. The distribution patterns below 200 m are very skewed. In the subregion to the north of the Gulf Stream, the distributions below 200 m depth have tails on the high temperature side, while, in the subregion to the south of the Gulf Stream, the distributions have tails on the low temperature side. It should be noted that the distributions have single a peak, and the bi-modal structure is disappeared. The distribution patterns to the north and to the south of the Gulf Stream are the same as those seen on the 300 m depth surface to the north and to the south of the Kuroshio Extension shown in Figs. A.7 and A.8, respectively. When the larger subregion of 5×5 degree mesh is used, it can be shown that bi-modal structure is generated also in the vicinity of the Kuroshio and the Kuroshio Extension.

The horizontal distributions of skewness and kurtosis at 500 m depth based on calculated values for 1×1 degree mesh are shown in Fig. A.14. The distributions are almost identical to those at 300 m.

The distribution pattern would have multiple peaks if analyzed regions are wide and contains multiple domains having water masses quite different from each other. So, we need to have special consideration to make quality control in such regions. Also, the values of skewness might become large in such regions.

A.7 Concluding remarks

In order to make quality check of higher grade, we need to know the nature of occurrence frequency distributions in the region under consideration. If the distribution is skewed, a 3σ criterion is hard to be applied in the procedure of range check. It is shown that large skewness values appear in many regions in the subarctic North Pacific, subarctic North Atlantic and their adjacent regions. We found skewed salinity distributions in surface layers in the sea near the mouth of Amazon River, due to the influence of freshwater discharge.

We need to make surveys where large skewed distributions are seen in the world ocean, but it should be reminded that the distribution nature can be changed due to size of subregions. If we use broad subregions where sharp fronts exist in it, the distribution might be bi-modal. Also, the skewness value is greatly increased if erroneous extreme values exist in the dataset. In the analysis of skewed nature of the distribution, we may apply range check by using a 3σ criterion for sufficiently larger subregions at first, in order to exclude such erroneous value. Even in that case, we should remind that skewness and kurtosis can

represent only some aspect of the skewed distribution. We always need to check the original distribution patterns.

Although we analyzed not only skewness but also kurtosis, kurtosis information basically gives information similar to skewness. In addition, these values are not sufficient to describe bi-modal structure of occurrence frequency. We may need much more sophisticated techniques to describe detailed nature of the distribution.

References

Marine Information Research Center (2001): MIRC Ocean Dataset 2001 Documentation, MIRC Technical Report No. 1, pp 169 (in Japanese).

Ocean Climate Laboratory, NODC (2002): World Ocean Database 2001. National Oeanographic Data Center Internal Report 16, 137pp.

Oguma, S., and Y. Nagata (2002): Skewed water temperature occurrence frequency in the sea off Sanriku, Japan, and intrusion of the pure Kuroshio Water. J. Oceanogr., 58, 789-796.

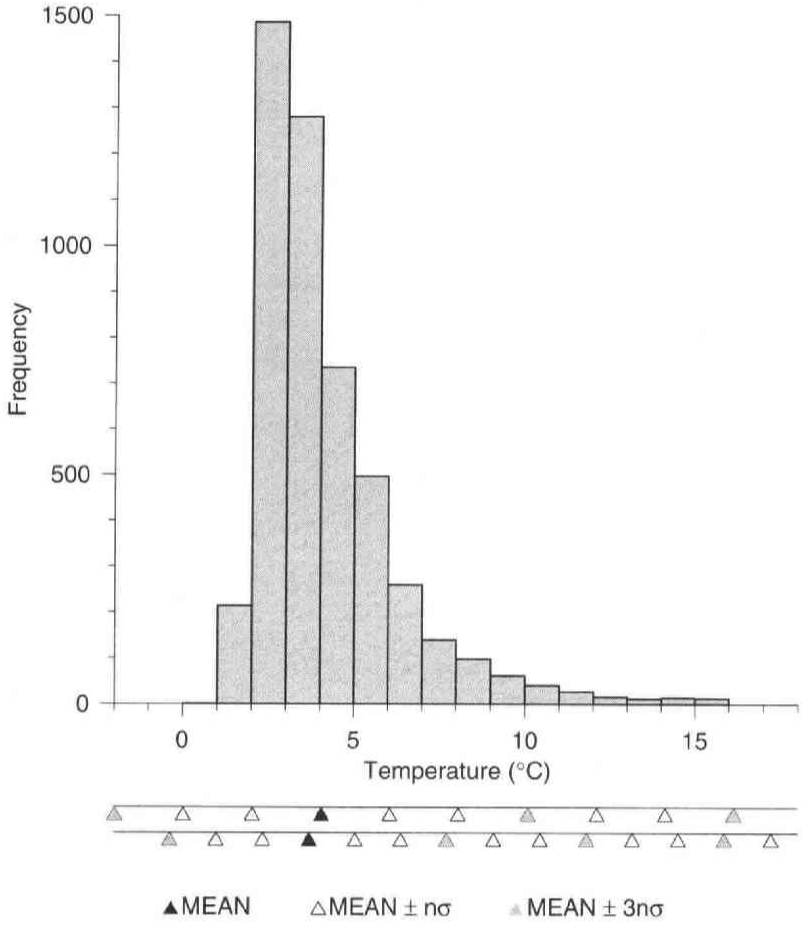

Figure A.1: Occurrence frequency distribution of temperature at 300 m depth off Sanriku Coast, Japan. Below the abscissa, two kinds of standard deviation scale are shown: the upper scale is based on the standard deviation calculated directly from the distribution shown, and the lower is based on the converged standard deviation, which was obtained by iterative procedure in which data lying outside the range $m \pm 3\sigma$ are omitted, and m and σ are recalculated using remaining data (Oguma and Nagata, 2002).

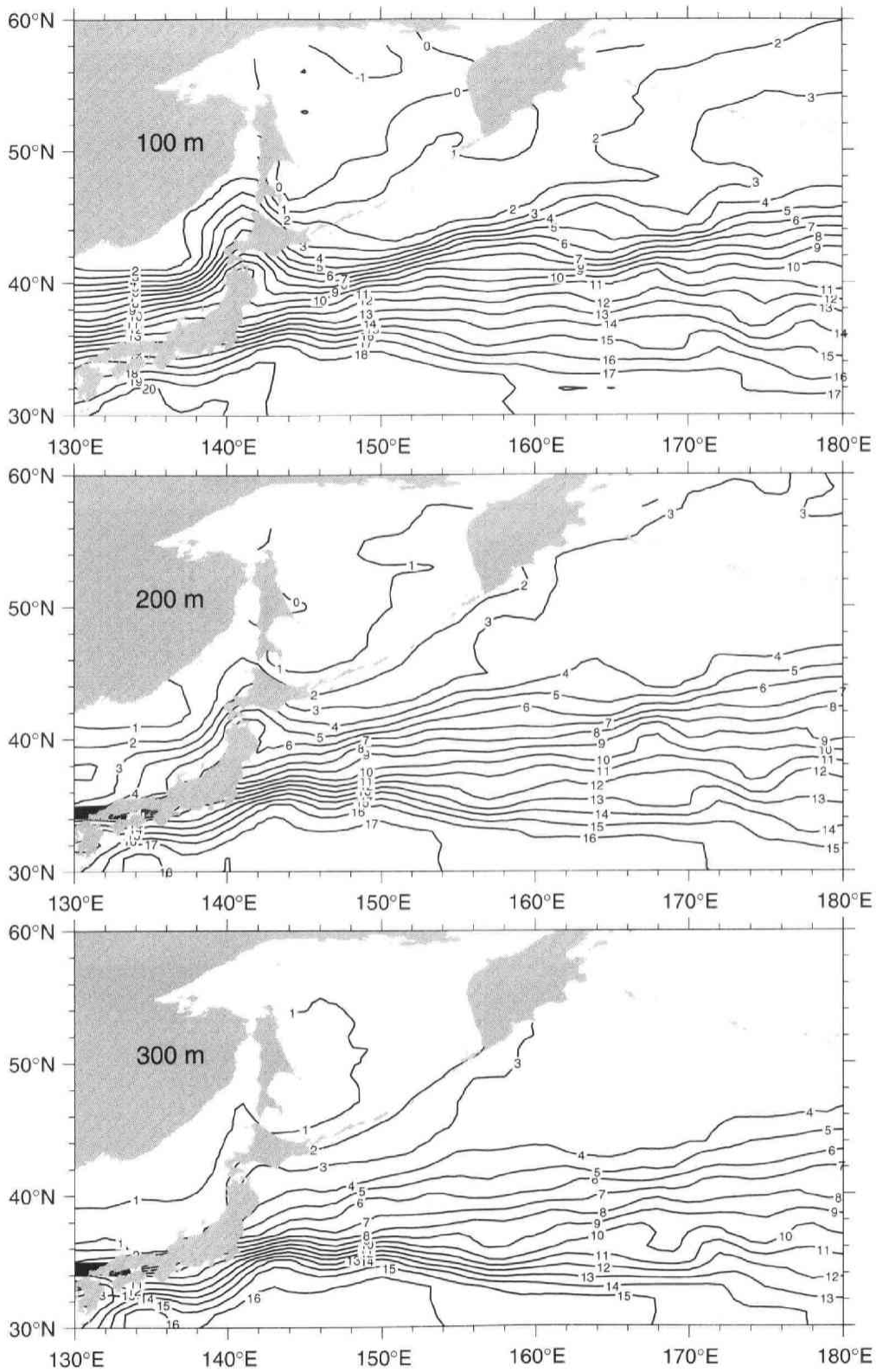

Figure A.2: Mean temperature distributions at 100 m (upper figure), at 200 m depth (middle figure), and at 300 m depth (lower figure) in the Western North Pacific. Numerals attached to isotherms indicate temperature in °C.

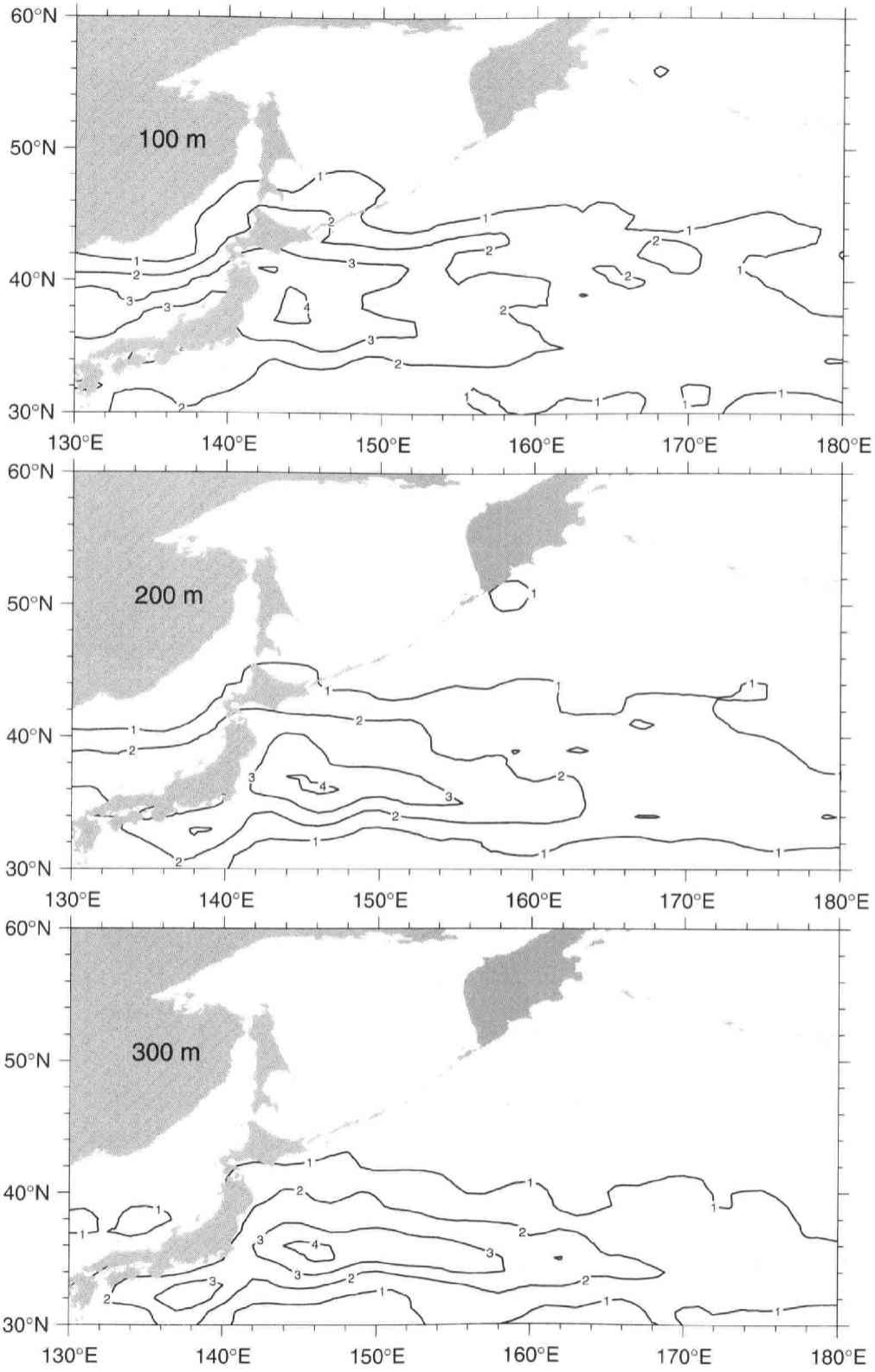

Figure A.3: Same as in Fig. A.2, except for standard deviation fields.

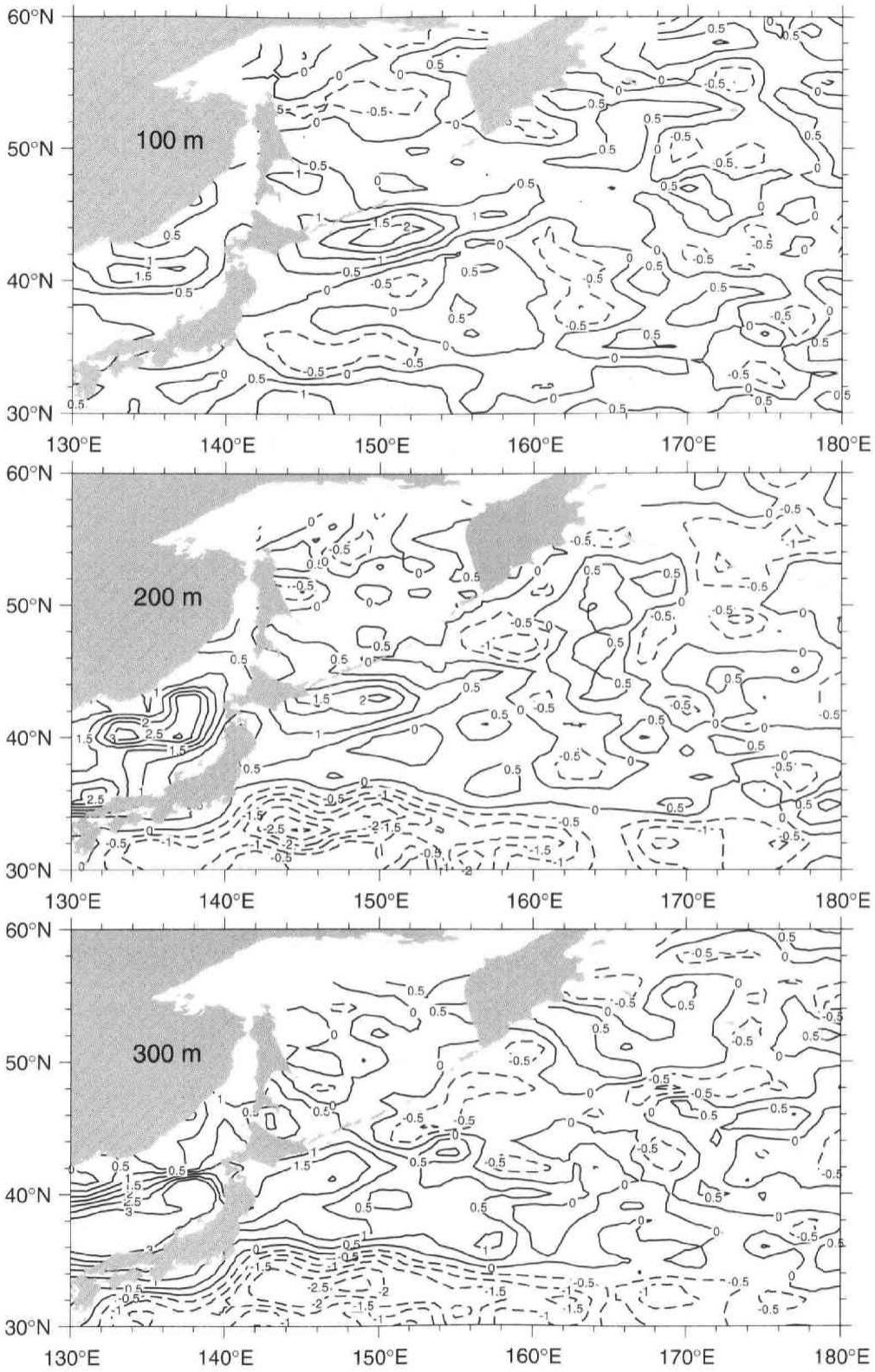

Figure A.4: Same as in Fig. A.2 except for skewness fields.

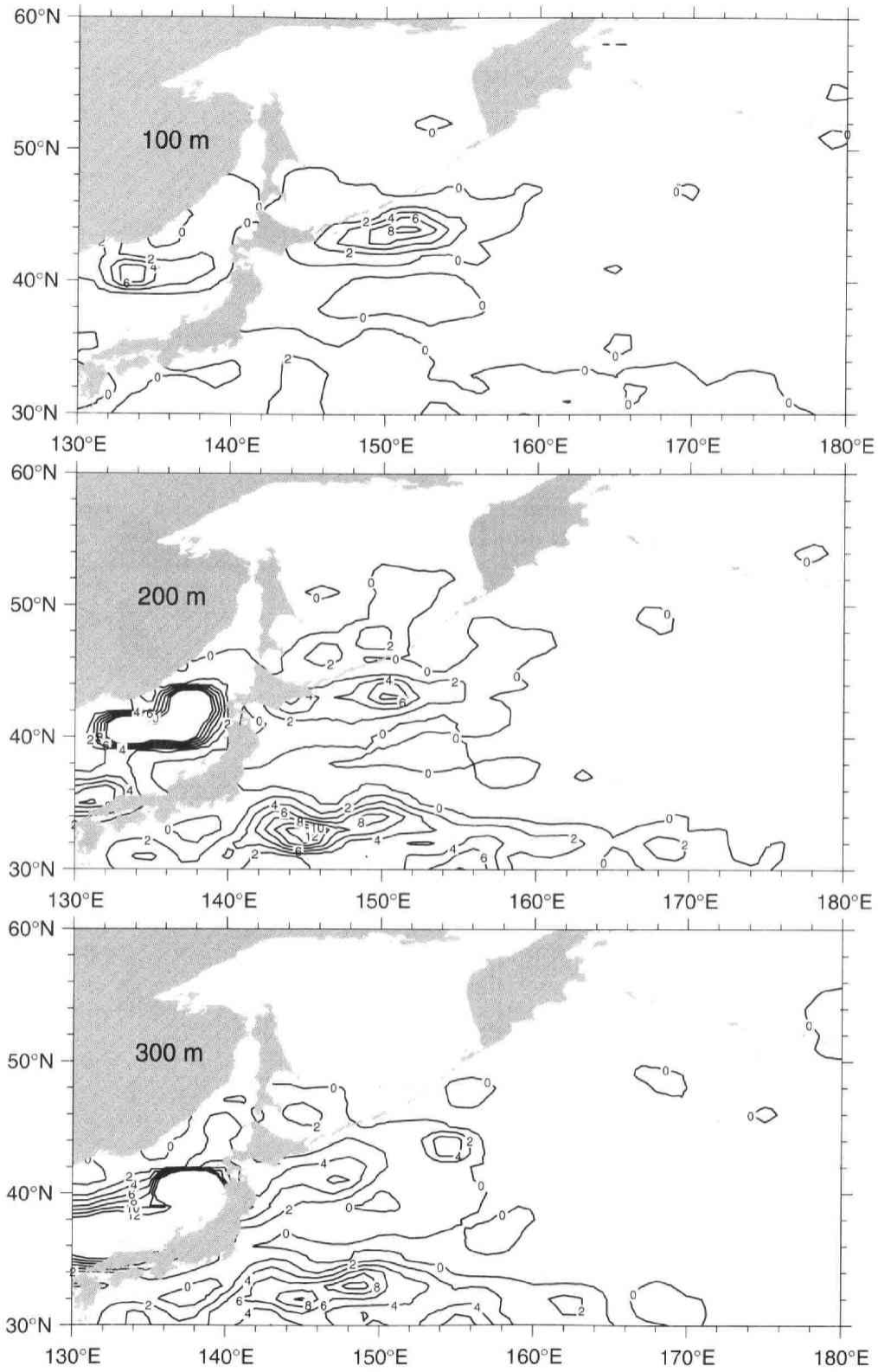

Figure A.5: Same as in Fig. A.2, except for kurtosis fields.

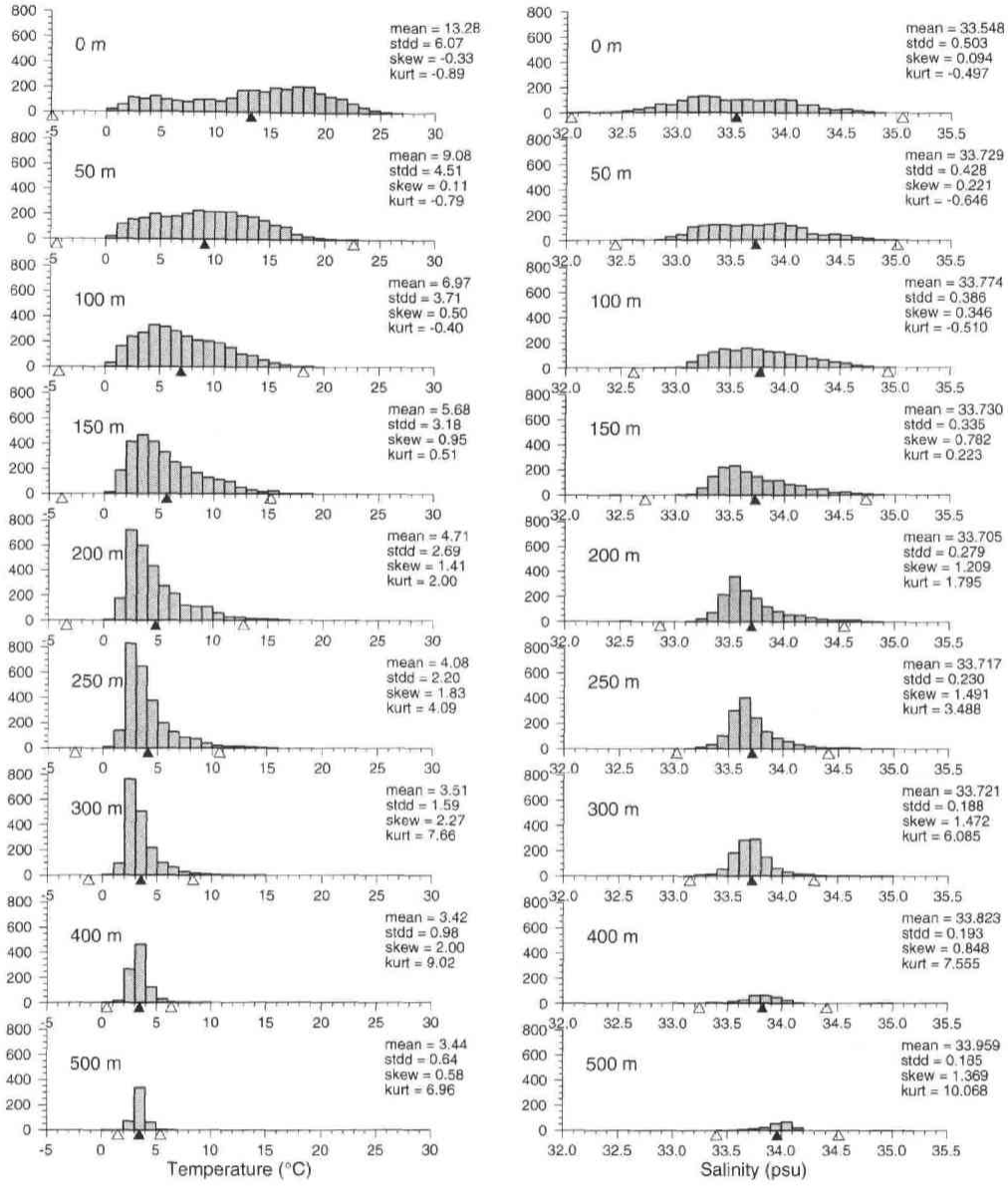

Figure A.6: Variations of the occurrence frequency distribution of temperature (left) and salinity (right) with depth in the subregion centered at 40°N, 143°E. The depth is indicated in the figure. Black triangles attached to abscissa indicate the mean value, and white triangles the mean ± three times of standard deviation. Values of mean, standard deviation, skewness, and kurtosis are shown for each figure.

144°E, 33°N (south of Kuroshio Extension)

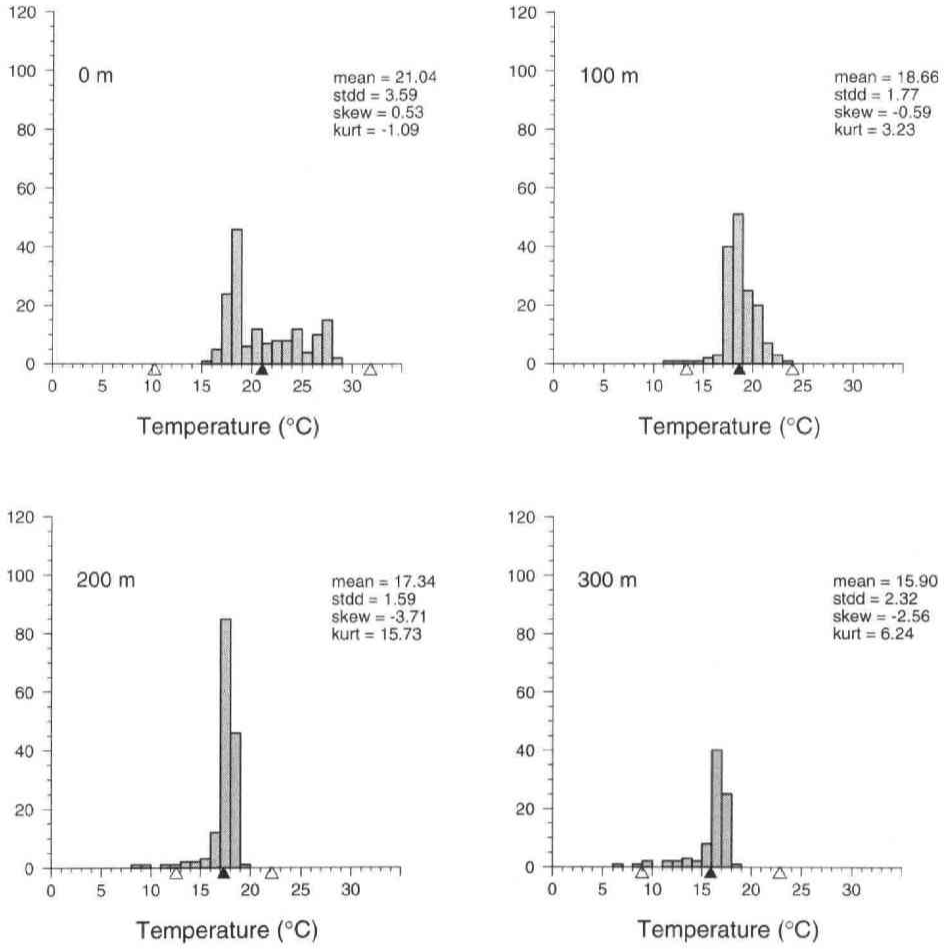

Figure A.7: Variations of the occurrence frequency distribution of temperature with depth in the subregion centered at 33°N, 144°E. The depth is indicated in the figure. Black triangles attached to abscissa indicate the mean value, and white triangles the mean ± three times of standard deviation. Values of mean, standard deviation, skewness, and kurtosis are shown for each figure.

150°E, 43°N (south of Kuril Is.)

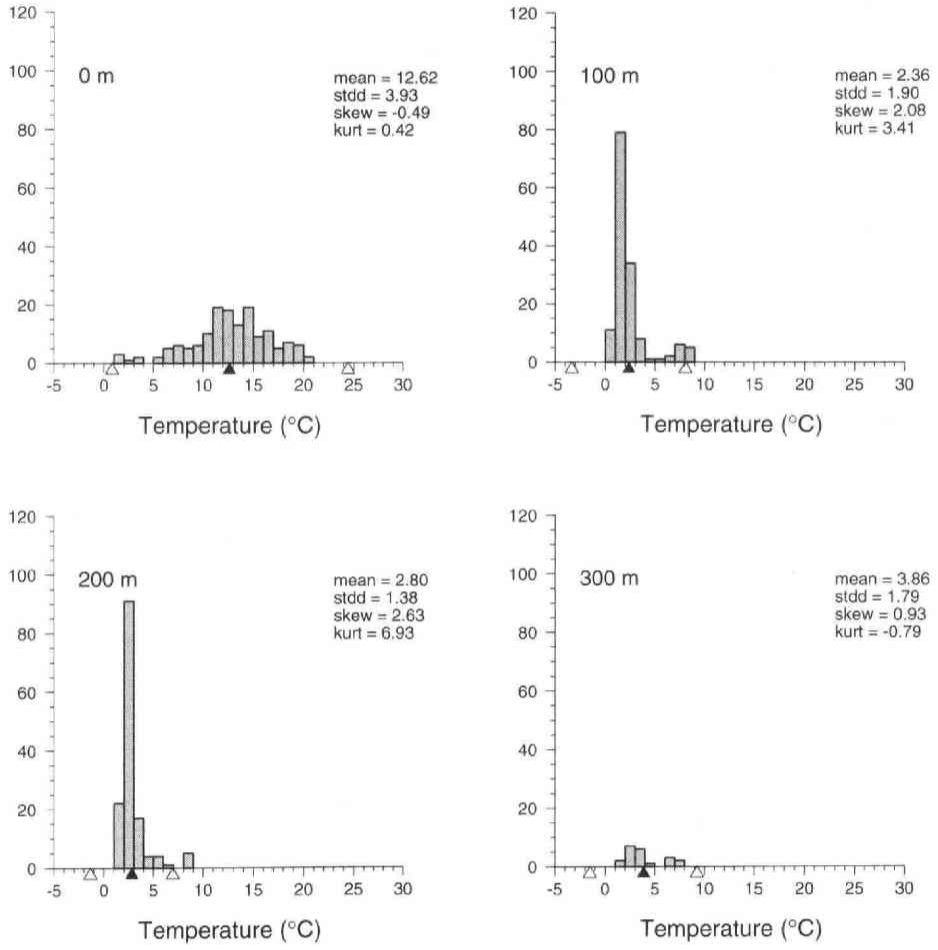

Figure A.8: Same as Fig. A.7 except for the subregion centered at 43°N, 150°E.

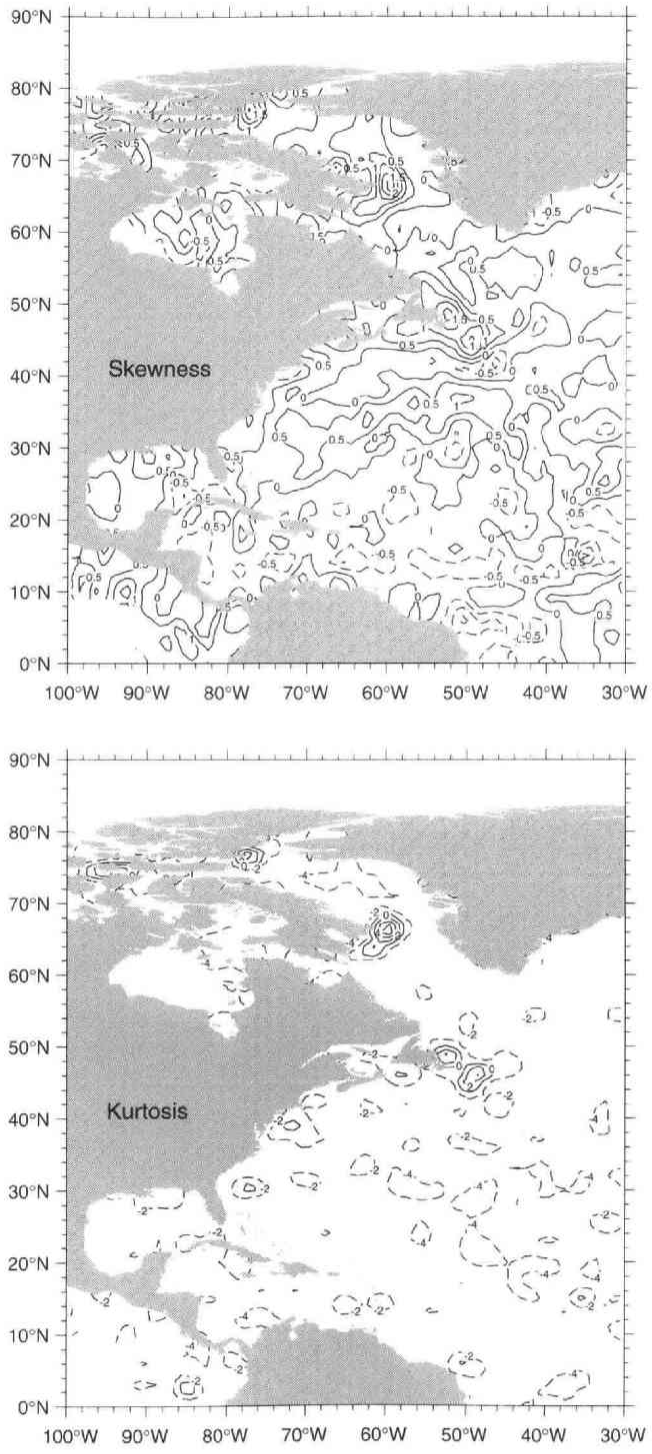

Figure A.9: Skewness (upper figure) and kurtosis (lower figure) distributions at 100 m depth in the Western North Atlantic.

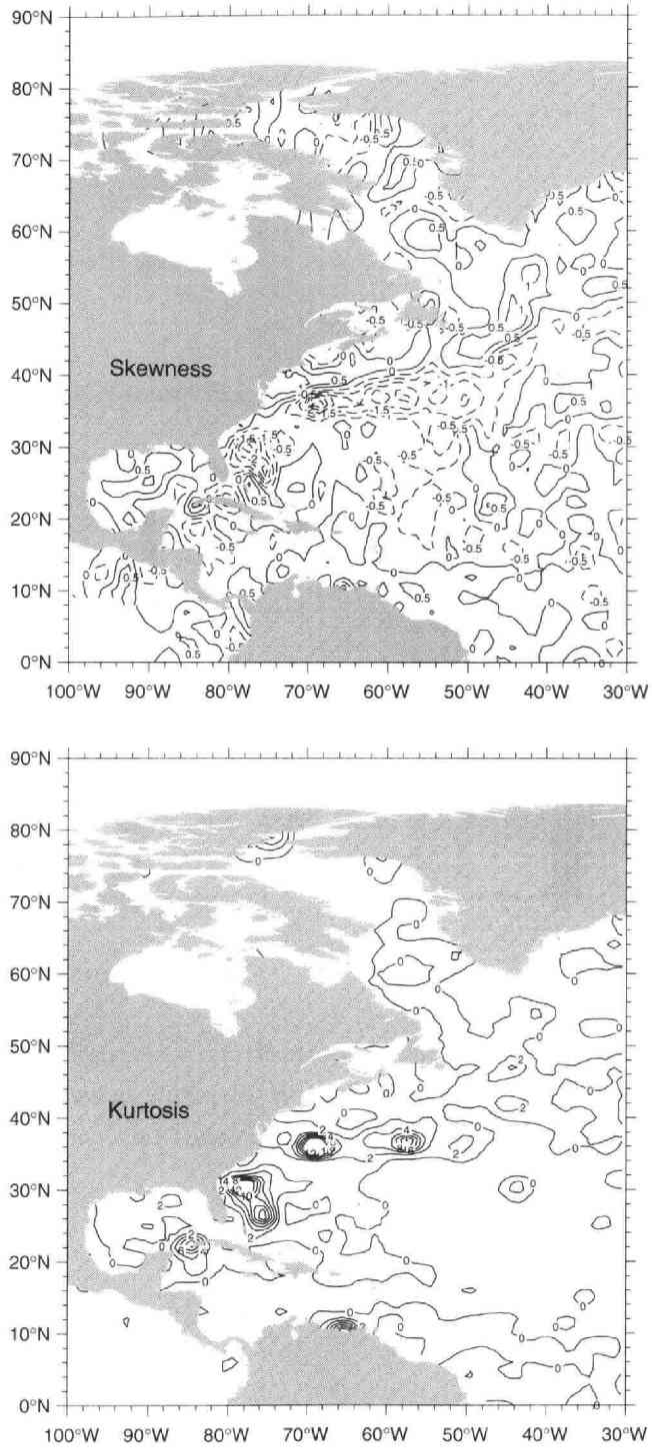

Figure A.10: Same as in Fig. A.9, except for at 300m depth.

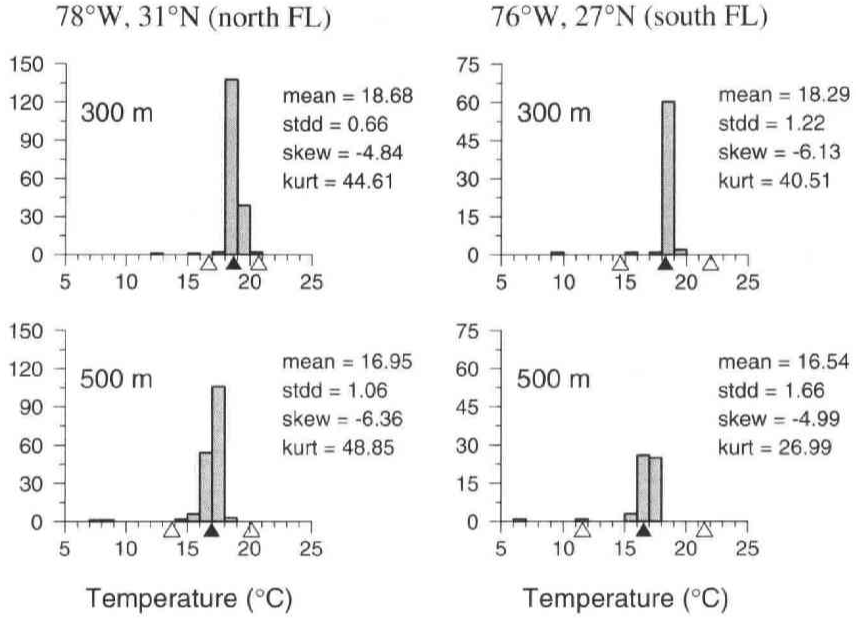

Figure A.11: Occurrence frequency distributions in the subregion centers at 31°N, 78°W (left figures) and in that centered at 27°N, 76°W (right figures). The distributions at 300 m depth are shown in the upper row, and those at 500 m depth the lower row.

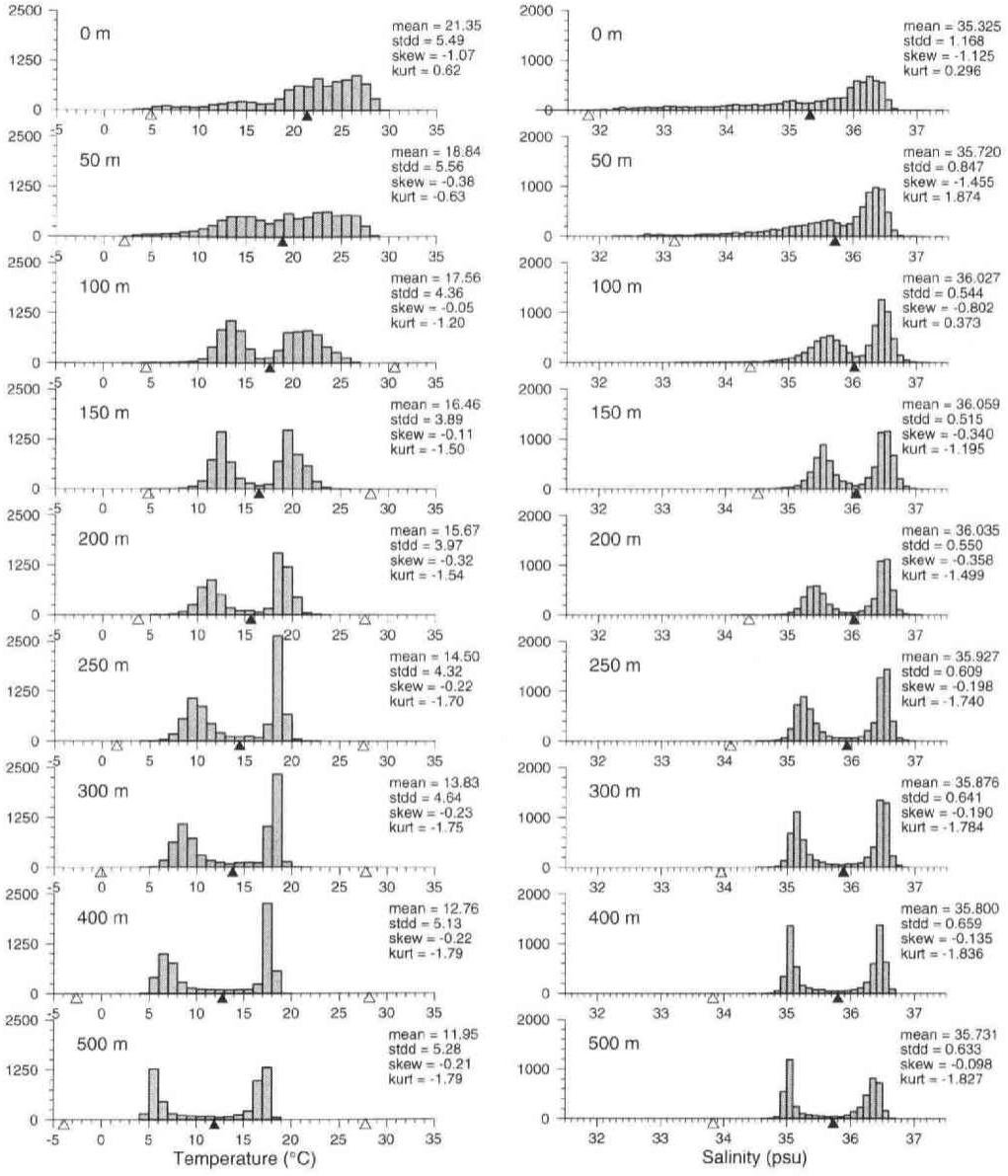

Figure A.12: Same as in Fig. A.6, except for the 5×5 degree subregion centered at 37.5°N, 70°W in the Western North Atlantic.

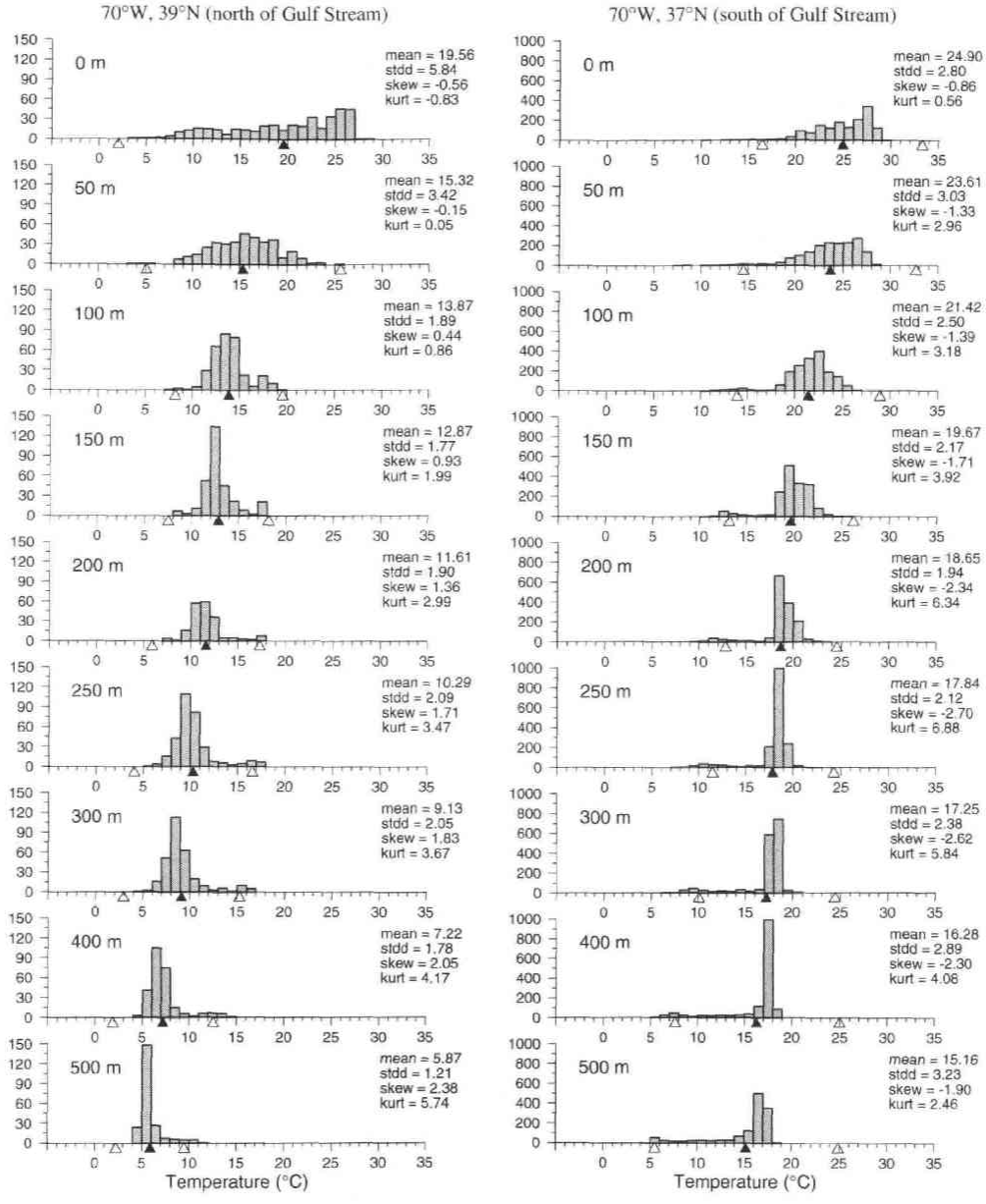

Figure A.13: Occurrence frequency distributions of temperature for various depths in the subregion centered at 39°N, 70°W (left figure) to the north of the Gulf Stream, and that at 37°N, 70°W (right figure) to the south of the Gulf Stream. The depth is indicated in each figure. Calculated mean, standard deviation, skewness and kurtosis are shown also in each the figure.

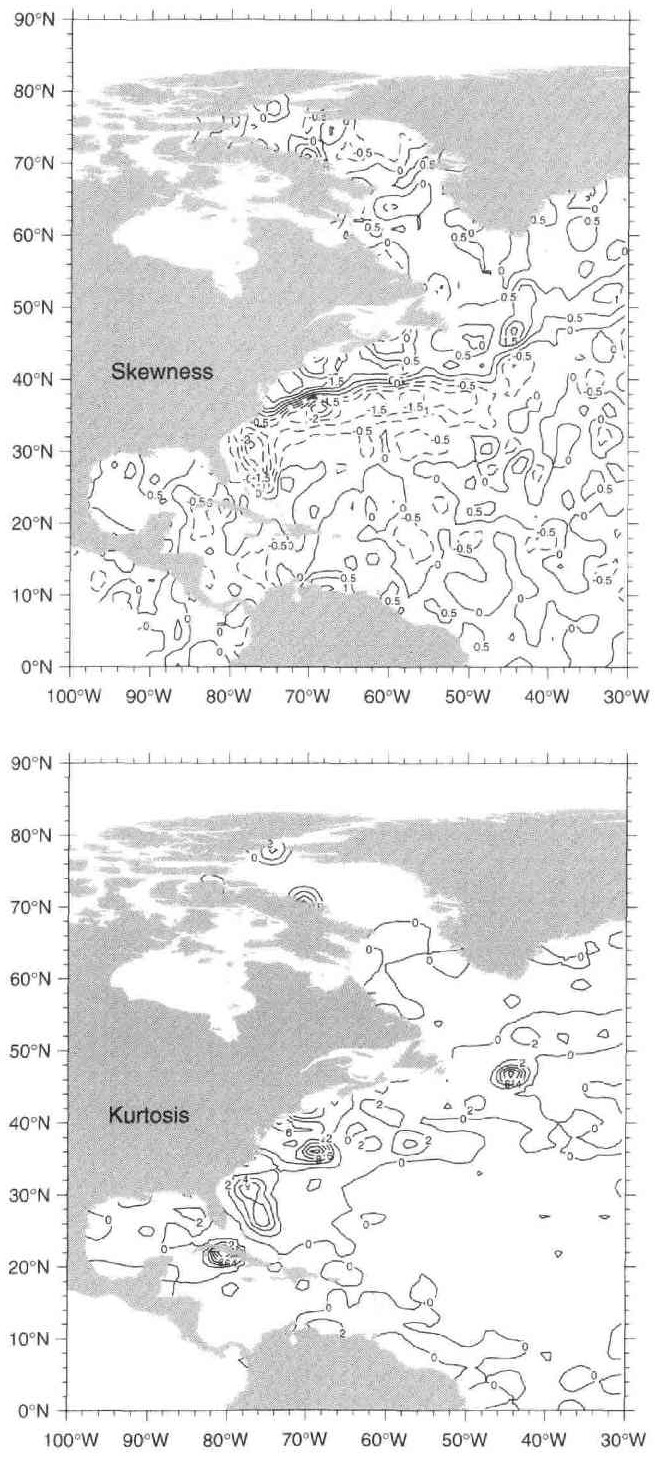

Figure A.14: Same as in Fig. A.9, except for at 500m depth.